REACTOR CORE MATERIALS

A Quarterly Technical Progress Review

Prepared for DIVISION of TECHNICAL INFORMATION,
U. S. ATOMIC ENERGY COMMISSION; by BATTELLE MEMORIAL INSTITUTE

August 1961

● VOLUME 4

● NUMBER 3

TECHNICAL PROGRESS REVIEWS

To meet the needs of industry for concise summaries of current atomic developments, the Atomic Energy Commission is publishing this series, Technical Progress Reviews. Issued quarterly, each of the reviews digests and evaluates the latest findings in a specific area of nuclear technology and science.

The four journals published in this series are:

Nuclear Safety, W. B. Cottrell, editor, R. A. Charpie, advisory editor, and associates, Oak Ridge National Laboratory

Power Reactor Technology, Walter H. Zinn and associates, General Nuclear Engineering Corporation

Reactor Core Materials (covering solid material developments), R. W. Dayton, E. M. Simons, and associates, Battelle Memorial Institute

Reactor Fuel Processing, Stephen Lawroski and associates, Chemical Engineering Division, Argonne National Laboratory

Each journal may be purchased ($2.00 per year for subscription and individual issues $0.55) from the Superintendent of Documents, U. S. Government Printing Office, Washington 25, D. C. See back cover for remittance instructions and foreign postage requirements.

Availability of Reports Cited in This Review

Unclassified AEC reports are available for inspection at AEC depository libraries and are sold by the Office of Technical Services, Department of Commerce, Washington 25, D. C. Some of the reports cited are not available owing to their preliminary nature; however, the information contained in them will eventually be made available in formal progress or topical reports.

Unclassified reports issued by other Government agencies or private organizations should be requested from the originator.

Unclassified British and Canadian reports may be inspected at AEC depository libraries. British reports are sold by the British Information Service, 45 Rockefeller Plaza, New York, N. Y.; Canadian reports (AECL series) are sold by the Scientific Document Distribution Office, Atomic Energy of Canada, Ltd., Chalk River, Ontario, Canada.

Classified U. S. and foreign reports identified in this journal as Classified may be purchased by properly cleared Access Permit Holders from the Division of Technical Information Extension, U. S. Atomic Energy Commission, P. O. Box 1001, Oak Ridge, Tenn. Such reports may be inspected at classified AEC depository libraries.

REACTOR CORE MATERIALS

A REVIEW OF RECENT DEVELOPMENTS

Prepared for DIVISION of TECHNICAL INFORMATION,
U. S. ATOMIC ENERGY COMMISSION,
by BATTELLE MEMORIAL INSTITUTE

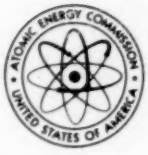

● AUG. 1961

● VOLUME 4

● NUMBER 3

foreword

Reactor Core Materials, one of a series of four quarterly reviews broadly covering the field of nuclear science and technology, is prepared by Battelle personnel from worldwide literature and covers materials and fabrication processes applicable to a nuclear reactor core. The coverage of this subject, however, is limited to materials that are solid at reactor operating temperatures. Pure chemistry, physics, core instrumentation, fuel processing, and source materials are not covered by this Review.

The authors and editors of *Reactor Core Materials* attempt to bring together new developments and significant findings in such a fashion that it can serve as a useful summary of current research for both management and the technical specialist. For the latter group of readers, it is intended that the extensive referencing will aid in locating sources of more detailed information.

R. W. DAYTON
E. M. SIMONS
R. W. ENDEBROCK
Battelle Memorial Institute

contents

Issued quarterly by the U. S. Atomic Energy Commission. Use of funds for printing this publication approved by the Director of the Bureau of the Budget on November 1, 1960.

Section I

FUEL AND FERTILE MATERIALS

Unalloyed Uranium

The diffusion coefficients for hydrogen in alpha uranium were measured by Mallinckrodt workers[1] using a desorption technique. In addition, previous determinations of hydrogen diffusivity, D, in the beta and gamma phases have been reevaluated statistically. The Arrhenius equations for hydrogen diffusion in the allotropic forms, calculated from the slope of the respective least-squares lines, are given below.

Alpha phase (500 to 662°C):

$$D_\alpha = 1.9 \times 10^{-3} \exp\left(\frac{-6.9 \times 10^3}{RT}\right)$$

Beta phase (662 to 772°C):

$$D_\beta = 5.04 \times 10^{-4} \exp\left(\frac{-4.4 \times 10^3}{RT}\right)$$

Gamma phase (772 to 1133°C):

$$D_\gamma = 1.73 \times 10^{-2} \exp\left(\frac{-11.9 \times 10^3}{RT}\right)$$

Beta-treated dingot uranium was alpha annealed in an attempt to refine the coarse-grain structure by a recrystallization process.[1] The effects of annealing time and temperature and dingot composition on the extent of recrystallization were determined. Extending the annealing time from 5 to 120 min at 1200°F increased the degree of recrystallization from 10 to 100 per cent. A similar increase was obtained by raising the temperature from 1080 to 1200°F at a constant annealing time of 120 min.

The average grain diameter (0.13 mm) of recrystallized, alloyed dingot uranium, which contained 150 ppm iron and 100 ppm silicon, was considerably smaller than the 0.31-mm grain diameter of unalloyed dingot uranium which contained 48 ppm iron and 18 ppm silicon. However, the unalloyed metal was completely recrystallized after alpha annealing at 1200°F for 20 min, as compared with a 120-min anneal required for the alloyed metal. This suggests that a second phase is present in alloyed dingot uranium and that this second phase inhibits recrystallization and grain growth during alpha annealing.

Grain refinement of the beta-treated grain structure was definitely achieved by alpha annealing. Alpha-phase vacuum outgassing of salt-bath beta-treated cores for grain refinement, stress relieving, and removal of hydrogen is one possible application of the beta-quench, alpha-anneal process.

The effect of thermal cycling on the creep of uranium was studied by the British.[2] Experiments performed isothermally at 500°C and with temperature cycles of ±40°C about this temperature show the considerable effect that cycling has on the creep rate. For example, creep rate at 0.5 tsi and 500°C is increased by a factor of at least 25 for cycles of ±40°C. The greater the amplitude of thermal cycling, the greater is the creep rate for a given stress; the effect on the creep rate is greater at lower applied stresses for a given thermal cycle. A theory is developed assuming that the internal stresses set up by the differential expansions of the individual crystals are not, of themselves, sufficient to cause plastic flow. This theory gives predictions of the magnitude of the effect which are in good agreement with the experimental results.

Uranium rods were extruded at temperatures near the alpha-to-beta phase transformation temperature by Nuclear Metals.[3] The billet temperature, extrusion-container temperature, reduction ratio, ram speed, and postextrusion cooling rate were varied. The microstructure

and crystallographic orientation varied with extrusion conditions; conditions which tended to raise the temperature of the extruding rod produced rods characterized by large grains (~500 μ) and a random crystallographic orientation. Some rods were made with a core of large grains of random crystallographic orientation surrounded by a thin rim (0.1 to 0.2 in.) of fine grains of <50 μ. The addition of 0.16 wt.% silicon to the uranium reduced the large grain size and retained the random orientation. It is presumed that the extruding uranium rods transform into the beta phase when the extrusion pressure drops abruptly beyond the die land.

In a study[4] of the preferred orientation that occurs as a result of cross rolling of uranium sheet, Dow Chemical workers made use of inverse-pole figures and calculated thermal-expansion coefficients. The preferred crystallographic orientation and thermal-expansion properties of uranium sheet can be summarized as follows:

1. Rolling of uranium produces a (0 0 1) texture in all cases in the short-transverse direction. The only effect that cross rolling has in the short-transverse direction is to change the shape of the texture about the (0 0 1) pole.

2. Cross rolling produces a high (0 1 0) texture in the transverse direction which tends to decrease to a moderately high density as the amount of cross rolling increases. The least amount of preferred orientation occurs in the transverse direction at 54 per cent of cross rolling; however, a (1 3 2) texture also begins to appear in the transverse direction at this point.

3. There is never any strong or detailed texture in the longitudinal direction as a result of cross rolling. The nearest approach to randomness in this direction was in the 54 per cent cross-rolled samples.

4. There will never be a random condition in all three principal directions at the same time. The textures will never be the same in any given direction.

5. The coefficient of thermal expansion in the short-transverse direction remains high and does not change as a result of cross rolling.

6. As the amount of cross rolling increases, the thermal-expansion coefficient in the transverse direction increases from a very low value to just above that for a random condition.

7. The thermal-expansion coefficient in the longitudinal direction behaves in a manner opposite to that in the transverse direction, i.e., from a value near that for a random condition to a very low value as cross rolling increases.

8. After cross rolling to a little more than 54 per cent reduction, the coefficient of thermal expansion may be nearly the same in the transverse and longitudinal directions; at other reductions the coefficients in the two directions will always be different.

Internal friction in alpha uranium depends on heat-treatment and decreases after beta or gamma-phase annealing according to Russian experimentation.[5] The internal friction changes isothermally during polymorphic transformations. The alpha-to-beta and gamma-to-beta transformations are accompanied by a decrease in internal friction, and the beta-to-gamma and beta-to-alpha, by an increase. Each phase has its own value of internal friction.

A recent issue of the *Journal of Nuclear Materials*[6] contains articles on uranium which cover the following topics: self-diffusion in the beta phase, diffusion of gold and aluminum in uranium, the effect of the $\alpha \rightarrow \beta \rightarrow \alpha$ transformation on the preferred orientation of alpha uranium, the effect of orientation and temperatures on the modes of deformation of uranium, and the thermal expansion of single crystals of alpha uranium. (M. S. Farkas)

Alpha-Phase Uranium Alloys

The constitution of the uranium-molybdenum-niobium system was studied by the British[7] at 1100, 1200, and 1300°C. Isothermal sections were obtained by metallographic and X-ray methods. The decomposition of the body-centered cubic gamma phase in alloys containing 5 at.% molybdenum and approximately 50 at.% uranium occurred very slowly at temperatures near the miscibility gap. Additions of molybdenum were found to decrease the rate of the monotectoid reaction, $\gamma_1 \rightarrow \alpha + \gamma_2$. Room-temperature lattice parameters of quenched, homogeneous, gamma alloys were obtained, and a hardness survey of the same alloys showed that a maximum hardness occurred at approximately 50 at.% niobium, whereas a minimum occurred at 85 at.% uranium.

Specimens of uranium, uranium–10 wt.% molybdenum, and thorium in the form of bare and organic- or metal-coated single coupons and composite assemblies that were joined by soldering, welding, or the use of machine screws were evaluated by Battelle[8] for corrosion re-

sistance. Both accelerated and long-term tests provided exposure to ambient, humid, salt-spray, and humid-freezing conditions. Environments involving high humidity or a salt fog caused a localized type of attack on all the materials. The uranium became badly pitted and roughened under almost all conditions studied. Vinyl type organic coatings blistered during exposure, particularly coatings on uranium. Aluminum coatings on uranium behaved similarly. No galvanic effects were observed in couples prepared from dissimilar metals, even at crevice areas and mating surfaces on specimens joined by machine screws.

The behavior of inert gases in samples of inoculated uranium and uranium alloys has been studied at Nuclear Metals.[9] Alloys included were uranium–1.6, –2.8, and –10 wt.% molybdenum, uranium–2 wt.% zirconium, uranium–0.3 wt.% chromium–0.3 wt.% molybdenum, uranium–1 and –2 wt.% carbon, and uranium–3.8 wt.% silicon. Helium was injected into metal samples by alpha-particle irradiation; krypton, by glow-discharge techniques. Following gas inoculation, samples were given various isothermal and thermal cycling heat-treatments to permit the formation of gas bubbles. The gas bubbles were observed in the light microscope after mechanical polishing and after chemical etching and in the electron microscope after cathodic vacuum etching. Helium-gas bubbles were observed in the cyclotron-irradiated samples following various heat-treatments between 475 and 1075°C. The majority of the gas bubbles in any sample, independent of heat-treatment, were between 0.05 and 2 μ in diameter (10^{10} to 10^{14}/cm^3) and accounted for up to 10 per cent porosity. Post-irradiation heat-treatments above 900°C gave rise to the formation of a small number (about 10^5/cm^3) of large bubbles between 10 and 150 μ in diameter which accounted for porosities up to several hundred per cent. The large volume increase caused by the bubbles formed during postirradiation treatments is similar to that observed in metallic reactor fuel elements irradiated at temperatures above 400°C. Effects of recrystallization and phase transformations on the behavior of the helium-gas bubbles were noted. The nucleation and growth characteristics of the small and large bubbles are discussed.

Irradiation studies by Argonne[10] of the uranium–5 wt.% zirconium–1.5 wt.% niobium alloy, variously fabricated and heat-treated, led to the following observations:

1. The most effective heat-treatment for dimensionally stabilizing swaged or round-rolled uranium–5 wt.% zirconium–1.5 wt.% niobium alloy consisted of a 24-hr isothermal transformation from the gamma phase at 650°C. This heat-treatment was subsequently used as a basis for specifying the heat-treatment to be given to the Experimental Boiling-Water Reactor (EBWR) fuel plates.

2. The most effective heat-treatment for dimensionally stabilizing flat-rolled material consisted of a 12 per cent reduction in thickness by cold rolling, followed by a 24-hr isothermal transformation from the gamma phase at 655°C.

3. The swaged alloy could not be heat-treated to bring about both dimensional stability and corrosion resistance.

4. Flat-rolled material would be made both dimensionally stable and corrosion resistant by first reducing the material 12 per cent in thickness by cold rolling, then transforming the alloy isothermally from the gamma phase for 24 hr at 665°C, followed by quenching from 800°C.

5. Zircaloy-2 cladding in thicknesses as small as 0.04 in. and metallurgically bonded to the fuel alloy partially restrained the irradiation growth of the fuel alloy.

6. Flat-rolled fuel alloy which was irradiated generally increased in length and width and decreased in thickness. (M. S. Farkas)

Gamma-Phase Uranium Alloys

A discussion of the band structure in uranium-molybdenum gamma-phase alloys is contained in a paper by Blatt.[11] Experiments dealing with the Hall effect, specific heat, and resistivity are reviewed, and the author finds the data to be consistent with the band model proposed earlier by Friedel. However, the need for additional data is pointed out, specifically on thermoelectric power, soft X-ray bands, and magnetic susceptibility.

A comprehensive review of corrosion behavior and theory as applied to uranium and various gamma-phase alloys is contained in a paper presented by Waber.[12a] Included is a discussion of the role of hydrogen penetration and of the influence of oxide film, especially the effect of stresses resulting from lattice mismatch between the base metal and oxide. A mechanism of corrosion involving hydroxide ion attack is presented.

Table I-1 NAA-38-3 CAPSULE IRRADIATION PRELIMINARY RESULTS

Composition, %	Estimated burnup, Mwd/metric ton of U	Estimated central temp., °F			Density, g/cm^3		Change, %	Change in length, %	Change in diameter, %
		First quarter	Second and third quarters	Fourth quarter	Preirradiation	Postirradiation			
U–10 Mo	7250	Steep flux profile: 700–800 during entire irradiation			17.10	16.05	6.20	0.43	0.267
U–10 Mo	9560	1200–1650		800–1200		12.23			12.7
U–10 Mo	9970				17.13	11.31	34.00	10.35	18.2

An experimental investigation of irradiation-induced disordering of the U_2Mo phase to produce gamma is described in a French report.[13] The change in structure was followed by X-ray-diffraction techniques. It was found that the change was initiated with exposures of about 10^{16} nvt and was completed after exposure to 1.2×10^{18} nvt.

Irradiation results for the uranium–10 wt.% molybdenum alloy were reported by Atomics International.* Data are shown in Table I-1. On the basis of the data obtained to date in their program, it is tentatively concluded that the alloy will serve well at burnups to 10,000 Mwd/metric ton of uranium and central temperatures to 1100°F. (A. A. Bauer)

Dilute Uranium Alloys

Aluminum-Uranium Alloys

The corrosion resistance of the bond between aluminum cladding and nickel-plated uranium has been studied by Savannah River.[12b] Aluminum-clad specimens that contained a drilled pinhole were tested in deionized water at 95 to 98°C. It was found that the corrosion resistance of the bond layer, i.e., the ability of the bond to confine attack to the vicinity of the defect, was dependent on the distribution of an "oxygen-rich phase" in the uranium-nickel diffusion zones. The oxygen-rich phase is not defined exactly because, although it has some X-ray-diffraction lines in common with UO_2, it is not recognizable as UO_2 by metallography; in fact, it usually can be seen only with the electron microscope. If the oxygen-rich phase occurs as dispersed particles through the UNi_5 layer, the corrosion confinement is good; however, if it is present as a more continuous layer between the UNi_5 and the U_6Ni, the corrosion is able to spread rapidly from the initial defect because of the rapid migration of hydrogen through the oxygen-rich phase layer.

Zirconium-Uranium Alloys

General Atomic[14] reports the temperature and stress dependence of the steady-state creep rate of zirconium-hydrogen-uranium (atomic ratio 1:1:0.03) in the temperature range 500 to 600°C. At 502°C, where the alloy is a mixture of beta (body-centered cubic solid solution of hydrogen in zirconium) and gamma zirconium hydride, the stress dependence of creep rate is represented by $\epsilon = K\sigma^n$, where σ = stress dependence and $n = 4.1$. Alloys were examined at stresses between 4000 and 8000 psi. Above the transformation at 553°C, $n = 4.7$, and at 568°C, $n = 4.9$. Stresses applied were 3000 to 6000 psi. On the basis of a stress of 6000 psi, the activation energy below the transformation is 80,000 cal/g-atom, whereas above the transformation the activation energy is 65,000 cal/g-atom.

It is interesting to note that the activation energies for creep in this alloy are much higher than those reported for self-diffusion of alpha and beta zirconium, i.e., 22,000 cal/g-atom in alpha and 27,000 cal/g-atom in beta. It appears likely that the rate-controlling step for creep in this alloy involves the diffusion of zirconium atoms in zirconium hydride.

Another interesting sidelight concerning the zirconium-hydrogen-uranium alloy is that, although brittle at room temperature, the alloy is quite ductile above 500°C. A specimen tested to failure at 568°C at a stress of 6000 psi exhibited an elongation of 70 per cent.

*W. A. Holland, Irradiation Properties of Uranium-Molybdenum Alloys, USAEC Report NAA-SR-6262, Atomics International, to be issued September 1961.

Miscellaneous Alloys

Two modifications of the crystal structure of U_2Zn_{17} have been observed.[15] One modification has hexagonal symmetry and the other has rhombohedral symmetry. These structures differed principally in the stacking of a basic structural layer. The hexagonal structure is related to Th_2Ni_{17}, and the rhombohedral structure is related to Th_2Zn_{17}. (R. F. Dickerson)

Plutonium and Its Alloys

An extensive investigation of the mechanical properties of unalloyed plutonium has been conducted by Hanford.[16] Average tensile properties of plutonium at various temperatures are shown in Table I-2. In general, the effect of an increase in temperature is a decrease in strength and an increase in ductility. The effects of testing speed on tension and compression properties in the alpha, beta, and gamma phases were determined. In the alpha phase, strength values increased to a maximum with increasing testing speed and then decreased. Beta-phase strength values increased rapidly with increasing testing speed, whereas the effect of test speed on gamma-phase strength was relatively small. In the alpha phase, creep rates at a stress of 10,000 psi varied from 15×10^{-4} to 330×10^{-4} in./(in.)(10,000 hr) for test temperatures of 31 and 100°C, respectively. A brittle fracture with an average impact-energy value of 2.6 ft-lb was observed in room-temperature tension impact testing. An average of 52,000 psi was obtained for the ultimate shear strength in torsion.

Table I-2 EFFECT OF TEMPERATURE ON TENSILE PROPERTIES OF ALPHA-, BETA-, GAMMA-, AND DELTA-PHASE PLUTONIUM[16]

(Testing Speed: 0.015 In./Min)

Test temp., °C	Strength, psi: Ultimate	Strength, psi: Yield (0.01% offset)	Modulus of elasticity, 10^6 psi	Elongation, %	Reduction of area, %	Phase
−30	57,300	50,300	14.7	0.018		Alpha
30	50,900	32,100	14.3	0.068		Alpha
70	43,800	15,200	12.6	0.43		Alpha
100	34,800	13,600	9.8	1.00		Alpha
110	33,100	12,300	10.0			Alpha
130	12,100	10,300	3.0	294.0	100.0	Beta
160	5,620	3,950		570.4	100.0	Beta
180	3,580	2,620		503.2	100.0	Beta
190	3,280	2,210	1.6	325.9	97.8	Beta
200	2,940	2,190		121.0	82.1	Beta
230	4,420	3,860	1.8	50.0	75.0	Gamma
265	3,470	2,900		57.2	77.0	Gamma
300	2,020	1,650	1.0	50.1	82.8	Gamma
325	895	790	0.38	67.3	98.0	Delta

Plutonium-aluminum alloys containing 0.36 to 1.23 wt.% aluminum have been investigated at Argonne.[17] Linear expansion coefficients for some of these alloys appear in Table I-3. Diffusion couples consisting of plutonium–1 wt.% aluminum alloy and Zircaloy-2 were heat-treated in a vacuum at 425 and 500°C for a period of one week. No evidence of a reaction layer between these two materials was noted. However, there was evidence that the materials in the couple at 500°C were not in intimate contact.

Table I-3 LINEAR EXPANSION COEFFICIENTS OF SOME PLUTONIUM-ALUMINUM ALLOYS[17]

Composition: Wt.% Al	Composition: At.% Al	Temp. range, °C	Linear expansion coefficient, 10^{-6}/°C
0.98	8.05	20–425	10.6
1.22	9.80	20–425	11.4
1.23	10.00	20–425	12.5

Alloys of uranium–20 wt.% plutonium–5, –10, and –15 wt.% fissium and the same alloys containing 1.5, 3, and 4.5 wt.% additional zirconium in the fissium are being studied[18] to determine the effects of changes in composition on a uranium–20 wt.% plutonium–10 wt.% fissium alloy. The uranium–20 wt.% plutonium–3.5 wt.% fissium–1.5 wt.% zirconium alloy was found to be body-centered tetragonal from 625 to 775°C. Lattice parameters for the alloy quenched from 775°C are $a_0 = 6.99$ and $c_0 = 6.78$ A. The uranium–20 wt.% plutonium–5 wt.% fissium alloy is body-centered cubic when quenched from 775°C. Quenching from 700°C produces a slightly distorted cubic cell; quenching from 625°C produces a tetragonal structure. The presence of the U_2Ru compound was indicated in diffraction patterns of uranium–20 wt.% plutonium–15 wt.% fissium alloy, whereas ZrRu was noted in alloys containing additional zirconium. The grain size of the alloys decreased with increasing fissium content.

The following alloys were found to exhibit adequate corrosion resistance when tested in 350°C water at Hanford:[19]

Al–11 wt.% Si–2 wt.% Pu
Al–1.3 wt.% Ni–1 wt.% Si–2 wt.% Pu
Al–2.0 wt.% Ni–2 wt.% Pu–0.1 wt.% Ti
Al–3.0 wt.% Ni–2 wt.% Pu
Al–3.5 wt.% Ni–2 wt.% Pu–0.1 wt.% Ti

No substantial increase in corrosion resistance was gained by increasing nickel content above 2.0 wt.%. Alloys which showed inadequate corrosion resistance were:

Al–1.8 wt.% Pu
Al–5 wt.% Si–2 wt.% Pu
Al–1 wt.% Si–2 wt.% Pu
Al–1 wt.% Ni–2 wt.% Pu
Al–3 wt.% Zr–2 wt.% Pu

Cast niobium–10 wt.% plutonium–10 and –30 wt.% zirconium alloys that are being investigated at Battelle[20,21] were found to contain the following phases: The primary phase was identified by X-ray-diffraction analysis as niobium-zirconium solid solution, whereas the secondary grain-boundary phases are believed to be zirconium-plutonium rich alloy phases. Diamond pyramid hardness (DPH) numbers of 202 and 244 were observed for alloys containing 10 and 30 wt.% zirconium, respectively.

On the basis of hardness data, 80 and 90 per cent cold-reduced thorium–5 and –10 wt.% plutonium alloys appear to recrystallize completely within 1 min at either 650 or 700°C.

(V. W. Storhok)

Thorium

Examination of refractory thorium and thorium-uranium compounds and their alloys is continuing at Battelle.[22] The rates of oxidation of a series of carbide alloys in air at 1100°F are shown in Table I-4.

Argonne[23] has irradiated a series of thorium-uranium alloys to burnups of 1.0 to 1.3 at.% at temperatures of 455 to 500°C. Visual inspection of cylindrical specimens containing 10, 15, and 20 wt.% uranium indicated that these alloys possess good irradiation stability. However, an alloy containing 28 wt.% uranium was badly warped after irradiation.

A series of thorium tensile specimens in NaK has been irradiated at the Materials Testing Reactor (MTR).[24] The maximum specimen temperature was estimated to be 320°C. The results of hardness tests on these specimens are shown in Table I-5. Results of tensile tests were reported previously. (W. Chubb)

Table I-4 OXIDATION RATES[22] OF THORIUM-URANIUM CARBIDES IN AIR AT 1100°F

Nominal composition, mole %	Weight gain, mg/(cm²)(hr)
ThC–10 UC	6.4
ThC–10 UC–2.5 Mo_2C	8.7
ThC–10 UC–5 NbC	6.7
ThC–10 UC–5 SiC	3.2
ThC–10 UC–5 ZrC	4.3
ThC_2–10 UC_2	3.5
ThC_2–10 UC_2–2.5 Mo_2C	3.4
ThC_2–10 UC_2–5 NbC	4.7
ThC_2–10 UC_2–5 SiC	3.7
ThC_2–10 UC_2–5 ZrC	3.7

Table I-5 HARDNESS OF THORIUM AS A FUNCTION OF IRRADIATION[24]

Burnup, at.%	Average hardness, R_A	Hardness range, R_A
0	16	14–17
0	27*	26–29
0.1	48	42–51
0.85	44*	42–46
1.5	48	34–59

*150 grains per inch. All others 20 grains per inch.

Dispersion Fuels

The objective of a continuing program at the Clevite Corporation[23] is to develop methods for producing improved aluminum-base fuel elements in which the fuel is contained in Fiberglas embedded in an aluminum matrix.

Initially, fabrication techniques were developed for converting aluminum-coated, uranium-free glass fibers into crack-free core material. This information was transferred to the fabrication of core sections containing depleted-uranium-bearing Fiberglas. These techniques can now be employed to process enriched-uranium-bearing Fiberglas into core sections for fuel plates.

The fabrication steps required for preparing fuel plates consist essentially of the following:

1. Consolidation of the aluminum-coated Fiberglas by hot pressing or by cold pressing followed by hot pressing.

2. Framing the compact in an aluminum picture frame.

3. Open rolling approximately 50 per cent.
4. Clad rolling into fuel plates.

The Fiberglas serves a twofold purpose. It acts as a carrier for uranium inasmuch as the U_3O_8 forms a solid solution with the normal glass constituents. Presumably, plutonium fuel could be substituted in this type of fuel material. Also, the glass serves to strengthen the aluminum at elevated temperatures.

It was found that reinforcing aluminum with Fiberglas provided materials with tensile-strength properties that were substantially higher than those of type 1100 aluminum, as well as most aluminum alloys, at elevated temperatures. Two types of Fiberglas materials are represented. These consist of (1) as hot pressed, in which the fibers were unfragmented and oriented in one direction, and (2) as rolled, in which the fibers were fragmented.

The as-hot-pressed material exhibited good strength-retention properties at elevated temperatures. For example, the tensile strength at room temperature was 25,250 psi. As the temperature was increased, the tensile strength decreased. It reached a plateau with an average tensile strength of 18,450 psi at temperatures from 250 to 800°F. This strength retention at elevated temperatures is significant, since conventional aluminum alloys lose most of their strength above 450°F.

The as-rolled Fiberglas-reinforced aluminum sheet prior to cladding also displayed a much better strength retention than commercial aluminum or any of the aluminum alloys at elevated temperatures. However, its strength was less than the as-hot-pressed material in the temperature range of 250 to 800°F. The decrease in the strength retention of the Fiberglas-reinforced material upon rolling is attributed to the fragmentation of the Fiberglas during rolling. Even so, the fiber-reinforced material after rolling remains substantially stronger than the commercial aluminum in the temperature range from 400 to 1000°F.

This concept, when proof tested by irradiation experiments, should provide a fuel element suitable for higher operating stresses in a test reactor, for operation in a small power reactor at 500 to 600°F, or for employing plutonium safely as a fuel.

Experimental work reported by Oak Ridge[25] is concerned with the development of a dispersion fuel plate with a high burnup potential for application in a 500°C sodium environment as core B of the Enrico Fermi Fast Breeder Reactor. The dispersion fuel product resulting from an 18-month program of materials evaluation and fabrication studies consists of 35 wt.% spheroidal UO_2 dispersed in type 347B stainless-steel powder and clad with wrought type 347 stainless steel. Methods for achieving a uniform distribution of spheroidal UO_2 in the matrix powder and for cladding the sintered powder compact by roll bonding are described. Examination of experimental plates reveals that the degree of UO_2 fragmentation and stringering encountered during processing is primarily a function of the degree of cold work employed in the finishing operation and the starting quality of the UO_2 powder. Cladding studies indicate that a sound metallurgical bond can be achieved with an 87.5 per cent reduction in thickness at 1200°C and that close processing control is required to meet the stringent tolerances specified.

Although basic fabrication procedures were well established, several problems peculiar to the core B fuel element remained to be resolved. One is to devise means for homogeneously incorporating the coarse spheroidal UO_2 particles in the stainless-steel matrix. Also, some concern existed as to whether appreciable difficulties would arise in roll cladding 0.112-in.-thick fuel plates, particularly since the ratio of cladding-to-core thickness was unusually small. Experiments were also conducted to determine the least amount of cold rolling that could be employed consistent with dimensional and flatness requirements of the plates, at the same time ensuring maximum integrity of the UO_2 particles. Detailed procedures covering composite-plate manufacture are presented.

At Battelle,[26] sintering, hot-press forging, and gas-pressure bonding were evaluated as techniques for preparing cermet fuel materials containing at least 60 vol.% UO_2 and having a minimum density of 90 per cent of theoretical. Minus 325-mesh chromium, molybdenum, niobium, and type 302B stainless steel were employed as matrix materials. Hydrothermal and spherical UO_2 powders were evaluated.

Cermets containing 80 vol.% UO_2 and exhibiting densities in excess of 90 per cent of theoretical were successfully prepared by both hot-press forging and by gas-pressure bonding mixed oxide and metal powders. Gas-pressure bonding produced specimens with a more uni-

form structure and was demonstrated to be capable of simultaneously densifying and cladding green-pressed cermet fuels. Spherical UO_2 powders produced the more homogeneous microstructures. Excellent microstructures were also obtained through the use of UO_2 powder coated with niobium by vapor-deposition techniques. An example is shown in Fig. I-1.

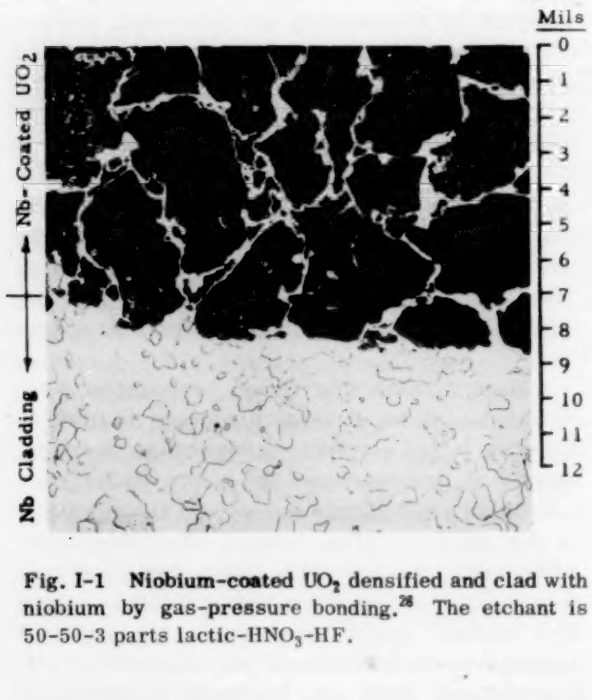

Fig. I-1 Niobium-coated UO_2 densified and clad with niobium by gas-pressure bonding.[26] The etchant is 50-50-3 parts lactic-HNO_3-HF.

So far as direct comparison is possible, the cermets were superior in strength to UO_2. Strength, which was measured by bend and compression tests, was density dependent. Thermal-conductivity values for the cermets were far higher than those for UO_2. The data are shown in Table I-6 and Fig. I-2.

Electrical-resistivity data were also obtained. These data were used to develop a mathematical correlation between electrical and thermal conductivities, but a complete analysis could not be made on the basis of present theories, owing to the limited number of measurements made.

The potentialities of a fuel element consisting of an enriched-uranium compound dispersed in a depleted uranium or thorium matrix would be influenced by the extent of isotopic exchange likely to occur at reactor temperatures. The consequences of interchange depend on both the diffusion of the enriched isotope into the matrix and the diffusion of uranium isotope into the

Table I-6 DESCRIPTION OF SPECIMENS USED FOR THERMAL-CONDUCTIVITY MEASUREMENTS[26]

Specimen	Nominal composition, vol.%	Density, % of theoretical
TC-81	UO_2–30 S.S.	97.0
TC-80	UO_2–20 S.S.	95.5
TC-102	UO_2–20 S.S.	98.4
TC-103	UO_2–20 S.S.	97.2
TC-82	UO_2–30 Mo	91.7
TC-90	UO_2–20 Mo	91.1
TC-105	UO_2–20 Mo	94.4
TC-104	UO_2–20 Cr	97.1
TC-115	UO_2–20 Nb*	85.3
TC-130	UO_2–20 Nb†	93.5

*Niobium-coated, −100 + 140-mesh spherical UO_2.

†Niobium-coated, −140 + 200-mesh hydrothermal UO_2.

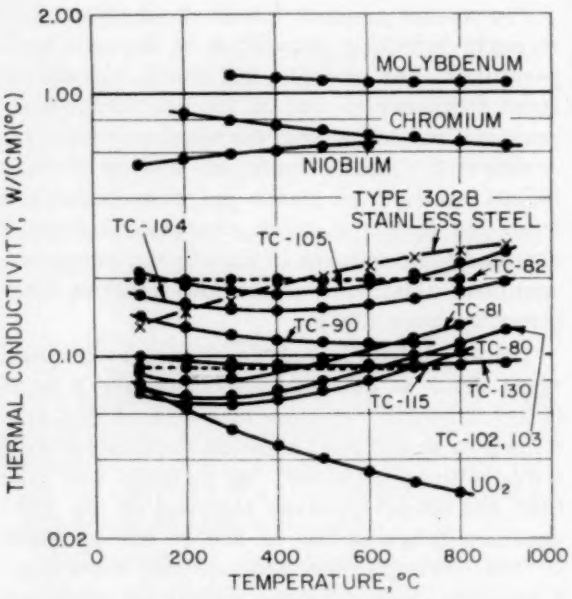

Fig. I-2 Thermal conductivity versus temperature for UO_2 cermets and their matrix metals.[26] (See Table I-5 for compositions of TC specimens.)

enriched-uranium compound. Workers at Nuclear Metals[27] investigated the extent of isotopic interchange occurring as a result of thermal diffusion in the system in which enriched UO_2 would be dispersed in a matrix of depleted uranium. The results obtained indicate that the increased concentration of U^{235} in the matrix would be negligible, even immediately at the interface. Thus radiation damage in the uranium matrix as a result of isotopic interchange is

negligible. The dilution of the enriched dispersed phase due to isotopic interchange becomes negligible at a distance of 3 μ or more into the UO_2 particle. The limiting factor in the interchange is the diffusion rate of uranium in UO_2. Experimental results gave approximate values of the volume diffusion of 4 to 45×10^{-18} cm^2/sec at 1000°C. Radiation damage in the matrix as a result of isotopic interchange was judged to be very unlikely. (D. L. Keller)

Refractory Fuel and Fertile Materials

Properties and Behavior of Uranium Oxide Fuels

A compilation of unclassified data on UO_2 has been assembled by Seddon at Harwell.[28] A bibliography of UO_2 references in the Russian literature from 1955 to June 1960 has been compiled by Wensrich.[29]

Recent thermal-conductivity measurements have been reported[30] for 85 per cent dense UO_2 from 833 to 2112°C. The values of thermal conductivity for the 85 per cent dense UO_2 and values corrected to theoretical density are given in Table I-7.

Table I-7 THERMAL CONDUCTIVITY[30] OF UO_2

Temp., °C	Measured thermal conductivity for 85% dense UO_2, watts/(cm)(°C)	Thermal conductivity normalized to 100% dense UO_2, watts/(cm)(°C)
833	0.025	0.029
1112	0.021	0.024
1168	0.021	0.024
1493	0.020	0.024
1738	0.017	0.020
2112	0.016	0.019

Studies at Chalk River[31] show that, from 1550 to 2440°C, grain growth as a function of time in UO_2 follows fairly closely the expression

$$D^2 - D_0^2 = Kt^{0.8} \exp(-87{,}000/RT)$$

where K is a constant depending on the particular material, D_0 is the initial grain size, and D is the grain size at time t. Observation of metallic uranium in material heated above 2000°C suggests that the UO_2 lattice can be oxygen deficient at high temperatures. The crystallographic orientation parallel to the major axis of columnar crystals of UO_2 formed under various conditions has also been determined.[32] Crystals formed from a melt have a [100] direction parallel to the major axis, whereas those grown from vapor have the [100], [111], or [110] directions parallel to their length, depending on the formation conditions. Bettis[33] and Atomics International[34] employ gas-adsorption techniques to measure surface areas associated with sintered UO_2. Krypton, butane, and ethane are used to measure surface areas ranging from 5000 to 20 cm^2.

Several recent reports cover the kinetics of oxidation of UO_2. A study of the oxidation of UO_2 and UO_2-containing fissia concentrations ranging from 0 to 5 per cent at oxygen pressures ranging from 3 to 800 mm Hg in the temperature range of 0 to 450°C has been made by Atomics International.[35] It is postulated that the oxidation of UO_2 to U_3O_8 is controlled by the following processes: (1) chemisorption of oxygen on the UO_2 surface, then adsorption of oxygen on the chemisorbed layer; (2) diffusion of oxygen through a 224 ± 74 A layer of U_3O_7 or U_4O_9 depending on the temperature, followed by (3) formation of U_3O_8 in the grain boundaries which causes the surface layer to spall off. The chemisorption reaction rate may be expressed as

$$R = 5.5 \times 10^{-7} P \exp(-12{,}800 \pm 2800/RT) \text{ moles oxygen/}(cm^2)(sec)$$

where P is oxygen pressure in millimeters of mercury. The diffusion coefficient for oxygen in the pure UO_2 material as a function of temperature was found to be

$$D = 5.5 \times 10^{-5} \exp(-21{,}900 \pm 1400/RT) \text{ } cm^2/sec$$

whereas for oxygen in UO_2 with fissia

$$D = 12.2 \times 10^{-5} \exp(-28{,}100 \pm 1100/RT) \text{ } cm^2/sec$$

Results of experiments at the Lawrence Radiation Laboratory show no indication of diffusion-controlled oxidation of UO_2 powder from 365 to 400°C at an oxygen partial pressure of 150 mm Hg. All oxidation curves were of the sigmoidal type, indicating only one oxidation step from UO_2 to U_3O_8. Oxidation of sintered 10 wt.% UO_2–ThO_2 at temperatures from 600 to 950°C and at an oxygen pressure of 779 mm Hg has been in-

vestigated at Atomics International.[36] From 800 to 950°C the rate of oxidation can be expressed as

$$R = 3.7 \times 10^{-3} \exp(-22{,}500/RT)$$

moles oxygen/(cm²)(min)

Under the conditions of the experiment, there was no evidence of any disintegration of sintered material due to the effects of oxidation.

Oak Ridge is continuing fission-product-release studies.[37] Measurements of fission-product release from thin plates of 97 per cent dense UO_2 during in-pile irradiation at temperatures ranging from 1000 to 2000°F showed that iodine, xenon, and krypton were released by a temperature-dependent process above 1300°F. The results of determinations of Xe^{135}- and Kr^{88}-escape from the UO_2 plates at various times during in-pile irradiation are shown in Fig. I-3. The points designated *A* and *B* were taken soon after the irradiation of the UO_2 was initiated, whereas the other data are based on measurements taken at random temperatures over a period of several days six months later. Not only did fractional release of krypton and xenon increase over this period by a factor of more than 100, but the ratio of xenon to krypton release increased, indicating a change in the fuel. It is thought that this change was due to oxidation of the UO_2 by oxygen impurities in the atmosphere to which the specimen was exposed rather than to radiation damage. Bursts of fission gas were released from the UO_2 when the temperature of the fuel was increased. The size of the burst was a function of the temperature change and, to some extent, the prior irradiation history. Bursts were also observed on rapid cooling; however, these were smaller than those obtained on heating. Diffusion coefficients calculated for Kr^{88}, which has a precursor with a short half life whose diffusion can be neglected, are shown in Fig. I-4. Diffusion coefficients of Xe^{135} were not given since there was evidence that the release data for this isotope were obscured by diffusion of its precursor, I^{135}.

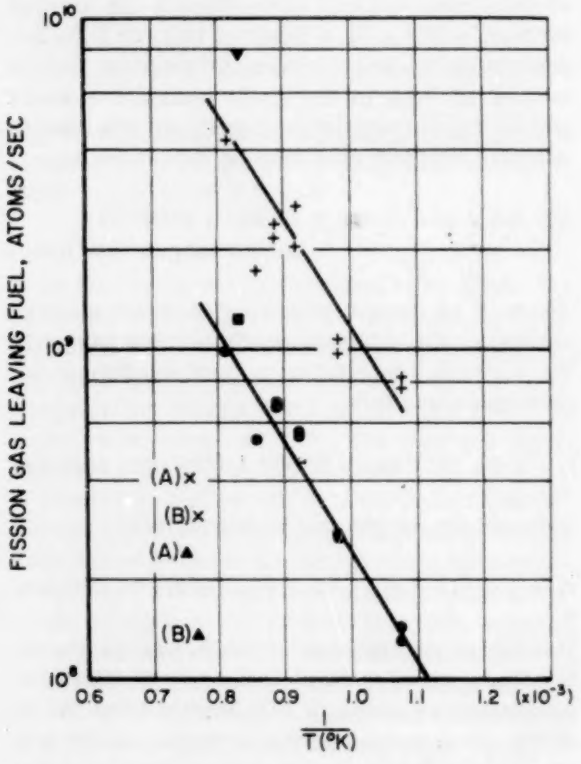

Fig. I-3 Temperature dependence of xenon-krypton evolution[37] from UO_2. Samples 1 to 8: ●, Kr^{88}; +, Xe^{135} [flux 3.5×10^{12} neutrons/(cm²)(sec)]; ■, Kr^{88}; ▼, Xe^{135} [flux 5.9×10^{12} neutrons/(cm²)(sec)]. Samples A and B: ×, Kr^{88}; ▲, X^{135} [flux 5×10^{13} neutrons/(cm²)(sec)].

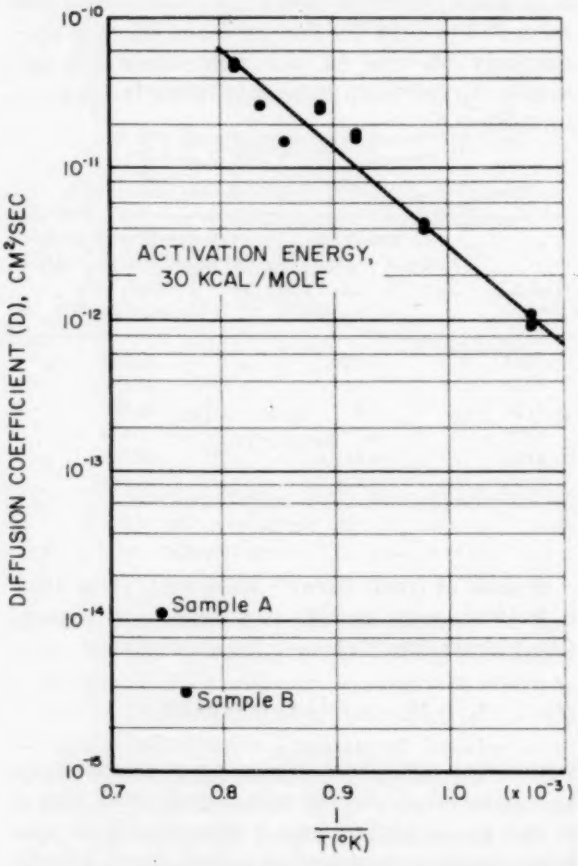

Fig. I-4 Diffusion coefficient[37] for Kr^{88} in UO_2.

The diffusion of Xe^{133} from slightly irradiated high-density platelets of 25 wt.% UO_2-ZrO_2 has recently been measured by Bettis.[39] Diffusion coefficients, including those for UO_2, are given in Table I-8. These values yield an activation

Table I-8 DIFFUSION COEFFICIENTS[39] FOR Xe^{133} IN 25 WT.% UO_2-ZrO_2 AND UO_2

Temp., °C	Diffusion coefficient, cm^2/sec	
	25 wt.% UO_2-ZrO_2	UO_2
700	1.6×10^{-18}	6.6×10^{-22}*
800	1.6×10^{-17}	4.0×10^{-20}
900	3.6×10^{-17}	2.2×10^{-19}
900	1.8×10^{-17}	
900	2.8×10^{-17}	
1000	1.1×10^{-15}	2.0×10^{-18}
1250	8.4×10^{-13}	4.0×10^{-16}

*Estimated.

energy for Xe^{133} diffusion in 25 wt.% UO_2-ZrO_2 of about 85 kcal/g-mole. This value is somewhat uncertain because of occasional sporadic bursts of Xe^{133} release which occurred during the course of the measurement.

An X-ray-diffraction study[40] of the uranium-aluminum-oxygen ternary system resulted in the phase diagram in Fig. I-5. No evidence was

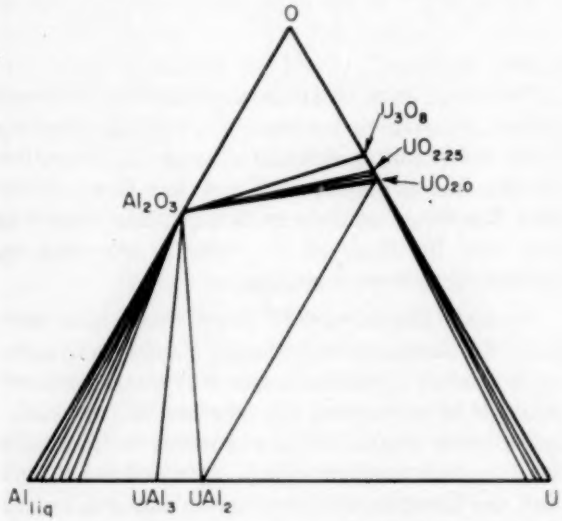

Fig. I-5 Uranium-aluminum-oxygen phase diagram.[40]

found for solid solutions between Al_2O_3 and uranium oxides.

Metallographic and X-ray studies by Bettis[41] of compositions ranging from 100 mole % UO_2 to 100 mole % ZrO_2 indicate that, for an anneal at 1875 to 1880°C for 66 to 72 hr, the material is face-centered cubic to 60 mole % UO_2. Lattice parameters of rapidly cooled compositions are given below:

UO_2		
Mole %	Wt.%	Lattice parameter *a*, A
100	100	5.470
90	95.3	5.439
80	90.0	5.409
70	83.7	5.380
60	77.0	5.349

At 50 mole % UO_2, where the cubic lattice parameter was found to be 5.315 A, metallography revealed the appearance of an acicular or platelet type structure within the individual grains which was also detected by a corresponding change in the X-ray-diffraction pattern. At 35 mole % UO_2, the platelet structure became more pronounced, and, at 30 mole % UO_2, the tetragonal phase changed from the platelets to an equiaxed grain which forms mainly at the grain boundaries of the plate type grains. At 15 mole % UO_2, the platelets disappear, leaving the equiaxed tetragonal structure throughout. A phase diagram based on other work on the UO_2-ZrO_2 system performed in England is described by Evans.[42] X-ray-diffraction studies were performed at Bettis[43] on UO_2, ZrO_2, and UO_2-ZrO_2 solid solutions that had been exposed to various levels of in-pile irradiation. The UO_2 structure remained stable up to 20×10^{20} fissions/cm^3. Beyond this level of exposure, the UO_2 gradually became amorphous, with the cubic X-ray pattern persisting to 30×10^{20} fissions/cm^3. ZrO_2 and UO_2-ZrO_2 solid solutions with the distorted fluorite type structure went to a higher symmetry when irradiated with fission fragments.

Metallographic studies have been conducted by Bettis[39] on UO_2-Y_2O_3 sintered at 1850°C for 63 hr and then cooled rapidly. A single-phase structure was found between about 20 and 50 mole % Y_2O_3, and a two-phase region was found with fluorite and thallium oxide type structures occurring between 60 and 85 mole % Y_2O_3. The Y_2O_3-rich thallium oxide type phase and the UO_2-rich fluorite phase have lattice parameters of 10.630 A and 5.350 A, respectively. There was also evidence of a two-phase region at 10 mole % Y_2O_3.

Irradiation experiments at Vallecitos[44] indicate that UO_2 powder with small additions of

TiO_2 exhibits better fission-gas retention than UO_2 alone. Stainless-steel fuel elements containing 22 per cent enriched UO_2 powder with and without TiO_2 compacted to densities ranging from 53 to 65 per cent were irradiated to peak burnups of 2 per cent total uranium atoms at surface heat fluxes up to 350,000 Btu/(hr)(sq ft). Krypton-85 release from UO_2 alone ranged from 39 to 100 per cent, whereas release values were significantly lower for UO_2 containing additions of about 0.5 per cent TiO_2. Central voids in the fuel containing the TiO_2 were found to be less pronounced than in fuel without TiO_2. Knudsen et al.[45] report that flexural-strength measurements at about 20 and 1000°C indicate that additions of 0.50 and 0.75 wt.% TiO_2 markedly increased the strength of sintered UO_2. Sinterability of the UO_2 was also enhanced by the TiO_2 addition.

Hanford[46] is continuing to investigate the UO_2-PuO_2 system. The liquidus for the UO_2-PuO_2 system has been determined and is presented in Fig. I-6. Results of thermal-expansion measurements on both UO_2 and PuO_2 as a function of temperature up to 1000°C are summarized in Fig. I-7. The discontinuous hump on the PuO_2 expansion curve which has been observed with three different specimens is not explained.

(R. H. Barnes)

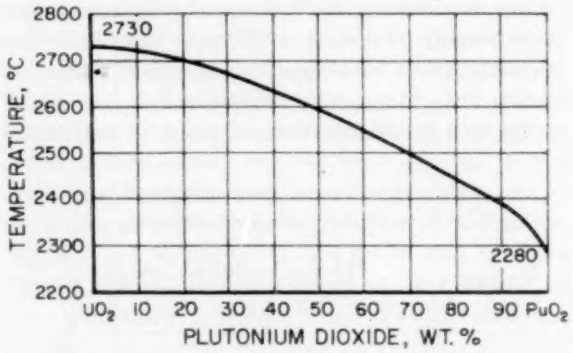

Fig. I-6 Liquidus for the UO_2-PuO_2 system.[46]

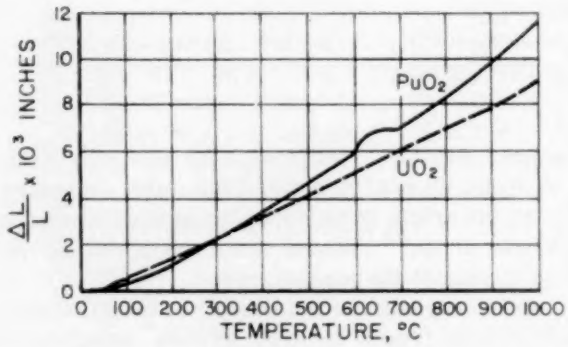

Fig. I-7 The expansion of UO_2 and PuO_2 as a function of temperature.[46]

Fabrication of Uranium Oxide Fuels

One of the principal reasons for the high cost of preparing fuel pellets by cold pressing and sintering has been variability in UO_2 powders. It has been necessary to employ high forming pressures, high sintering temperatures, or both, in order to use available material. Two recent observations hold promise of permitting further improvement in control of powder characteristics.

The development, on a laboratory scale, of a more economical process for fabricating dense UO_2 pellets is continuing at Olin Mathieson.[47] Several commercial lots of UO_2 powder of varying sintering characteristics have been activated by oxidation-reduction cycling, followed by oxidation to a minimum oxygen-to-uranium ratio of 2.25. Pellet densities in excess of 95 per cent of theoretical were attained by pressing such powders at 19 tsi, sintering the pellets at 1200 to 1300°C in nitrogen for 1 hr, and then reducing them to stoichiometric UO_2 in hydrogen.

Previous work had indicated that the beneficial effect of oxidation-reduction cycling resulted from the breaking down of coarse agglomerates during this procedure. It now has been shown that fluorine impurity in UO_2 inhibits sintering and that the fluorine is partially removed by oxidation-reduction cycling.

Verkerk and Brouwer[48] found that it was possible to stabilize high-surface-area UO_2 powders against oxidation during room-temperature storage by subjecting the powders to moisture-laden inert gases at the reduction temperature for 1 hr following reduction. The authors stated that the treatment caused formation of a nearly nonporous U_3O_8 layer on the UO_2 particles. Pressing characteristics of aged powders were enhanced, without harming sinterability. Sintering in moist argon or nitrogen for 1 hr at 1400 to 1500°C, and cooling in a dry oxygen-free mixture of hydrogen and nitrogen, resulted in stoichiometric UO_2 with density in excess of 95 per cent of theoretical. (H. D. Sheets)

Properties of Refractory Fuels Other Than Uranium Oxides

Published data on physical, mechanical, chemical, and irradiation properties of uranium carbide and uranium silicide are presented[28] in graphs and tables. Studies of these and other properties of uranium carbide are being continued. Meyerson et al.[50] are determining thermal conductivity, thermal expansion, and effects of thermal cycling on UC and UC + U mixtures. The solubility of uranium in UC is reported[51] to decrease its lattice parameter from 4.9600 ± 0.0005 A to 4.9520 ± 0.0002 A. Lattice-parameter data were obtained[52] which indicate two phases of the $U(C_xO_y)$ type. In this latter study, various mixtures of uranium, carbon, UC, UO_2, and U_3O_8 were reacted in argon at 1800°C. The resulting phases were identified by lattice-parameter measurements as $U(C_{0.73}O_{0.3})$ and $U(C_{0.3}O_{0.73})$. Thus differentiating $U_{1+x}C$, $U(C_xO_y)$, or $U(C_x,N_y,O_z)$ by lattice-parameter methods may lead to considerable uncertainty. Carbon-14 diffusion in UC is reported[21] to be 1.2×10^{-8} cm²/sec at 1500°C, 3.3×10^{-8} cm²/sec at 1600°C, and 2.1×10^{-7} cm²/sec at 1800°C. Battelle[21] is also investigating the hardness and irradiation behavior of uranium carbide containing 4.8 to 9.0 wt.% carbon. Microhardness data on uranium carbide are being obtained at Union Carbide.[53] Hot-hardness measurements on UC, U_2C_3, and UC_2 are reported.[21] Preliminary thermal expansion, modulus of rupture, modulus of shear, and Poisson's ratio for fabricated specimens of UC, UN, and U_3Si_2 are reported by Taylor and McMurtry.[54]

Alloys of UC with other refractory-metal carbides are being evaluated at Battelle.[21]

A new phase in the uranium selenide system has been reported by Khodadd,[55] i.e., cubic U_3Se_4, $a_0 = 8.804$ A, which has a density of 10.07 g/cm³. This selenide is attacked readily by dilute hydrochloric or acetic acids.

The physical properties of US and ThS are being compared with those of UO_2 and ThO_2 at Argonne.[17,56] Preliminary data are presented for thermal expansion, composition, grain size, and modulus of rupture.

Plutonium carbides are being investigated at Argonne[17,56] and at Hanford.[57–59] An abrupt change in the thermal expansion of PuC when heated above 400°C may be attributed to an excess of carbon and the reported[17,56] high-temperature solubility of Pu_2C_3 in the PuC lattice. Thermal-expansion coefficients are reported[57–59] to be 10.8×10^{-6}/°C for PuC and 14.8×10^{-6}/°C for Pu_2C_3. Addition of UC to PuC was reported by Hanford to eliminate the decomposition of the PuC to Pu_2C_3 and permit uniform melting.

The decomposition and melting of PuO_2 at 1700°C are being investigated at Hanford[57–59] and Battelle.[21] Melting has been attributed to decomposition of PuO_2 to Pu_2O_3. The compatibility of PuO_2 with various ceramics and metal powders is being studied at these sites. The limit of solid solubility of ZrO_2 in cubic PuO_2 is reported[59] to be approximately 60 wt.%. Vapor pressures of PuO_2 and PuO_2-ThO mixtures at 1973°K are reported[60] to be 7.9×10^{-6} atm. New compounds that have been reported[61] in plutonium systems include $PuAlO_3$, $PuVO_3$, $PuCrO_3$, and $BaPuO_3$. Crystallographic data are given.

The corrosion resistance of several thorium-base compounds (Th_2Al, $ThBe_{13}$, ThB_4, ThC, ThC_2, ThN, ThS, Th_3Si_2, and ThSi) in NaK at 1200°F is being studied.[21] The beryllide was corrosion resistant, the carbides lost considerable weight, and the other compounds had intermediate corrosion resistance to NaK. All the compounds withstood rapid cooling from 1000°C without cracking. A cubic perovskite type compound has been prepared[62] by reacting coprecipitated mixtures of barium and thorium oxalates at 1000°C. This compound is unstable in moist air at room temperature.

(D. A. Vaughan)

Fabrication of Ceramic Fuels Other Than Uranium Oxides

The AEC's Division of Reactor Development has prepared a summary of work being done under its Nuclear Technology Program. The reader desiring background information in fuels and materials developments during 1960 will find these reports[23,63] helpful.

Uranium carbide powder is now commercially available from several suppliers. Research is continuing on fabrication of cast UC fuel slugs, and increased effort is being directed toward powder-metallurgy fabrication techniques.[23]

The work of the first 1½ years of a casting-research program at Battelle[64,65] has been summarized. Recent significant developments indicate that the use of outgassed commercial

graphite in the skull melting and casting operation may result in better control of the carbon content of castings. Castings produced using outgassed graphite varied less than ±0.1 wt.% carbon, whereas castings produced from the same grade of graphite that had not been outgassed varied by ±0.3 wt.% carbon. Carbon variations attributed to the erosion of vacuum-outgassed AGOT nuclear-grade graphite electrode tips appear to be reduced when outgassed TSF reactor-grade graphite is used.[21,22]

Olin Mathieson[47,66] has been particularly interested in melting losses occurring when UO_2-graphite pellets are melted and cast. Longer melting times are required and material losses are greater using unreacted pellets, but homogeneity is good. Carbon content varied by not more than 0.1 wt.% from top to bottom of the castings. If the pellets are reacted in vacuum prior to melting, about 99 per cent of the theoretical UC yield is obtained.

Sylvania-Corning[67] reacted UF_4, silicon, and carbon at 1550°C and then arc-melted the products to obtain a two-phase material consisting essentially of UC with a dispersion of SiC.

The carbon content of UC powder prepared by the methane reaction has shown considerable variation, not only as reported by different facilities but among various lots of powder from a facility. Olin Mathieson uses propane to produce UC powder which consistently contains less than 100 ppm nitrogen and about 0.1 to 0.15 wt.% oxygen.[66] Previous high free-carbon content was found to result from pyrolytic decomposition of propane on the retort walls and was remedied by using copper inserts and trays.[47,66,68]

It is not surprising that UC produced from a UO_2-carbon mixture, which satisfies the equation $UO_2 + 3C \rightarrow UC + 2CO$, always contains a small amount of UO_2 since UO_2 generally contains a little more oxygen than that required for stoichiometry. Argonne[18] has reacted mixes of UO_2 and 13.4 to 13.0 wt.% carbon as part of an attempt to correlate the amount of carbon required to accommodate the UO_{2+x} stoichiometry.

Numerous investigators have reported considerable difficulty in sintering UC powder to densities approaching the theoretical value. Oak Ridge workers have studied the nature of the loss of material from UC during high-temperature sintering and have identified the ion species U^+, UO^+, and UO_2^+ by mass spectrometry.[69] This indicates that the oxide phase present as impurities may be responsible for loss of material. Battelle[20,22] has used the isostatic hot-pressing technique to fabricate UC bodies of 95 per cent or more of theoretical density which do not contain uranium or UC_2 but which do have small quantities of U_2C_3.

Slip casting of UC has been initiated at Union Carbide.[53,63] Slips having reasonable rheological properties were made using a xylene medium with Linde R61 silicone deflocculant or alcohol with formamide. Casting rate was controlled and mold release facilitated by washing the mold with a slurry of alumina in trichloroethylene-Carbowax solution. Cylindrical specimens ½ in. in diameter by 3 in. long with a green density of 6.8 g/cm^3 were sintered at 1850°C to densities in excess of 12 g/cm^3.

In a survey of different investigations aimed at preparing and fabricating UC, Accary and Caillat[70] find that, in general, a chemical reaction does not lead to high densification if there is a dependence on simple contact between discrete particles; however, chemical reaction can help sintering if densification can be achieved prior to the reaction.

Sintering of UN powder up to 91 per cent of theoretical density has been reported by The Carborundum Company.[54] However, vacuum sintering of UN powder at Battelle[6] resulted in decomposition of UN with a resulting liquid uranium matrix before significant densification could take place. Specimens with 95 to 96 per cent of theoretical density have been fabricated by isostatic hot pressing in niobium cans for 3 hr at 1480°C and 10,000 psi.[21] Recently, irradiation specimens have been fabricated without incident under the same conditions.[71] A small amount of nonmetallic second phase in these specimens is believed to be caused by the use of Carbowax 6000 as a binder in cold-pressing pellets prior to hot pressing, since a specimen hot-pressed under the same conditions with no binder reached 98 per cent of theoretical density and was virtually free of the second phase.[71]

Compaction of arc-fused ThO_2 and mixed ThO_2-UO_2 by pneumatic vibrators at Oak Ridge[72] consistently gave bulk densities of 87 per cent of theoretical. Compaction was best with a pneumatic vibrator which imparted a sharp impact to the tube on its upstroke but not on the downstroke.

A promising method of producing ThO_2 pellets involving the formation of cubes that are subsequently reduced to spheres by tumbling has been investigated at Oak Ridge.[73] A combination

of two methods (tumbling dry unfired cubes and tumbling wet, soft fired cubes at 1100 to 1300°C) appears most desirable. Polished spheres are finally fired at 1800°C.

The sintering rate of thoria compacts as a function of time was measured[73] from 600 to 1600°C at heating rates of 2.7, 4.0, and 8.0°C/sec. The sintering rate attained a peak value at 980°C and passed through a minimum at 1200°C. The initial peak occurred at an increase in density of 15 per cent. The temperature and degree of densification associated with the initial sintering rate peak were the same for each heating rate. The presence of a discontinuity in the sintering rate versus temperature curve suggests the influence of more than one material transport mechanism.

Hypostoichiometric PuC containing about 25 per cent Pu_2C_3 and stoichiometric Pu_2C_3 containing 10 per cent or less PuC have been prepared by powder-metallurgy techniques at Los Alamos.[74] The density of monocarbide pellets first sintered at 1250 to 1400°C was 10.5 g/cm^3. Further sintering of ground and re-pressed pellets resulted in densities up to 12.7 g/cm^3 (93 per cent of theoretical) for the monocarbide and 12.6 g/cm^3 (99 per cent of theoretical) for the sesquicarbide. Arc melting of the sintered pellets produced buttons up to 99 per cent of theoretical density containing less than 5 per cent plutonium sesquicarbide. Essentially, single-phase hypostoichiometric UC-PuC solid solutions were produced by these same procedures using pellets having a density of 12.7 g/cm^3 (93 per cent of theoretical) to produce an arc-melted button density of 14.0 g/cm^3.

The effect of a hydrogen atmosphere on the sintering of US must be redetermined in a pure atmosphere. X-ray examination shows UO_2 and UOS of almost equal intensity with no hydride apparent.[75] (E. O. Speidel)

Basic Studies of Radiation Effects in Fuel Materials

Radiation Effects in Metallic Fuels

Growth produced in alpha uranium by proton irradiation has been compared experimentally with that due to neutron-induced fission at Harwell.[76] The growth per unit concentration of point defects produced by protons is at least an order of magnitude less than that produced by fission, and recovery upon heating occurs only in the proton case. It is therefore concluded that the growth during fission cannot be explained solely in terms of point-defect migration.

Equations have been derived at National Lead[77] for the prediction of dimensional changes and stresses in thick-walled, hollow cylindrical, uranium fuel-element cores during thermal-neutron irradiation. The equations provide a means for combining discrete preferred-orientation data obtained from a finite series of X-ray-diffraction measurements. A comparison of calculated stresses with the creep strength of uranium should determine whether a plastic solution is necessary.

At General Electric,[78] krypton ions were put into uranium foil at 40 kv. The rate and temperature of release of the krypton gas was studied by the mass spectrometer. Evolution begins below 250°C and shows several peak rates. The temperature for release, in this case, is much lower than that found in other work on fission gases formed *in situ*.

The behavior of vacancies and fission-gas atoms in the uranium lattice has been studied in Japan.[79] It is shown that the processes for bubble formation depend upon the concentration of trapping sites and the irradiation temperature. By calculation it is shown that the swelling of irradiated uranium is least if the concentration of trapping sites is greater than 5×10^{-3}.

An analysis has been made[80] of bubble formation in irradiated fuels for the case where there is significant fission-gas solubility. It is shown that modes of bubble nucleation are not of primary importance. Bubble spacing, however, remains a most important feature, and the analysis suggests that spacing is strongly governed by the fission-gas diffusion coefficient and solubility where this solubility is not negligibly small.

An analysis has been made[81] of re-solution of fission gas during postirradiation heating of uranium. It is concluded that, for irradiated uranium, treatments such as thermal cycling or pressure cycling can affect the volume increase which occurs on subsequent high-temperature heat-treatment. On heating into the gamma range without such prior treatments, the observed volume increases can be interpreted quantitatively in terms of a re-solution of gas from the smaller bubbles, which results in growth of the larger ones. From the analysis of this process, the energy of solution of fission gases in gamma

uranium between 880°C and the melting point is deduced to be about 1.5 ev.

Postirradiation heat-treatment studies allow the product of the fission-gas solubility and diffusion coefficient to be readily determined experimentally. A knowledge of this product permits an estimate to be made of the volume increase occurring during irradiation at temperatures where the solubility is not negligibly small. (F. A. Rough)

Radiation Effects in Nonmetallic Fuels

Further studies of xenon diffusion in UO_2 are in progress at Chalk River.[82] Diffusion tests conducted on specimens as sintered, after impregnation with small amounts of oxygen and after removal of this oxygen, suggest that the initial accelerated release often observed is primarily the result of oxidized surfaces.

Diffusion coefficients of xenon in uranium carbides from 4.4 to 6.0 wt.% carbon have been measured. The results vary with composition and types of carbide in an unexplained fashion. D/a^2 varied from 6×10^{-12}/sec to as high as 1.8×10^{-8}/sec, depending on composition, etc.

Experiments have shown that measurable quantities of natural xenon will enter UO_2 during irradiation from 10 to 400 Mwd/ton of uranium. The observed effect will not be significant in limiting pressure buildup; but, since it may be masking effects that may become significant at longer irradiations, additional longer experiments are being conducted.

(F. A. Rough and J. B. Melehan)

References

1. Mallinckrodt Chemical Works, Process Development Quarterly Progress Report for October–December 1960, USAEC Report MCW-1463, Feb. 1, 1961.
2. W. S. Blackburn et al., The Effect of Thermal Cycling on the Creep of Uranium, *J. Nuclear Energy: Pt. A, Reactor Sci.*, 12: 162–171 (1960).
3. A. D. Donaldson, Structures Resulting from Extrusion of Uranium at Temperatures High in the Alpha Phase, USAEC Report NMI-7004, Nuclear Metals, Inc., Oct. 19, 1960. (Classified)
4. G. R. Mallett, Preferred Orientation in Cross-Rolled Uranium, USAEC Report RFP-216, Dow Chemical Co., Rocky Flats Plant, Feb. 13, 1961.
5. A. I. Dashkovskii et al., Internal Friction in Uranium, USAEC Translation AEC-tr-4407, 1960.
6. R. W. Cahn et al., *J. Nuclear Materials*, 3(1): 1–15, 30–40, 67–88 (1961).
7. G. H. Bannister and J. R. Murray, Some Observations on Uranium-Molybdenum-Niobium Alloys, *J. Less-Common Metals*, 2: 372–382 (October 1960).
8. E. Stephan et al., Corrosion of Thorium and Uranium Under Storage Conditions, USAEC Report BMI-1507, Battelle Memorial Institute, Mar. 21, 1961.
9. A. Boltax and A. R. Lumbert, A Metallographic Study of the Swelling of Uranium and Uranium Alloys, USAEC Report NMI-1239, Nuclear Metals, Inc., Aug. 17, 1960.
10. J. H. Kittel, Effects of Irradiation on the EBWR Fuel Alloy Uranium–5 Wt.% Zirconium–1.5 Wt.% Niobium, USAEC Report ANL-5639, Argonne National Laboratory, July 1960.
11. F. J. Blatt, On the Metastable Gamma-Phase Uranium-Molybdenum Alloys, *J. Phys. and Chem. Solids*, 17(3/4): 177–187 (1961).
12. AEC-Euratom Conference on Aqueous Corrosion of Reactor Materials, Brussels, Belgium, October 14–17, 1959, USAEC Report TID-7587, July 1960.
    a. J. T. Waber, Aqueous Corrosion of Uranium and Its Alloys, pp. 307–389.
    b. C. L. Angerman and E. C. Hoxie, Aqueous Corrosion of Aluminum-Nickel-Uranium Bonds, pp. 405–433.
13. J. Bloch, Phase Change and Lattice Disordering Provoked by Irradiation in the Compound U_2Mo, French Report CEA-1561, 1960.
14. J. C. Bokros, Creep Properties of a Zirconium-Hydrogen-Uranium Alloy, *J. Nuclear Materials*, 3(2): 216–221 (February 1961).
15. C. L. Vold and D. T. Peterson, The Structure of U_2Zn_{17}, USAEC Report IS-246, Ames Laboratory, January 1961.
16. H. R. Gardner and I. B. Mann, Mechanical Property and Formability Studies on Unalloyed Plutonium, USAEC Report HW-65019, Hanford Atomic Products Operation, December 1959.
17. Argonne National Laboratory, Reactor Development Program Progress Report, February 1961, USAEC Report ANL-6328, Mar. 15, 1961.
18. Argonne National Laboratory, Reactor Development Program Progress Report, January 1961, USAEC Report ANL-6307, Feb. 15, 1961.
19. C. H. Bloomster and Y. B. Katayama, Aqueous Corrosion of Aluminum-Plutonium Alloys, USAEC Report HW-67098, Hanford Atomic Products Operation, Oct. 12, 1960.
20. R. W. Dayton and C. R. Tipton, Jr., Progress Relating to Civilian Applications During January 1961, USAEC Report BMI-1496, Battelle Memorial Institute, Feb. 1, 1961.
21. R. W. Dayton and C. R. Tipton, Jr., Progress Relating to Civilian Applications During March 1961, USAEC Report BMI-1509, Battelle Memorial Institute, Apr. 1, 1961. (Classified)
22. R. W. Dayton and C. R. Tipton, Jr., Progress

Relating to Civilian Applications During February 1961, USAEC Report BMI-1504(Del.), Battelle Memorial Institute, Mar. 1, 1961.

23. Nuclear Fuels and Materials Development, USAEC Report TID-11295, February 1961.
24. Hanford Atomic Products Operation, Quarterly Progress Report on Fuels Development Operation for July, August, and September 1959, USAEC Report HW-62656, Oct. 15, 1959. (Classified)
25. J. H. Cherubini et al., Fabrication Development of UO_2–Stainless Steel Composite Fuel Plates for Core B of Enrico Fermi Fast Breeder Reactor, USAEC Report ORNL-3077, Oak Ridge National Laboratory, Apr. 18, 1961.
26. S. J. Paprocki et al., Preparation and Properties of UO_2 Cermet Fuels, USAEC Report BMI-1487, Battelle Memorial Institute, Dec. 19, 1960.
27. D. S. Kneppel, Isotopic Interchange in Dispersion Fuels, USAEC Report NMI-1232, Nuclear Metals, Inc., Oct. 20, 1960.
28. B. J. Seddon, Uranium Ceramics Data Manual: Properties of Interest in Reactor Design, British Report DEG-R-120, 1960.
29. C. J. Wensrich, Molybdenum, Niobium, Tantalum, Tungsten, and Uranium Oxide in the Journal Literatures of the USSR, 1955–June 1960, USAEC Report UCRL-6110, University of California Lawrence Radiation Laboratory, Sept. 1, 1960.
30. R. D. Reisweig, Thermal Conductivity of UO_2 to 2100°C, *J. Am. Ceram. Soc.*, 44: 48–49 (January 1961).
31. J. R. MacEwan, Grain Growth in Sintered Uranium Dioxide, Canadian Report CRFD-999 (AECL-1184), January 1961.
32. R. H. Tuxworth, An Orientation Study of UO_2 Single Crystals, Canadian Report CRMet-988 (AECL-1170), November 1960.
33. S. Aronson et al., Surface Areas of Sintered UO_2 Compacts, in USAEC Report WAPD-BT-19, p. 83, Westinghouse Electric Corp., Bettis Atomic Power Laboratory, June 1960.
34. T. Smith, Measurement of Surface Area of Uranium Dioxide Powder and Sintered Pellets, USAEC Report NAA-SR-5319, Atomics International, Oct. 1, 1960.
35. T. Smith, Kinetics and Mechanism of the Oxidation of Uranium Dioxide and Uranium Dioxide Plus Fissia Sintered Pellets, USAEC Report NAA-SR-4677, Atomics International, Nov. 1, 1960.
36. T. Smith, Kinetics of Oxidation of a Thoria–10 Wt.% Urania Sintered Pellet, USAEC Report NAA-SR-Memo-5773, Atomics International, Oct. 19, 1960.
37. R. M. Carroll and C. D. Baumann, Experiment on Continuous Release of Fission Gas During Irradiation (An Interim Report), USAEC Report ORNL-3050, Oak Ridge National Laboratory, Feb. 23, 1961.
38. Reference canceled.
39. Westinghouse Electric Corp., Bettis Atomic Power Laboratory, Pressurized Water Reactor (PWR) Project Technical Progress Report for the Period October 24, 1960, to December 23, 1960, USAEC Report WAPD-MRP-89.
40. L. J. Dykstra, Maritime Gas-Cooled Program. X-Ray Study of the Ternary System U-Al-O, USAEC Report GA-1479, General Atomic Div., General Dynamics Corp., Sept. 19, 1960.
41. Westinghouse Electric Corp., Bettis Atomic Power Laboratory, Pressurized Water Reactor (PWR) Project Technical Progress Report for the Period December 24, 1960, to February 23, 1961, USAEC Report WAPD-MRP-90.
42. P. E. Evans, The System UO_2-ZrO_2, *J. Am. Ceram. Soc.*, 43: 443–447 (September 1960).
43. R. M. Berman, An X-Ray Diffraction Study of Irradiated Fluorite Type Materials, in USAEC Report WAPD-BT-21, pp. 33–42, Westinghouse Electric Corp., Bettis Atomic Power Laboratory, November 1960.
44. T. J. Slosek and B. Weidenbaum, Irradiation and Examination of Vibratory Packed UO_2 High Burnup Program Fuel Elements, USAEC Report GEAP-3108(Pt. 2), General Electric Co., Vallecitos Atomic Laboratory, Feb. 26, 1960.
45. F. P. Knudsen et al., Flexural Strength of Specimens Prepared from Several Uranium Dioxide Powders; Its Dependence on Porosity and Grain Size and the Influence of Additions of Titania, *J. Am. Ceram. Soc.*, 43: 641–647 (December 1960).
46. Hanford Atomic Products Operation, Plutonium Metallurgy Operation Quarterly Progress Report for October, November, and December 1959, USAEC Report HW-64136, Feb. 25, 1960. (Classified)
47. E. Gordon, Nuclear Fuel Research, Fuel Cycle Development Program Quarterly Progress Report, October 1 to December 31, 1960, USAEC Report NYO-2691, Olin Mathieson Chemical Corp., Feb. 10, 1961.
48. B. Verkerk and G. H. Brouwer, A Stabilized Uranium Oxide for Sintering Properties, Belgium Report RCN-2, 1961.
49. Reference canceled.
50. G. A. Meyerson et al., Uranium Monocarbide, *At. Energ.*, 9(5): 387–391 (1960).
51. J. Williams et al., The Variation in the Unit-Cell Edge of Uranium Monocarbide in Arc Melted Uranium Carbon Alloys, *J. Less-Common Metals*, 2: 352–356 (October 1960).
52. R. F. Stoops and J. V. Hamme, Study of Phase Relationship in the U-C-O System, USAEC Report ORO-364, North Carolina State College, Dec. 31, 1960.
53. J. J. Finley et al., Columbium Alloy Clad Uranium Carbide Fuel Element, USAEC Report ORO-365, Union Carbide Metals Co., Dec. 31, 1960.

54. K. M. Taylor and C. H. McMurtry, Synthesis and Fabrication of Refractory Uranium Compounds, Monthly Progress Report No. 11, November 1–November 30, 1960, USAEC Report ORO-371, Carborundum Co., Dec. 13, 1960.
55. P. Khodadd, A New Phase of the Uranium-Selenide System, The Selenide U_3Se_4 and Its Chemical Nature, *Compt. rend.*, 250: 3998–4000 (June 13, 1960).
56. Argonne National Laboratory, Reactor Development Program Progress Report, March 1961, USAEC Report ANL-6343, Apr. 15, 1961.
57. F. W. Albaugh, Reactor and Fuels Research and Development Operation Monthly Report, December 1960, USAEC Report HW-67954-A, Hanford Atomic Products Operation, Jan. 15, 1961. (Classified)
58. F. W. Albaugh, Reactor and Fuels Research and Development Operation Monthly Report, January 1961, USAEC Report HW-68350-A, Hanford Atomic Products Operation, Feb. 15, 1961. (Classified)
59. F. W. Albaugh, Reactor and Fuels Research and Development Operation Monthly Report, February 1961, USAEC Report HW-68712-A, Hanford Atomic Products Operation, Mar. 15, 1961. (Classified)
60. R. W. Dayton and C. R. Tipton, Jr., Progress Relating to Military Applications During February 1961, USAEC Report BMI-1505, Battelle Memorial Institute, Mar. 1, 1961. (Classified)
61. L. E. Russell et al., Perovskite Type Compounds Based on Plutonium, *J. Nuclear Materials*, 2(4): 310–320 (1960).
62. Y. Harada and S. W. Bradstreet, Synthesis of Refractory Mixed Oxide with Perovskite Structure, Report ARF-6046-2, Armour Research Foundation, Illinois Institute of Technology, Nov. 21, 1960.
63. Nuclear Fuels and Materials Development, USAEC Report TID-11295(Suppl.), February 1961.
64. W. Chubb and F. A. Rough (Eds.), Progress on the Development of Uranium Carbide Type Fuels, USAEC Report BMI-1370, Battelle Memorial Institute, Aug. 21, 1959.
65. F. A. Rough and W. Chubb (Eds.), Progress on the Development of Uranium Carbide Type Fuels (Phase II Report on the AEC Fuel-Cycle Program), USAEC Report BMI-1488, Battelle Memorial Institute, Dec. 27, 1960.
66. E. Gordon, Monthly Progress Report No. 17, February 1961, Report No. 10, Olin Mathieson Chemical Corp., Mar. 20, 1961. (Classified)
67. Sylvania-Corning Nuclear Corp., Informal Letter Progress Report for November 1960, USAEC Report TID-11224.
68. E. Gordon, Monthly Progress Report No. 16, January 1961, Report No. 9, Olin Mathieson Chemical Corp., Feb. 21, 1961. (Classified)
69. Oak Ridge National Laboratory, Gas-Cooled Reactor Project Quarterly Progress Report for Period Ending December 31, 1960, USAEC Report ORNL-3049, Mar. 9, 1961.
70. A. Accary and R. Caillat, Sintering with a Chemical Reaction as Applied to Uranium Monocarbide, French Report CEA-1750, 1960.
71. E. O. Speidel, Battelle Memorial Institute. (Unpublished)
72. Oak Ridge National Laboratory, Chemical Technology Division Annual Progress Report for Period Ending August 31, 1960, USAEC Report ORNL-2993, Sept. 26, 1960.
73. Oak Ridge National Laboratory, Apr. 6, 1961. (Unpublished)
74. A. E. Ogard et al., Preparation of Plutonium Carbides and Uranium Monocarbide–Plutonium Monocarbide Solid Solution, USAEC Report LAMS-2506, Los Alamos Scientific Laboratory, Feb. 28, 1961. (Classified)
75. Argonne National Laboratory, Reactor Development Program Progress Report, December 1960, USAEC Report ANL-6295, Mar. 15, 1961.
76. M. W. Thompson, An Experiment To Clarify the Role of Point Defects in the Radiation Growth of Alpha Uranium, British Report AERE-M-795, November 1960.
77. P. R. Morris and R. N. Thudium, Prediction of Dimensional Changes in Uranium Fuel Elements During Irradiation—The Elastic Solution Interim Report, USAEC Report NLCO-816, National Lead Co. of Ohio, Sept. 22, 1960.
78. F. J. Norton and C. W. Tucker, Jr., Krypton Evolution from Metallic Uranium, *J. Nuclear Materials*, 2(4): 350–352 (1960).
79. F. Hashimoto, Process for Formation of Bubbles Produced in Irradiated Uranium, *J. At. Energy Soc. Japan*, 2: 518–522; *Nuclear Sci. Abstr.*, 15: Abstract 1921 (September 1960).
80. G. W. Greenwood, The Scale of Bubble Formation in Irradiated Fissile Materials, British Report AERE-R-3554, December 1960.
81. G. W. Greenwood, The Role of Fission-Gas Re-Solution During the Postirradiation Heating of Uranium, British Report AERE-R-3572, November 1960.
82. W. H. Stevens, Atomic Energy of Canada, Ltd., 1961. (Unpublished)

Section II

MODERATOR MATERIALS

Graphite

Experiments are in progress at Hanford to evaluate the effects of production variables on the oxidation rate of graphite.[1] One variable that appears to have great influence on the rate of oxidation is the amount of graphite impurities. Seven samples varying in density, Δih purity particle size, and type of coke were oxidized at 600°C in an air stream flowing at 2.5 cu ft/hr. The results of the test are summarized in Table II-1.

Table II-1 OXIDATION OF GRAPHITE SPECIMENS[1] IN AIR AT 600°C

Graphite type	Δih* purity $(hr)^{-1}$	Oxidation rate, mg/(g)(hr)
SP-21	+0.027	25.2
TS	+0.180	19.2
SP-23	+0.317	18.7
CO	+0.360	16.0
SP-10	+0.671	14.7
CSF	+0.854	11.9
SP-7	+1.10	4.3

*Inhour.

The dependence of oxidation rate upon purity is best illustrated by comparing SP-10 and SP-7 graphites. Both graphites have the same coke source, particle size, and density. Both were processed identically except that traces of Fe_2O_3 were added to SP-10. This caused the Δih purity to drop from 1.10 to 0.671 and the oxidation rate to rise by a factor of 3.4.

The effect of irradiation temperature on the contraction rate of nuclear graphites is being studied at Hanford.[2] In general, the transverse contraction rate goes through a broad minimum between the temperatures of 650 and 950°C with the least contraction occurring at approximately 800°C. Needle-coke and CSF graphites show the same effect but differ in magnitude. The transverse contraction rate of needle-coke graphites is approximately 0.6 that of the CSF rate at all temperatures. The results are shown in Table II-2. (J. Koretzky)

Table II-2 CONTRACTION OF NUCLEAR GRAPHITES AT HIGH TEMPERATURES[2]

Irradiation temp., °C	Rate (arbitrary units)*		
	Needle-coke graphite (transverse)	CSF graphite (transverse)	Both graphites (parallel)
450	0.055	0.085	0.155
500	0.040	0.065	0.124
600	0.023	0.035	0.065
700	0.015	0.022	0.050
800	0.012	0.020	0.060
900	0.014	0.025	
1000	0.021	0.035	
1100	0.038	0.060	
1200	0.070	0.100	

*The "arbitrary" units above represent contraction in terms of per cent per 10^{21} nvt ($E > 0.18$ Mev) with the dose estimated from computer calculations. An arbitrary unit of 0.01 is believed to represent a contraction rate between 0.0013 and 0.0026 per cent per 1000 Mwd/adjacent ton.

Beryllium Compounds

Thermodynamic calculations were carried out at Battelle on potential reactions of BeO with water vapor and nitrogen.[3] Results of these calculations are summarized in Table II-3. As a standard for comparison, it should be noted that a rate of loss of 0.25 mil/year is assumed permissible. (J. Koretzky)

Table II-3 REACTIONS OF BeO WITH WATER VAPOR AND NITROGEN[3]

Operating temp., °F	Impurity or coolant	Pressure, atm	Vaporizing species	Loss of BeO, mils/year
1340	H_2O	0.00063	$Be(OH)_2$	0.36
1500	H_2O	0.00063	$Be(OH)_2$	1.7
1700	H_2O	0.00063	$Be(OH)_2$	12.0
1700	H_2O	0.023	$Be(OH)_2$	440.0
2550	H_2O	0.023	$Be(OH)_2$	2.4×10^5
2230	N_2	1.0	Be_3N_2	Nil

Beryllium

A general description of beryllium metallurgy, including occurrence of the ores, economic statistics through 1959, production methods, and physical, chemical, and mechanical properties of the metal and some of its alloys appeared in the Second Edition of *Rare Metals Handbook*.[4] Lockheed[5] has issued supplement No. 3 (229 references) to its survey of beryllium literature.

Alloy Development

The best alloy developed in a study[6] of beryllium alloys prepared by liquid-phase sintering had a nominal matrix composition of silver–6 wt.% aluminum–3 wt.% germanium. This alloy showed an ultimate tensile strength of 130,000 psi, a yield strength of 52,400 psi, and a total plastic deformation of 22 per cent. The modulus of elasticity was 2×10^6 psi, and the density was 2.07 g/cm^3. The matrix content of this material was calculated from the density to be about 3 vol.%.

Purification of Beryllium

The effect of impurities on the ductility of beryllium continues to occupy the attention of many laboratories. Before this question can be resolved, it is necessary to produce pure beryllium. Franklin Institute[7–9] has succeeded in producing single crystals of beryllium that have an improved ductility (basal plane slip) of approximately 50 times that of any beryllium produced thus far. Work is in progress to determine the elements primarily responsible for the customary brittleness and to learn the effective concentrations. Until recently, the highest purity for beryllium reported in the literature was described by Sinelnikov et al.[10] and Amonenko et al.[11] The latest publication[12] of this group reports the production of beryllium 99.987 per cent pure, not counting carbon and oxygen. Although the oxygen was much lower than that reported earlier (see Table II-4), carbon and oxygen were still 0.02 and 0.04 per cent, respectively. The authors suggested that the oxygen originates in part from decomposition of the beryllia crucibles and the carbon from vacuum pump oil that passed a liquid-nitrogen trap. The

Table II-4 A COMPARISON OF ANALYSES OF BERYLLIUM OBTAINED IN VARIOUS ATTEMPTS AT PURIFICATION

Source of metal	Impurity, ppm																
	Fe	Al	Si	Mn	Mg	Ca	Na	K	Ni	Cr	Cu	Cd	Pb	Cl	N	O	C (total)
Hooper and Keen,[13] distillation in tantalum*	55	<30	40	<1	30	<100	<25	<30	<3	6	(5)	<0.3	<6	(25)	(<10)	70	(150)
Sinelnikov,[10] double distillation in beryllia	12	10	30	10					10		5		10			1000† 400‡	200‡
Pearsall,[14] distillation in tantalum	110	20	20	<35	8	30			70	<50	50			50		10 (calc.)	
Kaufmann,[15] distillation in beryllia	200		<100	20	30	30										1400	
Martin,[12] zone refined	120	60	260	20	20				50	30						80	

*Numbers in parentheses refer to analyses of material produced on other runs.
†Obtained from Amonenko et al.[11]
‡Obtained from Ivanov et al.[12]

microhardness of the distilled acicular monocrystals was about 130 kg/mm^2, and the Brinell hardness of castings made from these crystals was 100 H_B. Meanwhile, Hooper and Keen,[13] using a modification of the Russian distillation process to refine commercial Pechiney flake in tantalum equipment, obtained material from a single distillation that was lower in both carbon and oxygen than was material the Russians had obtained by multiple distillation. However, the total of iron, aluminum, silicon, copper, nickel, magnesium, lead, and nitrogen in the Hooper and Keen distillate totaled 140 ppm compared to 97 ppm reported by Sinelnikov et al.

As part of an attempt to prepare pure beryllium by thermal decomposition of beryllium iodide, Nuclear Materials and Equipment Corporation is engaged in the preparation[16] of pure BeI_2.

In the United States, Mallett distilled beryllium in a beryllia crucible fitted with a tantalum condenser similar to the Russian equipment and produced high-purity metal.

Fabrication of Beryllium

Joining. A series of welding tests was made by the Budd Company[17] to determine the tension-shear properties obtainable from representative gauges and weld setups on beryllium. They found that a spacing for spot welds of $\frac{5}{8}$ to $\frac{3}{4}$ in. in 0.040-in. sheet is the minimum that can be used to avoid cracking. Sheet from the same starting thickness rolled to thicknesses below 0.040 in. was more difficult to weld. Preferred orientation appeared to be a big factor. Characteristically, cracks begin at the center of the weld nugget and propagate at approximately 120° intervals. The results obtained on thin (0.015 in.) sheet were erratic, suggesting that mill practices in reducing the gauge to below 0.020 in. may not be satisfactory for resistance welding.

Shrink fitting beryllium parts together by expanding the outer member through heat to increase its diameter so that the inner member can be put in place is the most common method of joining beryllium in final assembly.[18] On cooling, the outer member contracts and holds the two pieces together.

Brush Beryllium[19] reported that successful automatic welds, both with and without beryllium filler wire, have been made using a d-c straight-polarity power source. Postweld heat-treatments at temperatures ranging from 825 to 900°C appeared beneficial. Multiple-pass welds on thick material were not successful.

In order to measure the neutron level of the Liquid Metal Fuel Reactor (LMFR), a detector must be placed in a thimble and inserted into the graphite core assembly. The approximate dimensions of the thimble are 3 in. in diameter by 11 ft long by $\frac{1}{8}$ in. thick, with one end closed and the other flanged. Beryllium was chosen for the thimble because (1) it would not necessitate an addition of fuel to maintain criticality when inserted into the core assembly and (2) it has good resistance to corrosion by molten bismuth. The end cap and two or more lengths of tubing were successfully joined by tungsten-electrode inert-gas welding.[20]

Beryllium Extrusion. A bare extrusion process for producing a beryllium channel section has yielded very encouraging and reproducible results.[21] Both the billet temperature (1750°F) and the type of lubricant (glasses) appeared to be critical. The press was operated at a ram speed of 720 in./min. The high ram speed reduced heat losses to the container and made the results so consistent that, for the first time, the effects of small variations in technique could be evaluated.

Beryllium Forming. Brush QMV powder is presintered in a graphite mold to 90 to 99 per cent of theoretical density (5 hr in the vacuum at 1200°C) in a tube-making process.[22] The solid billet is then drilled, enclosed in a steel can, heated in air to 1050°C, and extruded with reduction ratios that are generally less than 12 to 1. After the steel jackets are removed, a hot-work die-steel plug type mandrel is then drawn through the tube to make the inside surface smooth and uniform. Colloidal graphite in oil is used as the lubricant. After cleaning, the tubes are annealed in vacuum at 750°C for 30 min and furnace cooled. A British patent[23] indicates that beryllium can be formed in air at temperatures below 750°C by supporting it with a ductile metal such as steel or aluminum to which the beryllium will adhere without welding. Beryllium sheet up to 0.080 in. thick can be formed at 630 to 670°C over mild steel of twice the thickness of the beryllium.

Physical Metallurgy of Beryllium

Studies of binary and ternary alloys to determine the stability of the beta phase in beryllium-

alloy systems were continued.[24,25] Tentative phase diagrams of the beryllium-rich portions of the chromium-, iron-, silver-, and silicon-beryllium systems were presented. In none of the ternary (beryllium-nickel-iron) or quaternary (beryllium-nickel-cobalt-iron) alloys studied was the beta-to-alpha transformation point depressed below about 1065°C. Rapid-strain-rate, high-temperature tensile tests on pure beryllium–8 at.% nickel alloy showed that neither was ductile at 1060°C, at which temperature no beta is present. At 1070°C the unalloyed beryllium exhibited a tensile strength of 8000 psi and no ductility. The beryllium–8 at.% nickel alloy, however, exhibited a 19 per cent reduction in area at 1070°C, at which temperature the alloy is all beta.

Green and Sawkill[26] explored the relation between plastic anisotropy and ductility in beryllium between 20 and 400°C. They applied Stroh's theory for the basal-plane fracture observed in zinc to beryllium. A qualitative explanation for the increase in ductility with temperature of polycrystalline beryllium was proposed.

It was found that aging treatments of 24 hr at 400°C improved the ultimate tensile strength and elongation of extruded beryllium rod but did not change the yield strength.[16] It was suggested that aging did not actually strengthen the matrix but merely removed sources of premature failure.

Metallography of Beryllium

Thin sections of beryllium for transmission electron microscopy can be prepared by directing a fine jet stream of electrolyte in an electrolytic etching apparatus at the center of the specimen to reduce the thickness[16] to 50 to 100 μ. The specimen as a whole is then electropolished until the first breakthrough. The area around the hole is usually thin enough for electron transmission.

Jacquet[27] gave detailed metallographic procedures for preparing specimens of magnesium alloys, magnesium, and beryllium. These procedures involve an electrolytic buffer and appear to offer advantages in simplicity and ease of operation.

It is reported[28] that an aqueous solution of copper sulfate containing a few hundred parts per million of copper will deposit copper at the grain boundaries of mechanically or electrolytically polished specimens of beryllium. Copper is deposited also at subboundaries, showing misorientations across the substructure for both electron and light microscopy.

A wide variety of beryllium specimens ranging from single crystals to finely polycrystalline material containing inclusions was studied by the point projection X-ray microscope.[29] The highly divergent beam of X rays from a source 1 μ in diameter gave, on the same photograph, a microradiograph of the specimen with a resolution of 1 μ and a divergent diffraction pattern. Together, these give information about the distribution of heavier elements or cracks in the beryllium, the variation in perfection of crystal lattice, and, for a single crystal, the orientation and lattice parameters of the specimen.

Additional evidence that some impurity which becomes soluble in beryllium at about 850°C and is precipitated on cooling was obtained by etching various specimens. These specimens, which included Nuclear Metals extruded bar, Pechiney extruded bar, and Brush hot-pressed block, were annealed for 24 hr at 900°C and water quenched or slow cooled at a rate of 2°C/hr to room temperature. The quenched specimens on etching showed distinctly thick grain boundaries, whereas it was difficult to distinguish the grain boundaries of the slow-cooled specimens by etching, although a considerably greater amount of precipitate was scattered throughout the grains.*

Preliminary electron-micrographic studies of oxidized beryllium suggest a penetration of oxygen along crystallographic planes of the metal. Similar observations with tantalum have been attributed to either dislocation-enhanced diffusion or dislocation-aided nucleation.[9]

Mechanical Properties of Beryllium

A handbook intended to provide a single source of reliable data for direct use in the design of parts fabricated from beryllium was issued by Lockheed.[30] Included are data on basic mechanical and physical properties of beryllium; joint and fastener properties; fatigue, impact, and dynamic modulus; and fabrication methods.

After determinations of notch sensitivity on beryllium block and sheet were made, it was observed that, although beryllium may not be considered insensitive to stress concentrations,

*Atomic Energy of Canada, Ltd., 1961. (Unpublished)

it is no worse in this respect than some of the other high-strength alloys which are currently being applied successfully in aircraft and missile design.[31,32]

A notched specimen of hot-pressed, hot-extruded beryllium cyclically stressed at 9000 psi was reported[33] to last about 52 hr at 1100°F, whereas an unnotched specimen of the same material under a static stress of 9413 psi at 1100°F lasted only 0.83 hr. It was concluded that, from a design standpoint, beryllium exhibits its best behavior and highest strength under fatigue loading conditions and is weakest under static loading conditions. Some doubt may be raised about these conclusions, however, since it is not clear that the surface conditions of the specimens were equivalent. Another report[34] on fatigue tests carried out to 100 million cycles on hot-pressed block and 10 million cycles on $\frac{1}{8}$-in.-thick sheet at various values of K_t showed that the average ratio of the endurance limit to the ultimate tensile strength was about 0.7. Sheet specimens showed an increase in fatigue strength between 50 and 75 per cent over those machined from QMV hot-pressed block.

A study of the mechanical properties of beryllium sheet with various surface finishes emphasized the importance of etching to remove surface defects caused by machining. Ductility was low in all cases, being limited by the presence of notches and preferred orientation in the sheet. Impact tests were found to be the most suitable means to distinguish between the quality of various surfaces.[35]

The stress-rupture properties of several grades of beryllium tubing were determined,[36] and the tentative curves shown in Fig. II-1 were obtained. The tubing produced by machining from hot-pressed block exhibited the highest stress-rupture strength, although the ductility of these tubes was considerably lower than that of comparable extruded tubes from other manufacturers.

Edgewise compression tests on honeycomb panels with beryllium skins 0.040 and 0.020 in. thick separated by cores of stainless steel $\frac{1}{2}$ in. high showed failures[37] at about 30,000 psi. Several reports on elevated-temperature properties of beryllium have recently become available. These included data on stress rupture and creep of Brush QMV beryllium and material with a high-oxide content from room temperature to 1500°F,[38a] and data on tensile, compressive, and shear properties for various strain rates over the temperature range of 800 to 1500°F.[38b]

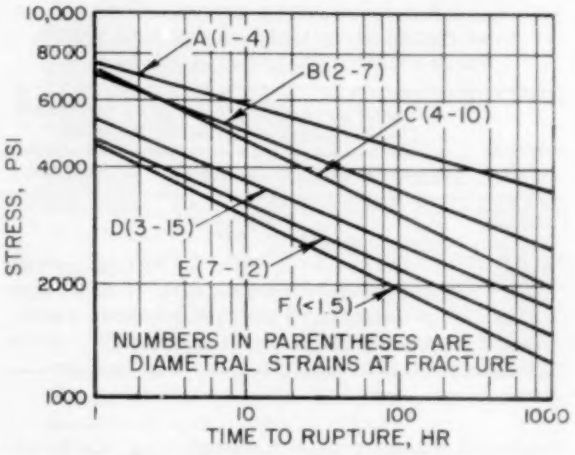

Fig. II-1 Stress rupture of beryllium tubes[36] at 600°C. *A*, machined from hot-pressed block, Brush Beryllium Co. *B*, machined from warm-extruded rod, Brush Beryllium Co. *C*, warm extruded, Brush Beryllium Co. *D*, Pechiney. *E*, Imperial Chemical Industries. *F*, Chesterfield.

Bernett[39] reported the short-time tensile properties of hot-cross-rolled beryllium sheet and vacuum-pressed block at temperatures up to 1500°F and high-stress creep properties in the same temperature range. The author concluded that, for short-time application at temperatures up to about 900°F, the creep rates of beryllium sheet and block materials are insignificant at even the maximum operating stress levels. As the temperature rises higher and higher above 900°F, creep becomes an increasingly critical design factor.

In work sponsored by Lockheed,[40] the thermal conductivity of seven commercial beryllium specimens was redetermined. The values ranged from 104 to 83 Btu/(hr)(ft)(°F) at 200°F and from 44 to 39 Btu/(hr)(ft)(°F) at 1900°F, depending on the BeO content and fabrication factors. The correlation between the electrical resistivity and thermal conductivity was good over this entire temperature range.

Anisotropy of electrical resistivity occurs near absolute zero in an extruded beryllium flat (Table II-5). Since anisotropy of resistivity at absolute zero cannot depend upon crystallography per se, it is postulated that it must be caused by (1) a preferentially precipitated impurity network occurring on a plane parallel to

Table II-5 EFFECTS OF TEMPERATURE ON ELECTRICAL RESISTIVITY OF SAMPLES TAKEN FROM AN EXTRUDED BERYLLIUM FLAT[16]

Temp., °K	Resistivity and standard deviation referenced to the extrusion direction, μohm-cm		
	Perpendicular	30° angle	Parallel
303.88		4.602 ± 0.0051	
303.28	5.262 ± 0.0078		
298.93			4.344 ± 0.0028
190.6	2.418 ± 0.0046	2.075 ± 0.0034	1.987 ± 0.0028
77.28	1.073 ± 0.0046	0.890 ± 0.0015	0.845 ± 0.0041
4.2	1.012 ± 0.0025		0.791 ± 0.0015

the basal plane or (2) the elongated grain structure in the extruded flat which presumably presents a greater concentration of high-resistance grain boundaries perpendicular to the basal planes than parallel to these planes.[16] Analysis of the thermal and electrical resistivity of beryllium at low temperatures shows that a reactor exposure of 10^{19} nvt (fast) should decrease the thermal conductivity of beryllium by approximately 0.04 watt/(cm)(°K) at temperatures of 20 to 30°K. Both high- and low-purity beryllium should be affected similarly. Warming to 250°K should cause rapid and complete annealing out of the radiation-induced change of thermal conductivity.[41]

Corrosion of Beryllium

The compatibility of beryllium with water vapor is being studied[36] at 600°C in flowing helium containing approximately 4 vol.% H_2O. The log-log plot of the weight change against time gave two straight lines intersecting at approximately $t = 5$ hr. The first part of the curve indicates the formation of a nonprotective film; the second part indicates the formation of a protective film. It appeared that the initial slope of the curve was due to the hydrolysis of Be_2C and that the sample was completely decarburized in 5 hr. (W. Hodge)

Solid Hydrides

On the basis of a study of internuclear distances in hydrides, made recently at Tufts University,[42] it has been concluded that there is no sharp difference between the "saltlike" hydrides and those of transition metals. An ionic model and one utilizing delocalized covalent bonding fit equally well. In the ionic model the H^- ion is found to have a radius of 1.29 A, assuming a coordination number of 4, whereas the single-bond radius for hydrogen is 0.37 A in the covalent model.

Zirconium Hydride

Thermal-expansion studies at Los Alamos[43] have shown that, for the delta-hydride phase, the average linear-thermal-expansion coefficient is 2.98×10^{-6}/°C for the temperature range 24 to 362°C. The data were obtained by X-ray-diffraction techniques. In the epsilon-hydride phase, a value of -1.4×10^{-6}/°C was found in the a direction and 30.6×10^{-6}/°C in the c direction. The average of 9.3×10^{-6}/°C for randomly oriented polycrystalline material agrees reasonably well with that previously reported by Yakel[44] and by Goon.[45]

(H. H. Krause)

References

1. D. R. deHalas, Hanford Atomic Products Operation, June 14, 1960. (Unpublished)
2. F. W. Albaugh, Reactor and Fuels Research and Development Operation Monthly Report, January 1961, USAEC Report HW-68350-A, Hanford Atomic Products Operation, Feb. 15, 1961. (Classified)
3. R. W. Dayton and C. R. Tipton, Jr., Progress Relating to Civilian Applications During January 1961, USAEC Report BMI-1496, Battelle Memorial Institute, Feb. 1, 1961.
4. C. A. Hampel (Ed.), Beryllium, in *Rare Metals Handbook*, 2nd Ed., pp. 32–57, Reinhold Publishing Corp., New York, 1961.
5. K. D. Carroll (Comp.), Beryllium — A Survey of the Literature, Report LMSD-288190(Suppl. 3), Lockheed Aircraft Corp., December 1960.
6. F. A. Crossley et al., Ductile Beryllium Alloys, Final Report, Report ARF-2187-6, Armour Research Foundation, Illinois Institute of Technology, Oct. 20, 1960.
7. Bureau of Naval Weapons News Release, Apr. 3, 1961.
8. M. Herman et al., The Preparation of High Purity Beryllium and the Study of Its Flow and Fracture Characteristics, Final Report, June 30, 1959–June 30, 1960, Report NP-9871, Franklin Institute Laboratories.
9. G. E. Spangler and M. Herman, Preparation and Evaluation of High Purity Beryllium, Nov. 2, 1960–Jan. 1, 1961, Report NP-9819, Franklin Institute Laboratories.
10. K. D. Sinelnikov et al., *Proceedings of the Second United Nations International Conference on the Peaceful Uses of Atomic Energy, Geneva, 1958*, Vol. 4, p. 296, United Nations, New York, 1958.

11. V. M. Amonenko et al., *Proc. Acad. Sci. U.S.S.R., Chem. Sect.*, 128(5): (1959).
12. V. Ye. Ivanov et al., Refining Beryllium by Vacuum Distillation, *Met. i Metalloved.*, 10(4): 581–585 (1960).
13. E. W. Hooper and N. J. Keen, The Purification of Beryllium Metal by a Distillation Process, British Report AERE-R-3321, November 1960.
14. C. S. Pearsall, Effect of Oxygen on the Ductility of Beryllium Prepared by High-Vacuum Distillation, USAEC Report MIT-1104, Massachusetts Institute of Technology, 1952.
15. A. R. Kaufmann et al., *Trans. Am. Soc. Metals*, 42: 785 (1950).
16. S. H. Gelles, Beryllium Research and Development Program, Report NMI-9505, Nuclear Metals, Inc., Nov. 10, 1960.
17. Preliminary Notes on Resistance Spot Welding Beryllium, Budd Co., Philadelphia, Pa.
18. How to Join Beryllium, *Metalworking Production*, 105: 19 (Jan. 4, 1961).
19. B. M. MacPherson and W. W. Beaver, Fusion Welding of Beryllium, Report NP-7901, Brush Beryllium Co., Aug. 15, 1959.
20. P. C. Thys, Liquid Metal Fuel Reactor Experiment. Investigation of Beryllium Welding Techniques for Reactor Port Thimble Joints, USAEC Report BAW-1100, Babcock and Wilcox Co., April 1960.
21. Northrop Aircraft, Inc., Program for the Development of Extruded Beryllium Shapes, Report NOR-61-6, Sept. 1–Nov. 30, 1960.
22. A. C. Hood and A. M. Bounds, The Conversion of Extruded Beryllium Tubing to a Close Tolerance Bore Tube, USAEC Report TID-11535, Superior Tube Co., Feb. 15, 1960.
23. N. A. Hill, Improvements in or Relating to the Forming of Beryllium, British Patent 848,269, Sept. 14, 1960.
24. S. H. Gelles and J. J. Pickett, Stability in the High Temperature Beta Phase in Beryllium and Beryllium Alloys, USAEC Report NMI-1218, Nuclear Metals, Inc., Oct. 10, 1960.
25. Nuclear Metals, Inc., Fundamental and Applied Research and Development in Metallurgy, Progress Report for November 1960, USAEC Report NMI-2091, Dec. 27, 1960.
26. A. P. Green and J. Sawkill, Plastic Anisotropy and Fracture in Beryllium, *J. Nuclear Materials*, 3(1): 101–110 (January 1961).
27. P. A. Jacquet, Nondestructive Metallography of Light and Ultra-Light Materials (Al, Mg, Be, and Their Alloys): Part 3, *Rev. Aluminium*, 37: 977–987 (September 1960).
28. J. Sawkill and J. E. Meredith, The Etching of Substructures in Beryllium, *Phil. Mag.*, 5: 1195–1196 (November 1960).
29. J. Sawkill and D. R. Schwarzenberger, X-Ray Microscopy of Beryllium, *Brit. J. Appl. Phys.*, 11: 498–503 (November 1960).
30. Lockheed Aircraft Corp., Beryllium Design Data, Report LMSD-48472, Apr. 29, 1959.
31. R. F. Crawford and L. A. Riedinger, Monthly Progress Report on Structural Design Data for Beryllium, Report LMSD-312201-9, Lockheed Aircraft Corp., Nov. 1, 1960.
32. L. A. Riedinger and R. F. Crawford, Structural Design Data for Beryllium, Report LMSD-312201-11, Lockheed Aircraft Corp., Jan. 1, 1961.
33. A. E. Riesen and R. T. Ault, Mechanical Properties of Beryllium, Report WADD-TR-60-425, Wright Air Development Div., Materials Central, September 1960.
34. R. L. Lowe, Fatigue Tests of Some Hot-Pressed Beryllium, Report LR-12954, Lockheed Aircraft Corp., Mar. 27, 1958.
35. C. O. Matthews et al., Beryllium Crack Propagation and Effects of Surface Condition, Report WADD-TR-60-116, Lockheed Aircraft Corp., Jan. 31, 1960.
36. Oak Ridge National Laboratory, Gas-Cooled Reactor Project Quarterly Progress Report for Period Ending December 31, 1960, USAEC Report ORNL-3049, Mar. 9, 1961.
37. J. N. Krusos, Development of Beryllium Composite Structures, Progress Report No. 11, Aeronca Manufacturing Corp., December 1960.
38. Symposium on Newer Metals, *ASTM Special Tech. Publ. No. 272* (1960).
    a. J. N. Hurd et al., Stress and Creep Properties of QMV Beryllium, pp. 95–115.
    b. W. W. Beaver et al., Effect of Purity and Manufacturing Variables on Elevated Temperature Properties of Beryllium, pp. 81–84.
39. E. C. Bernett, Evaluation of the Short-Time Mechanical Properties of Structural Beryllium, Aviation Conference of the ASME, Los Angeles, Calif., Mar. 12–16, 1961, Paper 61-AV-42.
40. Private communication, Dec. 9, 1960.
41. G. J. Dienes and A. C. Damask, An Estimate of the Effect of Radiation on the Thermal Conductivity of Beryllium, *J. Nuclear Materials*, 3(1): 16–20 (January 1961).
42. T. R. Gibb, Jr., and D. P. Schumacher, Internuclear Distances in Hydrides, *J. Phys. Chem.*, 64: 1407–1410 (October 1960).
43. C. P. Kempter et al., Thermal Expansion of Delta and Epsilon Zirconium Hydrides, *J. Chem. Phys.*, 33: 837–840 (September 1960).
44. H. L. Yakel, Thermocrystallography of Higher Hydrides of Titanium and Zirconium, *Acta Cryst.*, 11: 46 (1958).
45. E. J. Goon, The Nonstoichiometry of Lanthanum Hydride, USAEC Report NYO-7549, Tufts University, Mar. 30, 1959.

Section III

NUCLEAR POISONS

Control-Material Compounds and Dispersions

General Electric[1] has reported the results of compatibility studies of boron compounds dispersed in titanium, iron, zirconium, stainless steel, nickel, copper, silver, and aluminum. The diborides, HfB_2, TiB_2, and ZrB_2, were found to be least reactive, but all borides reacted to a certain extent with iron, nickel, zirconium, titanium, and stainless steel at 1000°C. The most severe reactions occurred between B_4C, YB_4, CuB_6, EuB_6, SmB_6 or YB_6, and nickel, iron, or stainless steel. No reaction was reported for any of the borides or copper at 1000°C, silver at 950°C, or aluminum at 550°C.

Helium-release measurements have been used at Bettis[2] on slightly irradiated B_4C to derive equations for computing the diffusion coefficients. Calculations were made assuming both uniform and nonuniform distribution of the helium. The results are shown in Table III-1.

Table III-1 HELIUM DIFFUSION COEFFICIENTS IN B_4^NC

Temp., °C	Geometric area D, cm²/sec: Nonuniform initial He distribution	Geometric area D, cm²/sec: Uniform He distribution	Gas adsorption area: Uniform distribution
600	2.4×10^{-13}	9.2×10^{-14}	3.2×10^{-16}
700	9.2×10^{-13}	2.4×10^{-12}	8.2×10^{-15}
800	5.6×10^{-11}	1.0×10^{-10}	3.6×10^{-13}
1000	1.6×10^{-10}	1.5×10^{-10}	5.1×10^{-13}

Phase equilibria in the boron-carbon system are being investigated at Armour.[3] For temperatures ranging from 1500 to 2000°C, boron carbide has a reported solubility ranging from 20 to 10 at.% carbon. The melting point of the carbide-graphite eutectic was reported as 2325 to 2350°C. The solubility of carbon in boron was very small, and the melting point of dilute carbon alloys could not be distinguished from that of boron (2040 to 2050°C).

Techniques have been described[4] which are applicable for production of nickel-boron cermets containing from 5 to 60 wt.% nickel. Powders are blended, cold pressed at 10 tsi, and then hot pressed at 1950°C in boron nitride-lined graphite dies. In this way, compacts were produced containing 10 wt.% nickel with a boron density of greater than 1.9 g/cm³.

Atomics International[5] found that a 1000-hr heat-treatment at 1800°F *in vacuo* had essen-

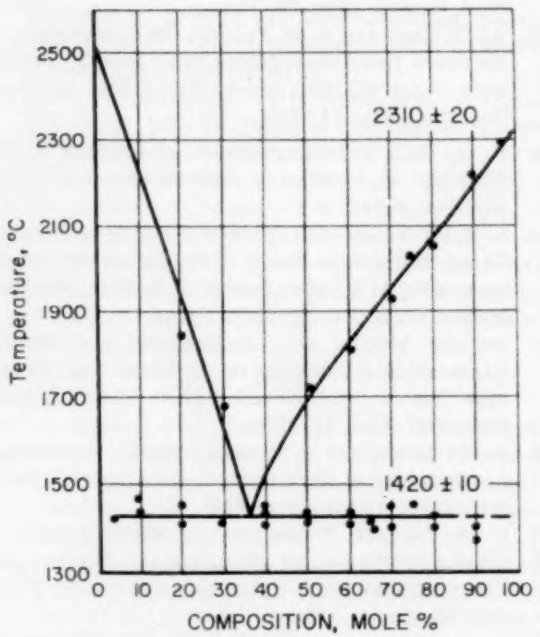

Fig. III-1 BeO-Sm_2O_3 phase diagram[6] in the region 1300 to 2500°C.

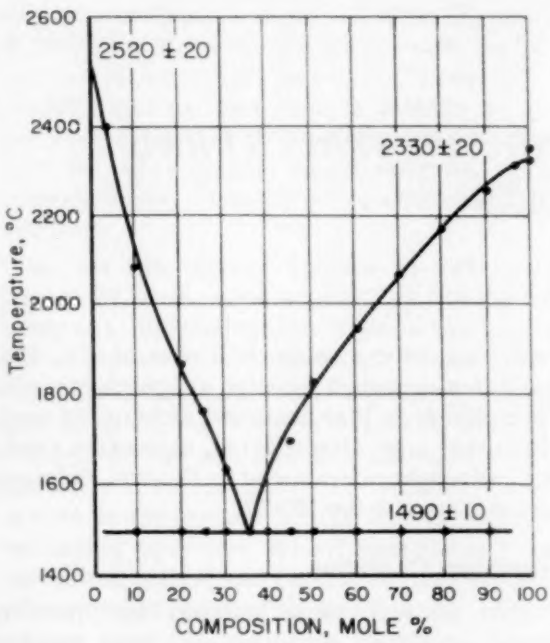

Fig. III-2 $BeO-Gd_2O_3$ phase diagram[6] in the region 1300 to 2500°C.

tially no effect on Multimet, Hastelloy X, type 347 stainless steel, and Haynes alloy 25 in contact with a mixed rare-earth oxide (50 per cent Gd_2O_3 – 50 per cent Sm_2O_3). Slight oxidation of Inconel X and a somewhat heavier oxidation of titanium were observed.

The systems $BeO-Sm_2O_3$ and $BeO-Gd_2O_3$ have been investigated.[6] Phase diagrams are reported in Figs. III-1 and III-2.

(G. W. Cunningham)

References

1. K. C. Antony and W. V. Cummings, Metallurgical Stability of Several Boride Dispersion Systems, USAEC Report GEAP-3530, General Electric Co., Atomic Power Equipment Dept., Sept. 20, 1960.
2. Westinghouse Electric Corp., Bettis Atomic Power Laboratory, Pressurized Water Reactor (PWR) Project Technical Progress Report for the Period December 24, 1960, to February 23, 1961, USAEC Report WAPD-MRP-90.
3. Armour Research Foundation, Illinois Institute of Technology, March 1961. (Unpublished)
4. P. Best and S. R. Twigg, Production of Boron-10 Compacts for Fast Reactor Control. Part II: Fabrication of Compacts of Density Greater Than 1.9 g B^{10}/cm^3, British Report DEG-R-4, Dec. 8, 1960.
5. R. D. Moeller, Compatibility of Various Materials with Rare-Earth Oxides at 1800°F, USAEC Report NAA-SR-Memo-5253, Atomics International, May 3, 1960.
6. S. G. Tresvyatskiy et al., Investigation of the Systems $BeO-Sm_2O_3$ and $BeO-Gd_2O_3$, *At. Energ.*, 9(1): 54–55 (1960).

Section IV

CLADDING AND STRUCTURAL MATERIALS

Corrosion

Niobium Corrosion

The effects of irradiation on the oxidation behavior of niobium have been studied at Oak Ridge.[1] Neutron dosages up to 10^{12} nv have no measurable effect on the oxidation rate or the nucleation process associated with oxidation at 400°C.

Crystalline Nb_2O_5 was produced at 96°C during anodic oxidation of niobium, according to Lakhiani and Shrier.[2] In contrast, recent Norwegian work[3] showed that Nb_2O_5 is formed only above 400°C during gaseous oxidation. Presumably, Nb_2O_5 is stable to temperatures at least as low as 96°C, and the unidentifiable oxides formed during gaseous oxidation below 400°C are metastable.

Studies at General Atomic[4] indicate that niobium and niobium alloys are probably unsuitable for use in the unclad, graphite-moderated version of the Maritime Gas-Cooled Reactor (MGCR). This reactor utilizes argon as a coolant, but trace amounts of CO and CO_2 in the argon cause embrittlement of niobium. In argon containing only 1 ppm CO_2, niobium was embrittled in 100 hr at 820°C. Binary alloys containing 1 to 5 wt.% zirconium or 5 to 20 wt.% titanium are also embrittled. Under carburizing conditions, niobium forms an adherent protective carbide.

The low-pressure, high-temperature oxidation studies at Oak Ridge[5] continue to indicate that alloying effects vary with gas pressure. Binary niobium alloys containing small percentages of tin and palladium oxidize as fast as unalloyed niobium at 1200°C at an oxygen pressure of 5×10^{-4} mm. However, an alloy of niobium–25 wt.% titanium–5 wt.% aluminum oxidized three times faster than niobium. This alloy is reportedly 100 times more oxidation resistant than niobium in 1 atm of air. Thus oxidation-resistant niobium alloys may be even less attractive than unalloyed niobium for use in relatively inert atmospheres, such as the argon-CO_2 atmosphere evaluated by General Atomic in connection with the MGCR.

Tantalum Oxidation

The internal oxide platelets that form in tantalum during oxidation have been found to penetrate parallel to the (3 2 0) planes.[6] This finding is in apparent conflict with the previous observation by Bakish[7] that these platelets form on the (1 0 0) planes. Oak Ridge identified polycrystalline TaO as one platelet constituent.

Sylcor[8] has developed a tin-aluminum hot-dip coating that protects tantalum from oxidation for several hours up to 3000°F. The coating consists of $TaAl_3$ and a tin-aluminum phase which is liquid at elevated temperature. Battelle[9] has determined that silicide and aluminum-modified silicide coatings protect tantalum alloys for periods up to 8 hr at 2700°F. These coatings are applied by pack cementation and appear to form a glassy oxide upon exposure.

(W. D. Klopp)

Corrosion of Base-Metal Alloys (Iron, Nickel, Cobalt)

Investigation of attack on Hastelloy X and Inconel in various environments associated with gas-cooled reactors was continued at Aerojet-General.[10] Tests in 99.5 per cent nitrogen–0.5 per cent oxygen at a temperature of 1750°F and a pressure of 300 psi were extended to 7500 hr. Hastelloy X continued to show good oxidation resistance, e.g., 1.5-mil penetration in reference gas and 2 mils in air. After 7500 hr in the reference gas at 1750°F, Inconel showed intergran-

ular penetration to a depth of 5 mils. Exposure of Hastelloy X to high-purity nitrogen or 99.9 per cent nitrogen–0.1 per cent CO resulted in nitriding and extreme loss of ductility (1 to 3 per cent elongation at room temperature) after 2500 hr. After similar exposures in air on the reference gas, 31 to 33 per cent ductility was retained.

Inconel 702, Inconel X, René 41, M252, and Haynes 25 were coated with KCl or LiF salt and oxidized in the 1600 to 1900°F temperature range under stress in a program at Crucible Steel Company of America.[11] The Haynes 25, René 41, and M252 showed the best creep-strength retention; on this basis the Inco alloys were considerably inferior. Little corrosion was observed in the absence of air. With air present, the salted materials did not form their normal protective scales, and general corrosive attack, intergranular penetration, and internal void formation were all operative corrosion mechanisms. Inconel, when exposed in a fused-salt bath (1472°F) for 50 days, exhibited selective corrosion of chromium and iron from the surface.[12]

Corrosion of Miscellaneous Metals

(Chromium, Magnesium, Yttrium)

A recent AEC report[13] reiterated the benefits derived in chromium through yttrium additions, i.e., radically improved air-oxidation resistance and room-temperature ductility.

Contained in a recent UKAEA monograph[14] are data on gaseous and aqueous corrosion of magnesium and its alloys. This is a convenient source of reference data and includes information on corrosion and ignition temperature in oxygen, air (dry and moist), CO_2, and pond water. Galvanic coupling effects are illustrated. Of particular note is that the ignition temperature of magnesium decreased by 60 to 180°F through coupling with nickel, brass, or aluminum.

Striking effects of metal purity on the oxidation behavior of yttrium were demonstrated at Ames Laboratory.[13] High-purity (99.9 per cent) yttrium formed a thin, adherent, dark oxide during air oxidation for 24 hr at 1652°F. Commercially pure yttrium, exposed in like manner, exhibited a voluminous, powdery, nonadherent scale. The addition of 5 per cent beryllium improved the oxidation resistance of yttrium.

(E. S. Bartlett)

Corrosion by Liquid Metals and Fused Salts

A program involving corrosion experiments with boiling potassium is in progress at Oak Ridge to provide information about the corrosion resistance of iron-, nickel-, cobalt-, and niobium-base alloys. In refluxing-capsule experiments in which potassium is maintained at 1500 and 1600°F, a trend showing weight loss for specimens located in the vapor zone and weight gain for liquid-zone specimens has been found. Inconel (nickel base) has exhibited less corrosion than type 316 stainless steel (iron base) or Haynes alloy No. 25 (cobalt base).[5] After 3000 hr of operation at a maximum temperature of 1600°F, a circulating boiling and condensing system fabricated of type 316 stainless steel displayed a maximum attack of 2 mils at the liquid-vapor interface in the boiler and about 3 mils of mass-transfer deposits in the cold zone. Circulating systems are being constructed of Haynes alloy No. 25 and of a niobium-zirconium alloy.

Pumping-loop studies to determine the long-time corrosion behavior of Inconel and INOR-8 exposed to fluoride salt mixtures of interest to the Molten-Salt Reactor Program at Oak Ridge are continuing. It was reported[15] recently that an INOR-8 loop which ran for nearly 20,000 hr displayed no evidence of attack of either hot- or cold-zone surfaces, although there was a small metallic deposit in one cold-zone area. Operating conditions for this system included: salt mixture, NaF-LiF-BeF_2 (27-35-38 mole %); peak temperature, 1200°F; temperature difference, 150°F; Reynolds number, 3000.

Zirconium taken from the Sodium Reactor Experiment (SRE) was examined[16] in terms of properties and characteristics after significant exposure at reactor operating temperatures (500 to 950°F). In the SRE, zirconium is used as a cladding material with sodium on one side and graphite on the other. In general, the material was virtually unchanged, although increases in oxygen and hydrogen content (to maximum values of 3300 and 1000 ppm, respectively) were noted. The sodium probably contributed the oxygen and part of the hydrogen. The hydrogen produced some loss of ductility at room temperature, but, at 200°F and above, the ductility appeared to be about the same as that of as-received material. Prior laboratory data indicate the possibility that fatigue life might be somewhat reduced by the oxygen impurity.

A summary of thermodynamic-property data for sodium and sodium vapor at temperatures in some cases as high as 2600°K has been presented.[17] Existing data were refined by extensive analysis of monomer and dimer effects in order to arrive at values for the vapor phase.

A treatise on embrittlement by liquid metals has been published.[18] (J. H. Stang)

Metal-Water Reactions

The experimental program to determine rates of reaction of molten reactor fuel and cladding metals with water is continuing at Argonne.[19] The principal laboratory-scale method involves the rapid melting and dispersion of metal wires in a water or steam environment by a surge current from a bank of condensers. Currently reported is a series of runs with 60-mil zirconium wires carried out in a new high-pressure reaction cell. Solid zirconium at temperatures near the melting point reacted (with room-temperature water at its vapor pressure of about 0.5 psia) to the extent of 4 to 5 per cent. At saturated vapor pressures of from 5 to 230 psia, 8 to 9 per cent reaction occurred. Liquid metal at the melting point gave about 8 per cent reaction with room-temperature water, whereas 30 per cent reaction was observed at pressures from 16 to 140 psia.

The results indicate that the over-all reaction depends strongly on the pressure of water vapor up to some point between 0.5 and 5 psia. A further increase in pressure causes no additional reaction. This limit suggests that the reaction becomes controlled by the transport of water vapor through a film of hydrogen generated by reaction. This latter process would be expected to be relatively independent of pressure.

Additional in-pile experiments in TREAT have also been conducted by Argonne.[19] Each transient with oxide-core pins resulted in rupturing and melting of the Zircaloy-2 jacket. The extent of metal-water reaction increased from 4.1 to 14.1 per cent as the reactor bursts became more energetic. It was concluded tentatively from results of runs with the oxide-core, metal-clad pins that the Zircaloy-2 jacket ruptured and melted more readily than the stainless-steel jacket. By comparing runs with clad and unclad cermet-core pins, it was also noted that dispersion of the fuel into particles is favored by the use of a jacket.

Another series of six metal-water transient irradiation experiments in TREAT with uranium wires was conducted.[20] The wires were 93 per cent enriched uranium with diameters of 34 and 64 mils. Reactor periods of 304 msec or less resulted in melting of the wires, and the uranium attained temperatures of about 1500°C with extensive formation of particles. One run with a bundle of three uranium wires to simulate a fuel-element cluster resulted in 12.9 per cent reaction. The three wires fused together, and some fine particles were produced. An experiment[1] with a single fully enriched uranium wire, 34 mils in diameter, gave 28.3 per cent reaction with complete conversion of the metal into particles.

Metal-water reaction experiments have been reported[21] for molten aluminum and molten aluminum–23.40 wt.% uranium alloy reacting with water vapor at essentially atmospheric pressure. Rates were determined by an automatically recording thermobalance; the experiments were performed over periods of 2 hr at constant temperatures between 1500 and 2300°F. It was determined that the reaction follows a linear rate law. The data for these experiments are shown graphically for the aluminum-uranium alloy.[22] Values for the rates of reaction increase rapidly from about 2 g/(cm²)(sec) at 1500°F to about 10 g/(cm²)(sec) as a maximum at 1600°F. Above this temperature the reaction rate slowly decreases to a value of less than 2 g/(cm²)(sec) at 2200°F.

Calculations performed[21] for the aluminum–23.40 wt.% uranium alloy indicate that, for conditions of no heat loss, a 0.01-cm-diameter molten particle would increase from 1600 to 1700°F in slightly over 2 min. This suggests that the reaction of molten aluminum-uranium alloys with water vapor at near atmospheric pressure does not constitute an explosive hazard in the operation of nuclear reactors.

(A. W. Lemmon, Jr.)

Radiation Effects in Nonfuel Materials

Defects: Structure and Properties

Metals. Focusing collisions in copper, silver, and gold irradiated with 0.3-Mev protons and 10-kev ions of argon and xenon have been explained in terms of three different processes.[23]

The first is a focused atomic collision in ⟨1 1 0⟩ directions where the momentum is transferred due to the geometric properties of the close-packed lines. No mass transfer is thought to occur in this process. Experiments show a maximum range of about 350 A in gold. The other two events, which occur along ⟨1 0 0⟩ and ⟨1 1 1⟩ directions, are thought to consist of successive replacements of the target atom by the projectile. The focusing here is due to the ring of atoms which circle the projectile's path. Predictions and experiments indicate a maximum range in copper of 35 A for the ⟨1 0 0⟩ and 120 A for the ⟨1 1 1⟩ events, and in gold, 50 A for ⟨1 0 0⟩ and 300 A for ⟨1 1 1⟩.

Granato and Nilan[24] have measured the stored-energy release of deuteron-irradiated copper. Deuterons of 11 Mev were used for the irradiation to a total dose of about 10^{15} deuterons/cm^2 in a specially designed calorimeter. Heat losses were minimized by using small samples and the relatively rapid anneal rate of 2°K/min. Annealing was studied from about 25 to 80°K. The normalized energy released was 0.83 cal/g to an accuracy of about 10 per cent. Using the data presently available, this energy release corresponds to a resistivity of 2.6 μohm-cm/1 per cent F. P. (Frenkel pair) with 1.2 atomic volumes per Frenkel pair. Other comparisons with recent annealing work at these temperatures serve as a basis for identifying the various annealing peaks. The agreement between experiments is also discussed.

Energy release in neutron-irradiated copper (1.7×10^{20} fast neutrons at 40°C) between 600 and 700°K has been measured by means of nuclear heating.[25] If the value 7.7 cal/mole is used for energy released after the irradiation, it is possible to estimate the number of defects annihilated. The assumption is that the annealing results from the migration and then annihilation of a single defect. When this method was used, the results calculated to account for the observed energy release were 5×10^{19}/mole interstitials, 2×10^{20}/mole vacancies, 4×10^{19}/mole interstitial-vacancy pairs, and 1×10^{12} cm/mole dislocations. Blewitt[26] and others have also reported on the hardening effects of neutron damage in copper. Their results seem to support a dislocations locking mechanism but are not conclusive as yet. Makin and Minter[27] have also studied irradiation-hardened nickel as well as copper. Meager results support Seeger's theory based on the dislocation locking mechanism due to generated obstacles. The dislocation hardening component is shown to be independent of temperature in copper but not nickel. They make no conclusions as to the mechanism of formation of the obstacles. Vacancy loops formed during neutron irradiation of copper and nickel are used by Greenfield and Wilsdorf[28] to explain radiation hardening. Doses up to 2×10^{19} nvt at 70°C produced loops from 50 to 250 A.

Neutron-radiation-enhanced diffusion in copper at 425°C has been studied by Goland[29] by observing helium-gas precipitation at grain boundaries according to methods developed by Barnes. This temperature in copper is below the temperature for self-diffusion so that the vacancies produced during irradiation are necessary for the gas precipitation. The size of the voids produced here is equal to the size of those produced at higher temperatures in unirradiated specimens. It is hoped that further work will allow a more quantitative analysis of the enhanced diffusion.

Annealing of neutron damage has been observed[30] in copper as low as 7.2°K. In studying the kinetics of annealing in neutron-irradiated copper and aluminum below 40°K, Blewitt, Coltman, and Klabunde observed a monotonic increase in activation energy with temperature. Both the isothermal and the change-in-slope method were used to measure the activation energies which turned out anomalously high. They concluded that the activation energy for the annealing in this range is not unique, and hence the analysis of the rate equation does not apply under these conditions.

Deuteron irradiation of tungsten shows a rate of damage almost proportional to $1/E$, where E is the energy of the incident deuterons.[31] This indicates that the mechanism necessary to explain secondary-defect production must have a weak energy dependence when averaged over a coulomb energy spectrum. For example, hard-sphere potentials yield an energy dependence of the form $(1 + \ln cE)$, where c depends on the masses of the deuterons and target.

Vacancy annealing in body-centered cubic metals has been discussed[32] in a survey on the mechanical properties and radiation damage in body-centered cubic transition metals. Mechanical deformation near room temperature will produce lattice vacancies. Electrical-resistivity measurements show that these defects have an activation energy for diffusion of 1.0 ev for nio-

bium, 1.3 ev for molybdenum, 1.35 ev for tantalum, and 1.7 ev for tungsten. Similar results are obtained in neutron-irradiated niobium, molybdenum, and tungsten. Vacancy annealing in niobium and molybdenum is accompanied by an increase in yield stress.

Divacancy migration has been observed in irradiated molybdenum[33] in the range of 200 to 400°C. There is also strong evidence in this temperature range for lattice interaction with interstitial lattice atoms, dislocations, and interstitial impurity atoms. Studies in copper show that the increase in residual resistivity can be explained in terms of the buildup of foreign atoms due to transmutation.

Annealing of neutron damage to doses of 10^{18} nvt (fast) has been studied[34] in iron irradiated from 35 to 78°K. Resistivity is measured at 20°K after various anneals. Two processes have been studied, the first at 100°K with an activation energy of 0.22 ev and the second at 200°C with an activation energy of 1.4 ev.

Niday[35] reports the range of 28 different fission products in metallic uranium. Radiochemical measurements of the amount of material leaving the surface are used to infer the ranges. Specifically, the mean range of a certain mass chain is found. The results agree with a semiempirical formula between the ranges and the initial velocities. Reliability of this method is discussed, and the results are reported to 1 per cent. Plots of range versus mass number show a definite lowering in total kinetic energy release (seen as a reduction in range) for U^{235} in the region of nearly symmetrical fission (mass numbers 104 to 130). Peaks appear in this curve at mass ratio of 1.25 which are very similar to the peaks in the fission-yield versus mass-number curve. This peaking of total kinetic energy released is also observed by other experimenters in ionization-chamber studies and direct velocity measurements. These results are not readily explainable with present theories.

Ranges of 2- to 60-kev recoil atoms of copper, silver, and gold have been measured by foil-sandwich techniques.[36] The recoils were produced by photoneutron reactions so that their energy could be varied by changing the bremsstrahlung energy and angle of incidence, relative to emission of the photons. The results were fitted to a theoretical model of Holmes and Liebfried for the range-energy relations so that the arbitrary constant now has an experimentally determined value. Rates of energy loss of carbon and oxygen ions passing through carbon, aluminum, nickel, silver, and gold absorbers have been measured in the energy interval[37] of 0.36 to 3.2 Mev. The results are reported to about 5 per cent and compared with theory. Ranges can be determined by numerical integration.

Rare-gas ions were accelerated up to 40 kv into metal films and foils.[38] No lattice distortion was observed with X rays even when 2 at.% argon was loaded into the metal lattice. This suggests that rare-gas ions coming to rest in such a lattice capture vacancies. Heating the bombarded foils in a mass spectrometer revealed interesting variations between different metals and gas ions. Further work incorporating these two techniques seems very promising for the study of rare gases in crystals.

The disoriented crystallites formed in the surface of silver crystals[39] during 130-ev argon positive-ion bombardment have now been studied at bombarding temperatures from 100 to 400°C and at various current densities of positive ions. The range of the angles occupied by disoriented crystallites decreases as either the temperature of bombardment increases or the ion current decreases. The results suggest that annealing effects are accelerated by the presence of point defects produced during the irradiation. Conclusions are drawn with regard to cleaning surfaces by ion bombardment. There appears to be no new texture structure induced by annealing. However, surface perfection should be sought by means of high-temperature, low-current-density bombardments.

Ferromagnetic relaxation behavior in irradiated nickel[40] was used to measure an activation energy of 0.81 ± 0.01 ev with an interstitial-atom-migration energy of 1.02 ± 0.03 ev. The damage was produced at 25°C with an integrated flux of 4×10^{17} nvt (fast) for 4 hr.

Defects in Metal Alloys. Ogilvie[41] discusses the surface effects produced in metals and metal alloys by bombardment with inert-gas ions having energies up to 4 kev. Metal atoms are reported to be knocked off the surface in preferred directions. It is also shown that metal atoms are driven into the material. Results of argon bombardment of Cu_3Au show a uniform surface layer that is rich in gold. The gold concentration decreases with gas-ion energy, being 68 at.% for 30-ev argon ions and 45 at.% for 3-kev ions. X-ray data indicate the high uniformity of this

damaged layer which suggests the necessity of a rapid discontinuity at some transition point in order to return to the original concentrations. Similar results are obtained with helium and xenon ions for bombarding energies in the range 14 ev to 3 kev.

Kernohan and Wechsler[42] have extended their studies of neutron-irradiated copper–15 at.% aluminum alloy from irradiation temperatures of 45 to 250°C. A metastable state below 200°C is eliminated by the enhanced atomic mobilities after irradiation. The activation energy for motion remains constant at about 0.5 ev. These results are compared with previous results of lower temperature irradiations.

Magnetic properties of 29 alloys of nickel, silicon, aluminum, and cobalt with iron were studied after a neutron irradiation[43] of $1.7 \times 10^{18}/cm^2$ (total) at 50°C. The anisotropy of highly ordered crystals, such as iron, nickel, silicon-iron, and low aluminum-iron, remains unchanged. Crystals of the highly disordered systems, nickel-iron, cobalt-iron, and high aluminum-iron, show a variation of anisotropy often corresponding to a decrease in order. The magnetostriction constants change, and their variation cannot be described in terms of ordering phenomena. The conclusion is reached, therefore, that at least two mechanisms are responsible for changes in the magnetic properties of these materials: changes in short-range order and the generation of point defects which affect the interaction of near neighbors. Nickel-iron properties are also affected by electron irradiation. Annealing studies in aluminum-iron show an increased rate of ordering in the irradiated specimens which is explained in terms of enhanced diffusion by means of the excess defects.

Defects in Other Materials. Micron-size interstitial loops have been observed[44] in neutron-irradiated graphite (3×10^{20} nvt at 300°C). These loops can be distinguished from vacancy loops because their Burger's vectors are in different directions. This produces different contrast effects in the electron microscope which allow the separation of loop types as suggested by Amelinckx and Delavignette. Eeles[45] thinks he has observed interstitial loops in graphite from small-angle X-ray scattering experiments. His irradiations were in the region of 150°C.

Neutron damage in graphite has been observed to force the carbon layers apart.[46] At 30°C, X-ray measurements indicate that this spacing can increase by about 16 per cent before saturation. As the irradiation temperature is increased, the spacing increase becomes less and saturation occurs at a lower level; e.g., there is only a 1 per cent spacing increase at 500°C. This damage which affects the physical properties of graphite can be annealed out. At present, the exact form of the defects producing this damage is not known.

Fission-recoil tracks have been observed[47] in thin flakes of mica by transmission electron microscopy. Tracks less than 300 A in diameter and greater than 4 μ in length have been seen superimposed on a general background produced by the neutron bombardment. Track damage has also been observed in the alkali halides[48] by means of transmission electron microscopy in replicas that were taken off cleavage faces previously damaged. Irregularly shaped tracks with cross sections in the region of 1 μ have been observed as well as smaller cross-sectional events.

The volume of damage produced per primary in fast-neutron-irradiated silica[49] was found to be $(67\ A)^3$. The volume was found from the intensity of scattered light. Angular dependence of the scattered light suggested that the regions of damage were rod shaped with a length of about 1800 A. These regions contain a volume approximately equal to the damaged volume calculated from macroscopic changes as well as from other estimates.

X-ray diffraction has shown that lithium precipitates out of LiF during neutron irradiation.[50] Large doses produce face-centered cubic lithium in epitaxially thin plates on the LiF lattice. Heating transforms this anomalous face-centered cubic structure to the ordinary body-centered cubic structure. The results are in good agreement with data from differential thermal microanalysis. X-ray line broadening of neutron-irradiated $BaSO_4$ reveals that the broadening is due to strains in the lattice as opposed to particle size.[51] Imperfections are found along (0 0 1) planes separated vertically by a distance of 1100 A.

Theories of Radiation Effects

Distribution of vacancy-interstitial pairs produced by successive knock-ons has been calculated for a substance like germanium.[52] A Monte Carlo method is used which was originally pro-

posed by Bohr and Seitz and Koehler. The ratio of close pairs to total pairs for a 10^4-ev primary is about 60 per cent. Taking into account replacement collisions, this ratio is reduced to about 30 per cent. The pairs exist in a region enveloped by a sphere with a diameter of 50 to 100 atomic distances. There is no tendency for the damage to concentrate in the direction of the primary, nor do the interstitials distribute themselves in the outer part of the damaged region.

A study was made of the defect cascades produced by high-energy radiations in crystals.[53] Various energy spectra were found to have little effect on the cascades, which leads to the conclusion that in nearly all practical cases one comes out mathematically with a very satisfactory approximation to the hard sphere. Balarin and Hauser[54] also show that in reactor neutron irradiations all collisions between primary knock-on atoms and other atoms of the same solid can be treated as collisions between hard spheres. This changes the often-used expression for the number of displaced atoms from $n = E_0/2E_d$ to $n = E_0/5E_d$. Considering this energy principle, the number of possible displacements in present theories is reduced by a factor of 2.5.

Lattice relaxation around the interstitial is used to calculate self- and migration energies of carbon and xenon in graphite.[55] Strains are calculated from equations for bending plates, assuming the graphite structure to be thin elastic plates held together by weak forces. These plates are subjected to transverse forces due to the interstitial atoms. A choice of suitable interaction energies between the interstitial and all other atoms is necessary for the final calculation. Self-energy in carbon is reported as 2.5 ev, and in xenon as 15.1 ev. Dienes has previously reported a value of 12.9 ev for carbon. Iwata et al. state that this difference suggests the importance of considering the lattice relaxation in doing such calculations. Migration energies are 0.016 ev for carbon and 0.03 ev for xenon. Ratios of strain energy to total self-energy are 0.49 in carbon and 0.79 in xenon.

A semiempirical method developed to evaluate interaction energies of close impurity-atom-interstitial pairs has been reported.[56] This theory indicates that undersize impurity atoms provide deep traps for interstitials, whereas oversize impurity atoms furnish several shallow traps with different interaction energies. The method was applied to annealing in irradiated copper. Stage II is interpreted as the liberation and annihilation of several kinds of shallow-trapped interstitials. Stage III is explained as the liberation and annihilation of deep-trapped interstitials.

Calculations by Schottky[57] on the various energies of trivacancy structures in the noble metals have been completed. He extends this theory in gold and compares it with experiments[58] by discussing the equilibrium concentrations of single-, di-, and trivacancies with temperature.

Analytical expressions have been developed[59] for the assessment of neutron damage in solids, which includes the dependence on the neutron-energy spectrum. A method of comparing spectra in terms of damage produced is discussed, as well as expressions for damage as a function of time and neutron energy.

Surveys on Radiation-Induced Defects

A summary of the radiation damage in body-centered cubic metals has been presented by Thompson.[60] The report indicates the consistency in drawing inferences from face-centered cubic experiments. Most of the conclusions are based on such analyses. Much of the experimental work has been previously reported.[61,62] Thompson[63] has also presented a discussion on the observed nature of primary radiation damage in solids. This discussion points out the importance of focusing collisions and the necessity of including such focusing energies when comparing theories to experiments.

Koehler[64] discusses the production and annealing out of radiation damage in noble metals and ordered alloys. He states that 1.4-Mev electrons occasionally produce secondary displaced atoms, whereas 9-Mev deuterons produce clusters containing up to 10^4 displaced atoms and pile damage produces even larger regions of displacement. Thermal spikes, focusing, and alloy disordering are also discussed. A survey has been made on the general effects produced by radiation damage in cladding materials.[65] Fast-neutron damage that produces point defects and dislocation loops is considered, as well as gas-bubble formation. The effects of these defects on the mechanical properties are discussed.

Three general reviews of the effects of radiation in metals should be mentioned; their authors are Peckner,[66] Seitz,[67] and Billington[68] et al.

Smith[69] and Hickman[70] presented papers at a recent symposium on Phase Transformations in Metals. Both papers are in the form of surveys. Smith reported on radiation-induced phase transformations in metals and alloys, and Hickman's paper was concerned with the nucleation and growth of gas bubbles in irradiated metals.

Billington and Crawford[71] have published a book entitled *Radiation Damage in Solids*. The review is general but not necessarily comprehensive (in the authors' own words) and is slanted toward the experimental solid-state scientist. The treatment begins with a general introduction that leads into a discussion of the interactions between radiation and matter and their consequent influence on properties. The main analysis of effects is separated by means of the materials in which the damage is produced: metals, alloys, covalent crystals, minerals, ionic crystals, and semiconductors. Special chapters are added for the damage effects in uranium and graphite because of their importance and interest.

(T. G. Knorr)

Effects of Radiation on Mechanical Properties of Nonfuel Materials

The relative effectiveness of cladding and its influence on fuel materials during irradiation was investigated at Hanford.[72] Metallic and ceramic fuel elements were clad with Zircaloy-2, stainless steel, and aluminum alloys and then irradiated. Changes in the relative strength properties of fuel cladding and bond areas were noted in the Zircaloy-2–uranium system. Interface materials in the stainless steel–uranium and the Zircaloy-2–UO_2 systems were studied. The burst strength of Zircaloy-2 tubes containing UO_2 has been investigated at Bettis[73] after irradiation. These were blanket fuel rods of the PWR core 1 which were irradiated to total integrated fast fluxes (>0.6 ev) of 4.1×10^{21} to 5.5×10^{21} neutrons/cm^2. A comparison of the burst strengths of irradiated and unirradiated Zircaloy-2 tubes is shown in Table IV-1. These data show an approximately 25 per cent increase in burst strength after irradiation. The tensile properties of annealed Zircaloy-2 irradiated to 7.13×10^{20} neutrons/cm^2 (>1 Mev) were determined by Phillips Petroleum.[74] The change in properties is shown in Table IV-2. These data show an increase of approximately 50 and 20 per cent in the 0.2 per cent offset yield strength and ultimate tensile strength, respectively.

In work at Oak Ridge[75] the tube-burst properties of AISI type 304 stainless steel are being investigated while being subjected to fluxes of 2×10^{13} neutrons/(cm^2)(sec) (>1 Mev). The rupture life is being determined as a function of time at specific tangential stresses. The results show rupture times for test conditions in and out of reactor at 1500 and 1600°F. These data are given in Table IV-3. In Table IV-4 the results of tube-rupture tests at 1300°F are given for the in-reactor conditions but not for the out-of-reactor conditions. It appears that, at a test temperature of 1500°F for the range of stresses studied, the rupture strength is reduced by 1500 psi under neutron bombardments. Insufficient data are available for a comparison at 1300 and 1600°F.

The effect of irradiation on the welds in AISI type 304 stainless steel has been investigated at Savannah River.[76] The type 304 stainless-steel plate welded with type 308 filler metal was irradiated at <100°C to maximum exposures of 1.2×10^{21} fast neutrons/cm^2 (>0.1 Mev). The increase in tensile strength and the decrease in ductility in the weld metal, heat-affected zone, and the parent plate are shown in Figs. IV-1 to IV-3.

The effect of postirradiation annealing on the impact properties of pressure-vessel steels has been investigated at the Naval Research Laboratory.[77] They have found that heat-treatment is effective in recovery of notch ductility properties for those materials irradiated at <200 and at 575°F. The effectiveness of particular heat-treatments was strongly dependent on irradiation temperature. Recovery was not as complete for steels irradiated at 575°F as for

Table IV-1 POSTIRRADIATION BURST STRENGTH OF ZIRCALOY-2 TUBES[73] CONTAINING UO_2

Burst pressure, psi	Calculated tensile strength, psi	Total integrated fast flux (>0.6 ev), 10^{21} neutrons/cm^2
11,000	80,000	0
11,500	83,000	0
14,900	108,000	4.1
13,300	96,000	4.3
14,200	103,000	4.5
14,600	106,000	4.7
13,700	99,000	5.1
14,200	103,000	5.3
13,200	95,000	5.5
13,200	95,000	5.7
13,700	100,000	4.9

Table IV-2 DATA OBTAINED FROM TESTING IRRADIATED AND NONIRRADIATED TENSILE SPECIMENS OF VARIOUS MATERIALS[74]

Material	Radiation received, nvt >1 Mev	Yield strength (0.2% offset), psi	Ultimate tensile strength, psi	Elongation in 1 in., %	Reduction of area, %	Rockwell Hardness	
						Before	After
2024, Al	0	45,300	71,600	26	29	B71	
2024, Al	2.04×10^{19}	48,700	71,100	25	32	B71	B68
2024, Al	1.22×10^{20}	48,200	74,300	26	36	B71	B71
2024, Al	5.59×10^{20}	56,100	79,400	25	27	B71	B77
2024, Al	9.84×10^{20}	66,200	84,900	24	29	B71	B79
6061, Al	0	40,000	47,200	21	46	B44	
6061, Al	5.17×10^{20}	43,700	50,200	22	49	B44	B46
6061, Al	1.17×10^{21}	42,800	51,900	21	48	B43	B50
356, Al	0	26,000	33,100	4	6	B33	
356, Al	2.04×10^{19}	29,100	36,700	6	10	B32	B36
356, Al	1.22×10^{20}	33,500	42,000	6	7	B29	B45
356, Al	5.59×10^{20}	42,400	45,900	6	6	B32	B52
356, Al	9.84×10^{20}	52,100	54,400	3	6	B32	B57
Inconel X SA	0	163,300	203,400	22	41	C38	
Inconel X SA	1.78×10^{20}	194,600	195,700	12	47	C37	C36
Inconel X SA	5.86×10^{20}	205,500	205,500	11	44	C37	C36
Inconel X SA	2.20×10^{21}	201,100	201,200	11	44	C39	C34
Inconel X SA	3.47×10^{21}	194,800	197,900	12	39	C37	C39
Inconel X DA	0	118,000	174,000	29	36	C26	
Inconel X DA	8.54×10^{20}	174,000	180,500	12	42	C28	C32
Inconel X DA	1.40×10^{21}	169,000	178,000	10	35	C27	C33
Inconel 702	0	90,500	145,300	44	53	B94	
Inconel 702	8.54×10^{20}	*	172,000	13	53	B94	C27
Inconel 702	1.40×10^{21}	171,500	171,500	14	53	B99	C28
17-4 PH, S.S.	0	144,700	148,500	16	65	C25	
17-4 PH, S.S.	2.04×10^{19}	179,400	181,000	13	53	C26	C32
17-4 PH, S.S.	1.30×10^{20}	194,500	197,000	12	44	C26	C33
17-4 PH, S.S.	5.14×10^{20}	205,500	206,400	11	44	C26	C35
17-4 PH, S.S.	1.18×10^{21}	209,500	209,900	10	41	C26	C35
17-4 PH, S.S.	2.87×10^{21}	214,300	215,400	9	29	C25	C34
304 S.S.	0	77,200	107,500	46	68	B97	
304 S.S.	2.04×10^{19}	126,300	126,900	32	61	B98	C24
304 S.S.	1.30×10^{20}	129,300	130,000	31	66	B98	C24
304 S.S.	5.14×10^{20}	129,600	131,200	32	61	B98	C25
304 S.S.	1.18×10^{21}	130,500	130,500	33	61	B97	C25
304 S.S.	2.87×10^{21}	129,200	129,400	31	65	B97	C24
304 S.S.†	5.72×10^{21}	103,300	113,800	50	68	B91	C27
304 S.S.‡	5.72×10^{21}	103,700	114,200	54	68	B91	C26
304 S.S.§	5.72×10^{21}	100,600	111,700	50	66	B92	C24
316 S.S.	0	67,100	91,400	60	76	B92	
316 S.S.	1.20×10^{19}	101,200	105,200	44	68		A59
316 S.S.	9.90×10^{19}	104,800	108,300	44	68		A60
316 S.S.	5.62×10^{20}	107,500	109,400	42	68		A59
316 S.S.	1.28×10^{21}	107,100	110,600	42	67		C19
347 S.S.	0	67,200	96,200	56	68	B93	
347 S.S.	5.17×10^{20}	116,400	116,600	36	64	B93	C21
347 S.S.	7.96×10^{20}	116,600	117,000	35	65	B93	C20
347 S.S.	4.74×10^{21}	115,900	116,400	36	62	B93	C28
347 S.S.¶	4.74×10^{21}	107,000	116,900	34	63	B94	C29

Table IV-2 (Continued)

Material	Radiation received, nvt >1 Mev	Yield strength (0.2% offset), psi	Ultimate tensile strength, psi	Elongation in 1 in., %	Reduction of area, %	Rockwell Hardness Before	Rockwell Hardness After
AM-350, S.S.	0	156,300	194,800	18	46	C40	
AM-350, S.S.	5.9×10^{19}	191,600	217,400	13	44	C41	C41
AM-350, S.S.	1.17×10^{20}	192,400	220,000	16	50	C41	C42
AM-350, S.S.	7.31×10^{20}	207,000	226,900	16	57	C40	C46
Zircaloy-2	0	56,400	77,400	29	44	B87	
Zircaloy-2	5.9×10^{19}	74,200	89,500	19	44	B88	B94
Zircaloy-2	1.17×10^{20}	73,900	89,600	19	44	B87	B93
Zircaloy-2	7.31×10^{20}	84,400	93,300	19	44	B87	B94

*Yielded before 0.2 per cent offset.
†Single specimen.
‡Single specimen annealed 5 hr at 640°F.
§Single specimen annealed 22 hr at 640°F.
¶Single specimen annealed 4 hr at 640°F.

Table IV-3 RESULTS OF TUBE-BURST TESTS OF TYPE 304 STAINLESS STEEL IN AIR IN THE ORR[75]

[Flux: 2×10^{13} neutrons/(cm^2)(sec) (>1 Mev)]

Specimen	Stress, psi	Temp., °F	Irradiation dose at rupture, Mw-hr	Time to rupture, hr
*, †	6300	1500	0	510‡
*, †	6300	1500	0	490
97	6300	1500	0	184
*, †	5800	1500	0	690
*, †	5250	1500	0	1330
*	5250	1500	0	1250
9-7	5000	1500	5,400	337
9-8	5000	1500	8,300	518
*, †	4200	1500	0	2450
*	4200	1500	0	1650
7-3	4000	1500	12,300	895
9-6	4000	1500	8,900	672
17-3	4000	1500	36,900	851§
17-10	3500	1500	50,080	>1600¶
17-1	3000	1500	50,080	>1600
17-9	3000	1500	50,080	>1600
17-8	5060	1600	3,750	49
*, †	3700	1600	0	265
17-5	3000	1600	13,500	414
17-6	2600	1600	27,100	870
17-4	2200	1600	43,900	1430
17-7	2200	1600	47,400	>1505**

*Out-of-pile specimens.
†These specimens are 6 in. long. All other specimens are 2½ in. long.
‡All out-of-pile data were received from J. W. Woods and J. T. Venard of the ORNL Metallurgy Division. The stresses were recalculated to correspond with those used for the in-pile specimens.
§This specimen was stressed after 11,500 Mw-hr of irradiation at 1500°F.
¶Three specimens held at 1500°F had not ruptured when the experiment was terminated.
**This test was terminated when the thermocouples failed and control was lost.

Table IV-4 RESULTS OF IN-PILE TUBE-BURST TESTS OF TYPE 304 STAINLESS STEEL AT 1300°F IN AIR[75]

[Flux: 10^{13} neutrons/(cm^2)(sec) (>1 Mev)]

Specimen	Stress, psi	Time to rupture, hr
15-2	13,000	130
3	13,000	197*
6	13,000	144
8	13,000	122
4	11,000	512
7	11,000	480
10	11,000	462
1	9,000	1680
5	9,000	>1850†
9	9,000	>1850†

*Irradiated at 1300°F for approximately 8400 Mw-hr prior to application of stress.
†Test concluded before rupture.

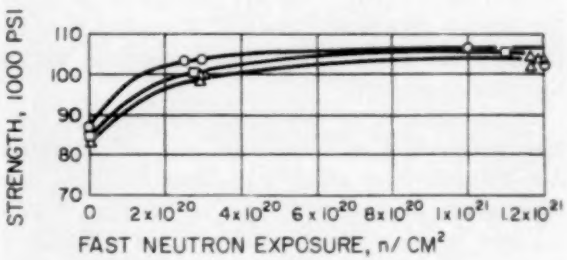

Fig. IV-1 Effect of irradiation on the ultimate strength of welded stainless steel.[76] ○, weld metal. □, heat-affected zone. △, parent plate.

those irradiated at <200°F. It was also noted that a short-time heat-treatment of a few hours was just as effective as a long-term treatment for the recovery of radiation-induced transition-

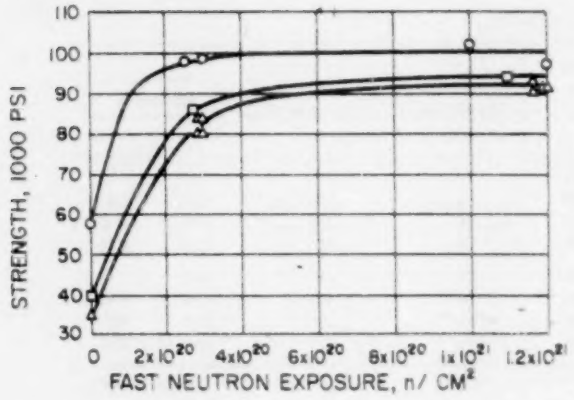

Fig. IV-2 Effect of irradiation on the yield strength of welded stainless steel.[76] ○, weld metal. □, heat-affected zone. △, parent plate.

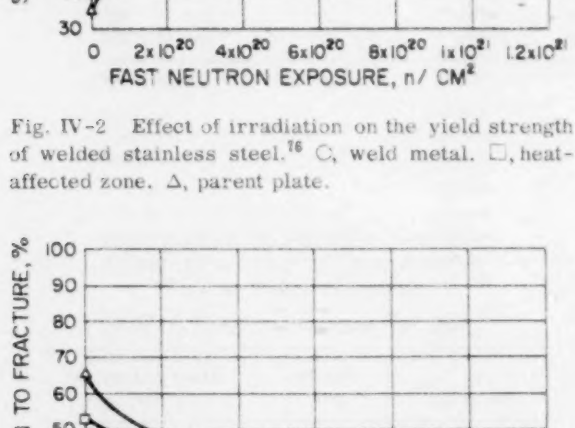

Fig. IV-3 Effect of irradiation on the ductility of welded stainless steel.[76] ○, weld metal. □, heat-affected zone. △, parent plate.

temperature shifts. The percentage of recovery for steels irradiated at < 200°F appeared to be independent of total neutron exposures within the ranges studied.

A comparison of the room-temperature tensile properties of irradiated and unirradiated AM-350 stainless steel, a hardenable alloy, has been made at Hanford[78] and at Phillips.[74] The changes in properties as determined at Hanford are shown in Table IV-5.

Data reported by Phillips are shown in Table IV-2. Although the unirradiated properties reflect a difference in lot variation of material, these differences apparently are reduced by irradiation. The exposures reported are the greatest to date for many of these materials. The effect of short-time annealing on the properties of types 304 and 347 stainless steel irradiated to 5.72×10^{21} neutrons/cm^2 has produced a slight reduction in yield strength and ultimate strength after heat-treatment, but the resulting strengths were still approximately 60 and 20 per cent, respectively, higher than the unirradiated stainless steels.

Table IV-5 ROOM-TEMPERATURE TENSILE PROPERTIES OF IRRADIATED AND UNIRRADIATED AM-350 STAINLESS STEEL[78]

Flux, thermal neutrons/ cm^2	Yield strength (0.2% offset), 1000 psi	Ultimate tensile strength, 1000 psi	Elastic modulus, 10^6 psi	Elongation, %	
				Uniform	Total
0	171.3*	209.9	33.1		10
7×10^{19}	186.5	217.7	30.2	5.4	7.4
3.19×10^{20}	199.0	225.8	29.7	3.5	5.9
6.25×10^{20}	206.5	230.5	28.7	4.0	5.4

*0.1 per cent offset.

Workers at Oak Ridge[75] have been studying the effect of elevated-temperature irradiation (500 to 700°C) on beryllium. Specimens from material prepared by hot pressing, hot extrusion, and hot rolling were compared. Bend tests conducted at room temperature after 1.0 to 1.5×10^{20} neutrons/cm^2 (>0.66 Mev) exposure indicate that embrittlement has not resulted from the irradiation. Photomicrographs show some increased porosity after irradiation.

(F. R. Shober)

Selected Metallurgical Aspects of Cladding and Structural Materials

Aluminum

Armour[79] investigated dispersion strengthening of corrosion-resistant aluminum alloys by powder-metallurgical methods. The tensile strength of extruded rods was tripled by dispersions made with powders of Al_2O_3, $AlPO_4$, SiO_2, B_4C, and SiC. Corrosion resistance was not affected.

An extensive study by Roberts[80] of the effects of powder-metallurgy fabrication of both commercial and experimental aluminum-base alloys has led to the following conclusions:

1. The powder-metallurgy fabrication of aluminum alloys of current commercial analyses (3003, 2024, 5083, and 7075 alloys) will result in very significant refinement of the microconstituents present in the alloys, accompanied by

greatly increased resistance to recrystallization.

2. In the experimental aluminum-zirconium-magnesium-copper precipitation-hardening alloy system, extrusions of highly alloyed composition are producible which do not recrystallize during solution heat-treatments.

3. Extrusions that are structurally inhomogeneous may be obtained from structurally and chemically homogeneous supersaturated alloy powders due to accelerated precipitation in the most highly worked zone of the extrusion. This results in the presence of a surface zone or skin of the most desirable type of microstructure. The degree of structural inhomogeneity between the extrusion surface and its center will decrease as the amount of the sluggish elements in supersaturated solid solution is increased.

4. The use of excessively high extrusion temperatures or prolonged exposure to temperatures above the 800 to 900° F range will alter the characteristics of the dispersions and reduce the amount of strain hardening of the matrix.

Chromium-Alloy Systems

High-purity alloys of the chromium-nickel-niobium system with a range of up to 50 wt.% niobium were investigated by the Russians.[81] Quasi-binary sections were constructed in the examined part of the ternary system, as well as isothermal sections at 1100 and 1175°C. A new ternary intermetallic compound was discovered with a composition of approximately $Ni_8Cr_5Nb_2$. This compound crystallized from the liquid state at 1175 ± 5°C and disintegrated at 1160 ± 5°C, undergoing a eutectoid transformation.

Additional research by the Russians[82] on the chromium-nickel system (limits of 50 per cent nickel) showed that eutectoid transformations in this system are actually absent. The variation of the solubility of nickel in chromium with temperature (determined roentgenostructurally) indicates that this solubility falls sharply from 40.50 per cent nickel to practically zero on lowering of the temperature from 1340 to 850°C.

(J. A. DeMastry)

Niobium-Alloy Systems

The phase diagram of the ternary system, niobium-molybdenum-vanadium, was determined by Russian investigators[83] utilizing melting-point observations and microstructural examination. Unlimited solid solubility was found. While establishing the solidus curve, it was found that the melting point is lowered from 2450 to 1800°C as the vanadium content is increased. The niobium corner of the diagram presented the lowest hardness in the system, ranging from 105 to 220 kg/mm^2. The highest heat resistance was shown by alloys with high niobium content; those containing large amounts of molybdenum and vanadium were easily oxidized.

The following characteristic temperatures in the niobium-NbC phase diagram were determined by workers at Los Alamos:[84] a eutectic temperature between $NbC_{0.08}$ and $NbC_{0.39}$ of 2335 ± 20°C, a peritectic temperature between $NbC_{0.52}$ and $NbC_{0.56}$ of 3090 ± 50°C, and a melting-point maximum at about $NbC_{0.86}$ of 3500 ± 75°C. Congruent vaporization *in vacuo* takes place at a composition near $NbC_{0.71}$ at 2800°C. At about 2000°C, Nb_2C has a very narrow range of homogeneity. Lattice parameters for the Nb_2C phase in equilibrium at the phase boundary were found to be $a_0 = 3.128 \pm 0.001$ A, $c_0 = 4.972 \pm 0.001$ A when NbC was present and $a_0 = 3.126 \pm 0.001$ A, $c_0 = 4.965 \pm 0.001$ A when the niobium phase was detected.

A large number of stacking faults in niobium with their associated partial dislocations were demonstrated by transmission electron microscopy by European Associates investigators.[85] Photomicrographs show some aspects of the stacking-fault ribbons within which the characteristic interference fringe can be seen. These ribbon dislocations cover an extensive area; thus it is possible to observe, in certain cases, the interaction of the individual particles. These are similar to those observed by Whelan on stainless steel and by Matthews on evaporated foils of silver, gold, and copper.

Elastic constants of single crystals of vanadium, niobium, and tantalum were reported by Westinghouse[86] at $T = 27$°C. They are, in units of 10^{11} dynes/cm^2 for C_{11}, C_{12}, and C_{44}: vanadium, 22.8, 11.9, 4.26; niobium, 24.6, 13.4, 2.87; and tantalum, 26.7, 16.1, 8.25, respectively. The shear anisotropies, $A = 2C_{44}/(C_{11} - C_{12})$, are anomalously small for these elements as compared with other cubic-system elements. An analysis of the shear anisotropy, based on Fueh's model, is given, and it was found essential that the next nearest as well as nearest neighbor ion-ion interaction be considered.

The results of preliminary studies at Oak Ridge[87] on the aging behavior of wrought

niobium–1 wt.% zirconium alloys follow: The aging phenomena in the niobium-zirconium alloy were influenced by the annealing temperature. Higher annealing temperatures led to more pronounced aging effects. No correlations were found between observed aging effects and surface contamination from the experimental containers used or from the annealing furnace. The aging or nonaging behavior of the alloys could be correlated with their oxygen-nitrogen ratio and to a lesser extent with their oxygen-carbon ratios. There was a positive correlation between the amount of oxygen added to the alloy and the tendency for aging to occur; when sufficient oxygen was added, the aging tendency could be virtually eliminated.

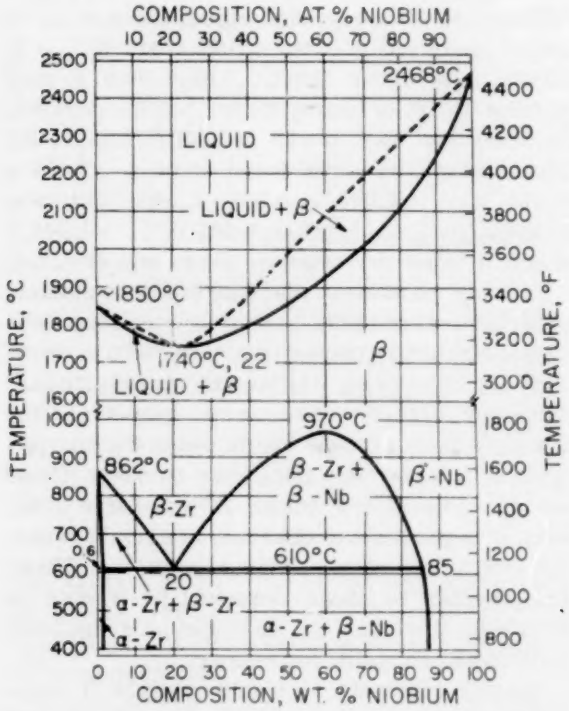

Fig. IV-4 Equilibrium phase diagram of the zirconium-niobium alloy system.[13]

Figure IV-4 shows the equilibrium phase diagram of the niobium-zirconium alloy system which was determined by the Division of Reactor Development of the AEC.[13]

(J. A. DeMastry)

TiN Dispersion in Molybdenum

Research on molybdenum performed in England[88] has resulted in the development of a highly stable dispersion of TiN in molybdenum. This stable dispersion was obtained by isothermal heat-treatment in nitrogen of a 1 wt.% titanium-molybdenum alloy in the temperature range of 1100 to 1500°C.

(J. A. DeMastry)

Zirconium-Alloy Systems

The zirconium-dysprosium phase diagram determined by the Bureau of Mines[89] shows a single eutectic system with the eutectic isotherm extending from 30 to 95 wt.% dysprosium at 1280°C. The solid solubility of dysprosium in beta zirconium is of the order of 30 wt.% at 1280°C and decreases to approximately 10 wt.% at 890°C. At this temperature the peritectoid reaction occurs and extends over the range of composition from 10 to more than 80 wt.% dysprosium. The maximum solubility of dysprosium in alpha zirconium appears to be 12 wt.% at 690°C and decreases to approximately 7 wt.% at 400°C.

The effects of beryllium and uranium in Zircaloy-2 are reported by Hanford.[78] Additions of 0.35 to 4.20 wt.% beryllium and 0.0 to 4.8 wt.% beryllium with 250, 500, 750, 1500, and 2500 ppm uranium were studied. Metallographically, the beryllium tends to separate as a second phase after a 30-min heat-treatment at 900°C followed by a cold-water quench even at concentrations as low as 0.35 wt.% beryllium. The phase diagram indicates solid solubility up to 2 wt.% beryllium at this temperature. At 1.95 wt.% beryllium the basic Zircaloy structure changes to a dendritic structure in a matrix of the intermetallic compound $ZrBe_2$. At 3.26 wt.% beryllium the dendritic structure gives way to the eutectic structure. Uranium is not readily observed in the structure up to 500 ppm. There does, however, appear to be an apparent increase in the tendency to form subgrains in the Zircaloy with an increase in the uranium content. The microhardness increases sharply from 200 DPH for 0.35 wt.% beryllium to 380 DPH for 4.2 wt.% beryllium. Uranium appears to make the structure harder and more brittle.

The effects of nitrogen on the lattice constants, unit cell volume, and hardness of zirconium as reported by Bettis[90] are shown in Figs. IV-5 to IV-7, respectively.

Chalk River,[91] after extensive study of the effects of hydrogen in zirconium, has published data on hydrogen solubility (Table IV-6). Results show that increasing niobium content pro-

Table IV-6 TERMINAL SOLID SOLUBILITY OF HYDROGEN VERSUS TEMPERATURE[91]

Temp., °C	Terminal solid solubility, ppm			
	Zirconium	Zircaloy-2	Zirconium–1.9 wt.% niobium	Zirconium–2.6 wt.% niobium
260		71	127	
300		95	167	179, 174
350		203	233	334, 324
400	~220	270	326	557, 557
450	320	473	499	
500	496	638	888	

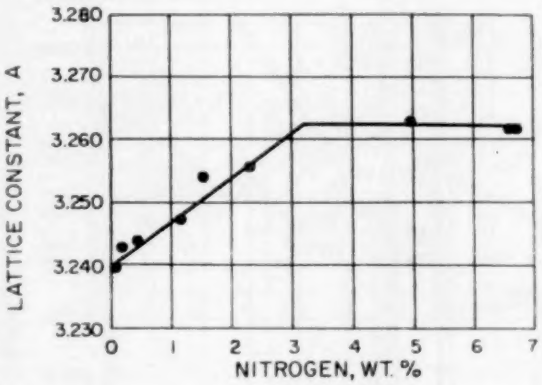

Fig. IV-5 Lattice constant versus wt.% nitrogen.[90]

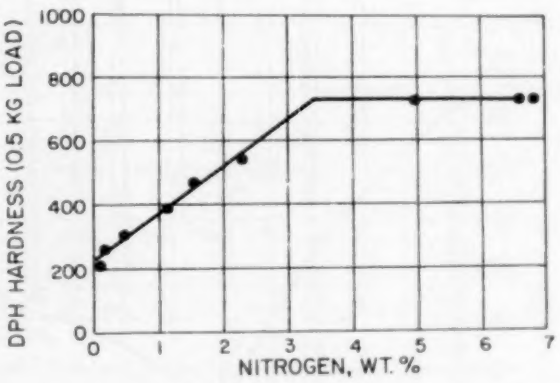

Fig. IV-7 Hardness versus wt.% nitrogen.[90]

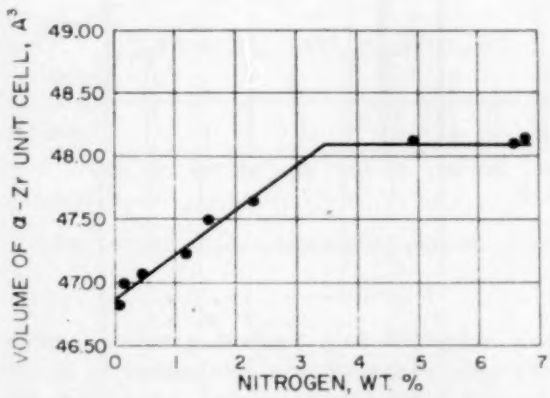

Fig. IV-6 Volume of alpha-zirconium unit cell versus wt.% nitrogen.[90]

duces a corresponding increase in hydrogen solubility. The heat of transport for hydrogen in zirconium alloys containing yttrium and niobium is shown in Table IV-7.

Yttrium-Alloy Systems

Figures IV-8 to IV-10 show phase relations for yttrium-iron, -nickel, and -copper, respectively, as determined by Denver Research.[92]

A summary of the phase relations of yttrium and selected rare-earth metals was presented by Research Chemicals.[93] Erbium and yttrium form simple binary eutectic systems with titanium. No compounds are present. The transition temperature of titanium is not significantly affected. Copper, tin, and calcium form intermetallic compounds with erbium and yttrium. The melting points of the rare earths are rapidly lowered, eutectics forming with the respective compounds. Vanadium forms extensive (and chromium limited) liquid immiscibility regions with erbium and yttrium. Eutectics are formed at the rare-earth end of these systems. Terminal solubilities are low in all of the above systems.

The erbium-zirconium system is characterized by appreciable solubility of zirconium in erbium and extensive solubility of erbium in both alpha and beta zirconium. A high-temperature peritectic reaction involving beta erbium is suggested. The yttrium-zirconium system is similar in all major respects except that the solubility limits at both ends of the system are somewhat lower. Preliminary investigation of

Table IV-7 HEAT OF TRANSPORT OF HYDROGEN IN ZIRCONIUM ALLOYS[91]

Alloy	Time, days	Temp. range, °C	Initial concentration, ppm	Heat of transport, kcal/mole
Zirconium–0.5 wt.% yttrium	47	300–496	72	5.8
	47	302–494	72	5.7
Zirconium–2.6 wt.% niobium	41	302–497	68	5.9
	41	300–496	68	5.3

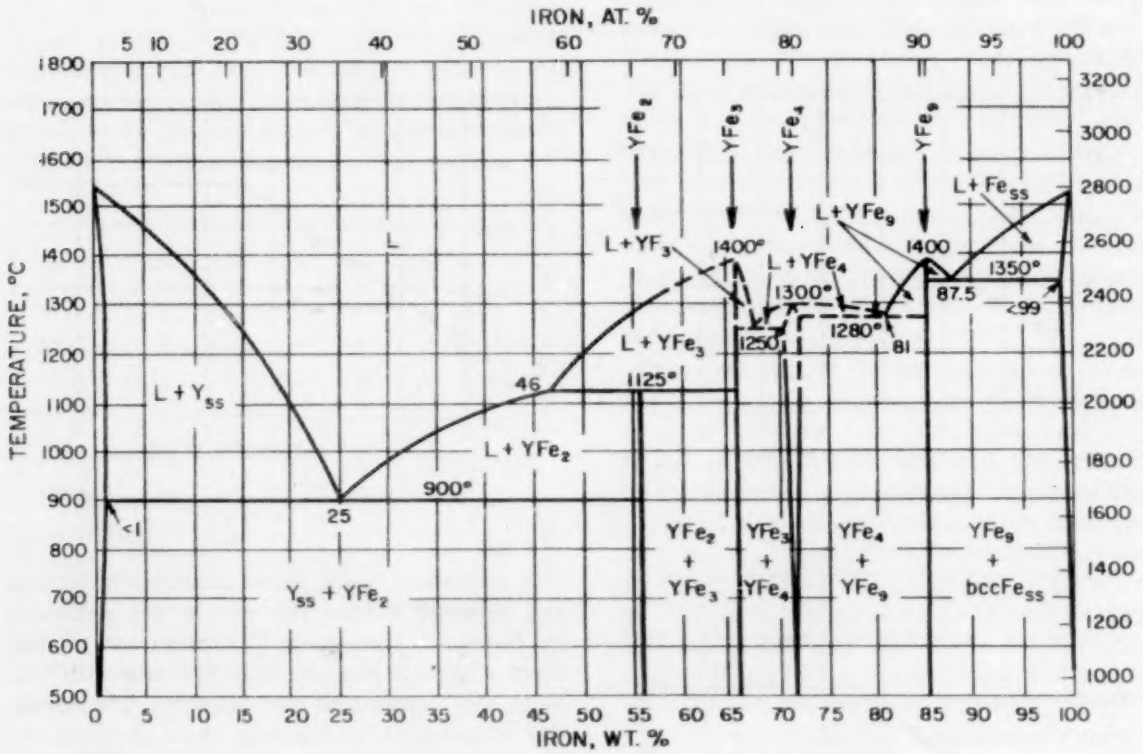

Fig. IV-8 Phase relations of the yttrium-iron system, showing temperatures of peritectic and eutectic reactions.[92]

the gadolinium-zirconium system also indicated similarity in all major respects.

Beryllium and yttrium form an intermetallic compound. The terminal solubility of yttrium in beryllium is low. No eutectic reaction is observed at the beryllium end of the system.

(J. A. DeMastry)

Diffusion Studies

In studies at Battelle[94] the thermal diffusion of hydrogen in beta zirconium was investigated at two compositions, $ZrH_{0.44}$ and $ZrH_{0.86}$, and at temperatures from 630 to 860°C. A diffusion cell containing a sample of zirconium hydride was subjected to a thermal gradient, and the hydrogen pressure was determined at the hot and cold ends of the specimen. From the variation of pressure with temperature, the heat of transport could then be determined. It was found that the results varied little with composition; however, the heat of transport was found to increase with temperature, ranging from 6 to 12 kcal/mole. The thermal conductivity was found to vary with increasing temperature from 0.042 to 0.052 cal/(cm)(sec)(°C). The thermal diffusion of hydrogen in Zircaloy-2 has been investigated at Hanford.[95] The distribution of absorbed hydrogen within Zircaloy-2 process tubes under various thermal-gradient conditions was studied

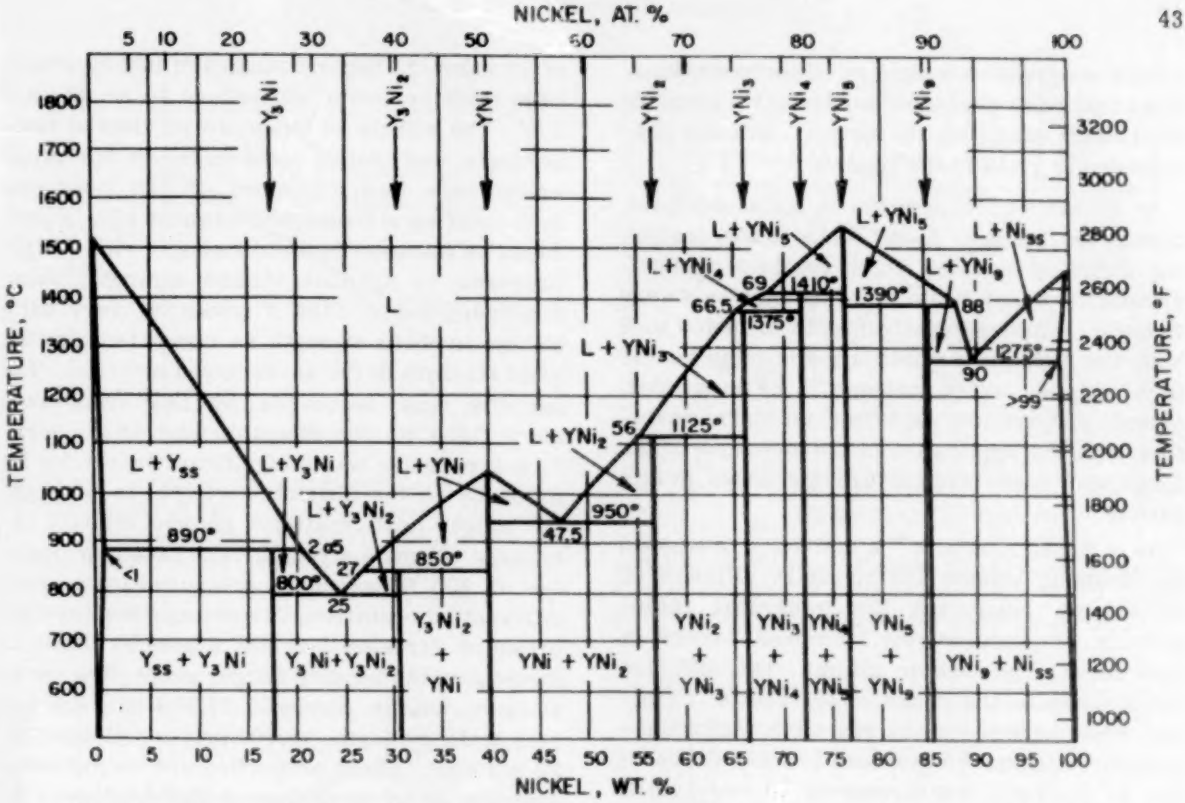

Fig. IV-9 Phase relations of the yttrium-nickel system, showing temperatures of peritectic and eutectic reactions.[92]

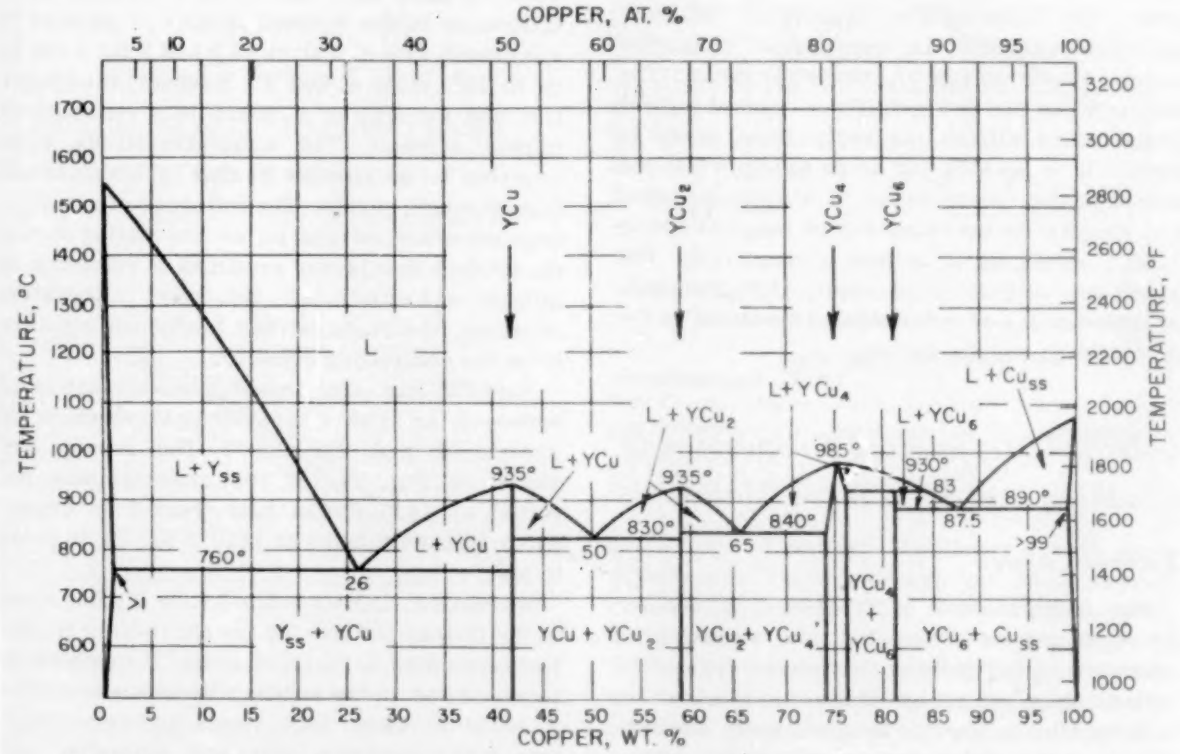

Fig. IV-10 Phase relations of the yttrium-copper system, showing temperatures of peritectic and eutectic reactions.[92]

in this program. A summary of the basic equations that were developed to predict the behavior of systems exhibiting the thermal-diffusion phenomenon is given in the report.

In an article[96] of a book on X-ray analysis, Lublin describes an X-ray technique for analyzing diffusion couples which employs a monochromatic X-ray beam that impinges on a very fine slit, a holder for aligning the diffusion zone with the slit, and a scintillation counter for the high counting rates that are to be measured. Sample preparation, experimental instrumentation, and the application of the technique to the aluminum-nickel system are discussed in this article.

In a Russian article[97] a method is discussed for studying volume and boundary diffusion of metals by measuring the integrated radioactivity of successively removed layers of specimens. The author claims that diffusion coefficients in the range of 10^{-13} to 10^{-14} cm^2/sec could be determined with ease. Autoradiographic techniques were used to make it possible to perform measurements on very small samples. In the case of relatively refractory metals (such as iron, chromium, cobalt, nickel, zirconium, tantalum, molybdenum, and tungsten), the temperature dependence of self-diffusion assumes an exponential character beyond the threshold of recrystallization. The author notes that the mobility of atoms at a given temperature differs markedly from metal to metal. It is pointed out as an example that the self-diffusion coefficients of aluminum, iron, and tungsten in the temperature range of 500 to 1000°C differ by 10 orders of magnitude. The paper also includes a discussion of studies made of diffusion and of the bonding of the atoms in the iron-carbon-silicon system.

(D. C. Carmichael)

Selected Mechanical Properties of Cladding and Structural Materials

Zirconium Alloys

The extensive use of Zircaloy-2 in nuclear reactors and its anticipated use has prompted continued investigation of its mechanical properties. Many variables such as fabrication, heat-treatment, service temperatures, and service conditions are being investigated to determine their effect on the mechanical properties of Zircaloy-2. Several studies of this type have been made by Bettis (references 14, 98, 99*a*, and 100). The effects of temperature, time at temperature, and cooling rates on the tensile properties have been examined. It was found that heat-treating at temperatures above 1700°F produced an increase in yield strength with a slight decrease in ultimate tensile strength. Heat-treatment below 1750°F produced very little change in yield strength as compared with the yield strength of the as-received material. The ductility was decreased by heat-treatments above 1450°F. The effect of time at temperature apparently was insignificant except for its influence on the ultimate strength; in this case the longer heat-treatment showed slightly increased ultimate strength. The tensile properties at 600°F have been measured by several different laboratories. The average tensile properties of Zircaloy-2 at 600°F used by Bettis to investigate the bending fatigue properties were: ultimate tensile strength, 33,350 psi; 0.2 per cent yield strength, 18,500 psi; and elongation, 39 per cent. These properties are for material annealed 20 hr in vacuum at 750°C followed by furnace cooling. The results obtained are summarized graphically in Figs. IV-11 to IV-14. These graphs show that there is no significant difference in the notched fatigue properties of specimens with K_t values of 3 and 9 for a life of up to 10^6 cycles at 600°F. However, for longer life and for a K_t of 9, there is a reduction of fatigue strength. The notch sensitivity, q, is reported to be similar to that of titanium and high-strength steels. The influence of a superimposed static stress on an alternating stress on notched specimens produces a reduction in fatigue strength. At the lower alternating stresses, the static-stress component appears to be the controlling condition.

Bettis[100] has also investigated the effect of hydrogen on the Charpy-impact strength of Zircaloy-2 and Zircaloy-4. The results are shown in Fig. IV-15. The material was hot rolled at 1475°F and heat-treated in argon-filled Vycor capsules at 1450°F for 24 hr prior to test.

Workers at Carborundum[90] have studied some of the factors influencing the short-time tensile tests on rolled Zircaloy-2 at 600°F, a procedure incorporated in the military specification MIL-Z-19859 in 1959. Such items as temperature variation, specimen size and geometry, and strain rate were considered. At Du Pont[101] the

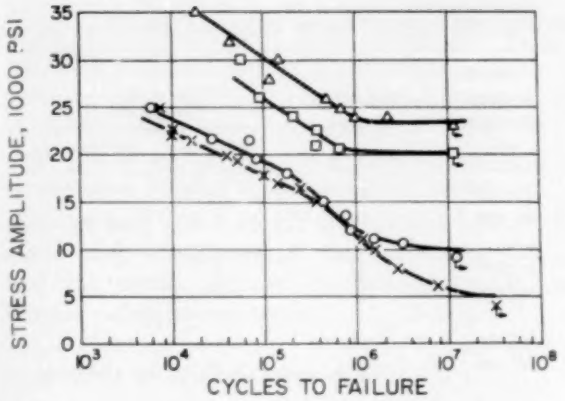

Fig. IV-11 Zircaloy-2 base annealed; reversed bending fatigue tests at 600°F zero mean stress; heat OM-160 tensile properties at 600°F; ultimate tensile strength 33,350 psi; 0.2% offset yield strength 16,500–22,500 psi; per cent elongation[90] 33–44. Δ, K_t = 1; □, K_t = 1.6; ○, K_t = 3.0; ×, K_t = 9.

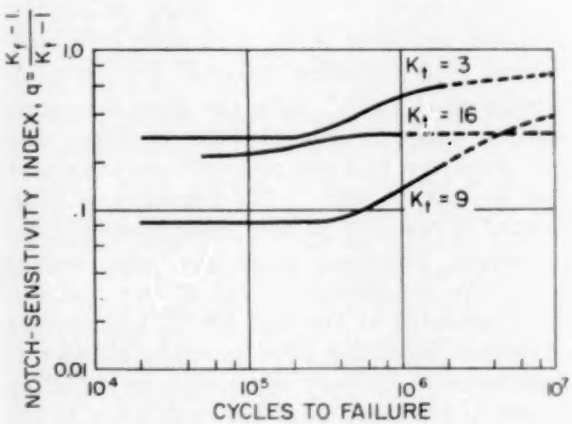

Fig. IV-12 Zircaloy-2, base-annealed condition.[90]

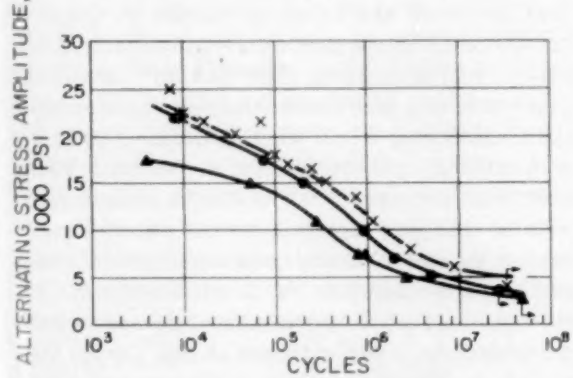

Fig. IV-13 Combined bending and static-load fatigue tests on Zircaloy-2, base annealed, notched specimens; K_f = 9; heat[90] OM-160. $A = \frac{\sigma \text{ alternating}}{\sigma \text{ static}}$; × = A = ∞; ● = A = 1.7; ▲ = A = 0.6.

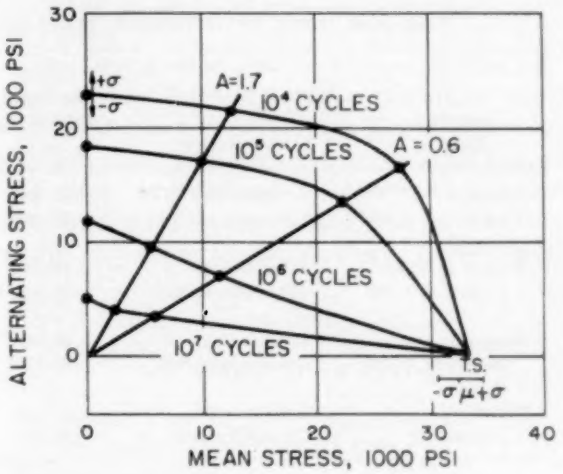

Fig. IV-14 Modified Goodman diagram for Zircaloy-2, base annealed, V-notched specimens; K_t = 9; combined bending and static fatigue tests[90] at 600°F.

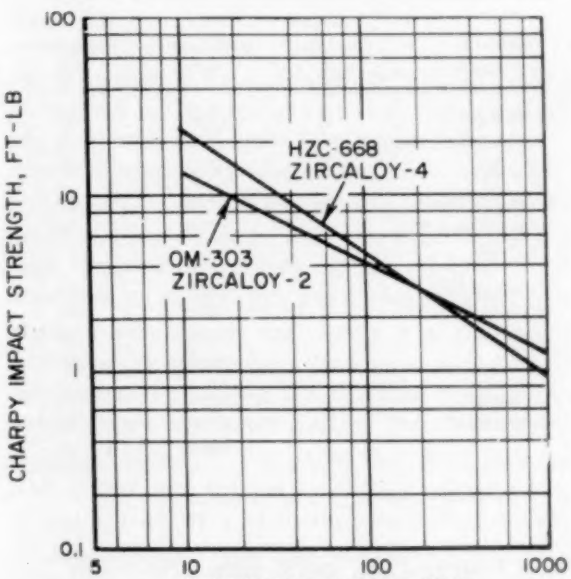

Fig. IV-15 Charpy impact strength[100] versus hydrogen content for Zircaloy-2 ingot OM-303 and Zircaloy-4 ingot HZC-668.

properties of swaged Zircaloy-2 sheath were determined. These sheaths had been swaged around UO_2 powder. The results from additional tensile and tube-burst tests are shown in Tables IV-8 and IV-9. A very extensive study was made by Knolls[102] on the mechanical and physical properties of Zircaloy-2. Approximately 470 specimens from one ingot were used to examine five test variables. Those included

Table IV-8 RESULTS OF TENSILE TESTS ON ZIRCALOY-2 SHEATHS AT ROOM TEMPERATURE[101]

Material condition	Orientation	Yield strength (0.2% offset), psi	Ultimate tensile strength, psi	Reduction of area, %	Elongation, %	
					Uniform	To fracture
As-received; annealed, 2.204 in. OD	Longitudinal	47,000	73,300	45	15	21
	Circumferential	68,000	77,400	52	6	18
Swaged in three passes to 2.065 in. OD	Longitudinal	78,500	81,600	36	8	8
	Circumferential	71,000	87,400	38	3	6
Swaged in two passes to 2.128 in. OD	Longitudinal	68,000	75,500	44	11	13
	Circumferential	57,000	82,100	48	5	11
Vibratory compacted	Longitudinal	47,000	71,400	48	17	22
	Circumferential	61,000	73,400	54	10	18

Note: All specimens had a gauge length of 2 in. and a width of 0.500 in.

Table IV-9 RESULTS OF HYDRAULIC BURST TESTS ON ZIRCALOY-2 SHEATHS AT ROOM TEMPERATURE[101]

Material condition	Stress ratio, σ_a/σ_λ*	Max. pressure, psi	Max. local elongation, %
As-received; annealed, 2.204 in. OD	½	2900	46
	0	2700	65
	0	2700	80
Swaged in three passes to 2.065 in. OD	½	3400	16
	0	3000	32
Swaged in two passes to 2.128 in. OD	½	3250	18
	½	3500	20
	0	3050	70
	0	3050	48
Vibratory compacted	½	2700	52
	½	3100	42
	0	2600	90

*σ_a = axial stress, σ_λ = hoop stress.

were temperature, grain size, anisotropy, hydrogen content, and specimen geometry. The results on tensile properties, creep properties, low-cycle fatigue, and thermal-expansion coefficient are given.

A number of investigations on the properties of Zircaloy-2 are being carried out by the Canadians.[91] The effect of hydrogen in the form of hydride has been studied using Charpy-impact specimens and drop-weight specimens. No effect was noted from a 10-μ-thick hydride layer on Charpy-impact specimens tested between room temperature and 300°C. Drop-weight tests on specimens containing 30 ppm precipitated hydride showed crack penetration through the entire thickness of 0.25-in. plate only after the test temperature was decreased to −80°C. Plates 0.4 in. thick having 7 ppm hydrogen behaved similarly at −115°C. Creep properties, both long and short term, of 19.3 per cent cold-worked NPD prototype material are being investigated at 300°C. Data are given for specimens in tests as long as 8400 hr. Other data are given for 18.5 per cent cold-worked material in test at 400°C. The recovery of cold-worked Zircaloy-2 is also being studied by the Canadians. Materials which were cold worked at the two conditions, 12 and 25 per cent, are being annealed at 300 and 400°C. Comparison of tensile properties after annealing shows that considerable recovery is achieved by annealing at 400°C for three days but very little in 180 days at 300°C.

Other zirconium alloys receiving somewhat less attention are those developed to improve the elevated-temperature strength and corrosion behavior of zirconium. The British[103] have been experimenting with a zirconium-niobium-copper alloy containing 2 to 7 wt.% niobium, 0.25 to 3.0 wt.% copper, and the balance zirconium. These additions increased the strength considerably without changing significantly the corrosion behavior or the thermal-neutron-capture cross section. The addition of 5 wt.% niobium to a zirconium−1 wt.% copper alloy appears to have increased the creep strength at 500°C by a factor of 4. The short-time hardness and creep properties of binary zirconium alloys have been investigated by the Russians.[104] Greatest increase in creep resistance in alpha solid solutions was attained with 5 to 10 at.% titanium and 1 to 5 at.% tin. The least creep-resistant alloy

was found to be the 50 at.% zirconium-titanium alloy. The Canadians[91] have creep tested, at 300, 400, 450, and 500°C, a zirconium–2.5 wt.% niobium alloy which had been heat-treated 1 hr at 880°C, water quenched, and annealed in vacuum for 6 hr at 500°C. At 300°C, twice the stress was needed to produce the same creep rate as was obtained for Zircaloy-2 under the same test conditions. It was noted, however, that the creep strength decreased rapidly at temperatures above 400°C.

Properties of Nickel-Base Alloys

Inconel X, Inconel 713C, and Hastelloy X continue to hold promise for many high-temperature nuclear-reactor applications. Investigation of the tensile, stress-rupture, and creep properties of Inconel X at 1000, 1200, and 1400°F have been completed at Langley Research Center.[105] The effect of six different heat-treatments was studied. Aging heat-treatments gave the greatest 10-hr rupture strengths at all test temperatures. Shorter aging times gave material with superior stress-rupture properties at 1400°F. A good summary of the data is presented. Creep-rupture tests conducted by General Atomic[106] show that the creep properties of Inconel X in helium at 1300°F are about the same as those in air at 1500°F. The fatigue properties of Inconel 713C have been determined at 1500°F in helium and at 1300°F in a helium-air mixture. Investigators at Aerojet-General[10] have determined the tensile properties at room temperature of Hastelloy X after exposure to nitrogen plus 0.5 per cent oxygen mixture, air, high-purity nitrogen, and nitrogen plus 0.1 per cent carbon monoxide mixture. Reductions in ultimate tensile strength, yield strength, and ductility after long-time (1000 to 5000 hr) exposures to these gases have been noted. It was thought that reduction in properties was associated with excessive formation of a carbidelike second phase. A considerably lesser effect was noticed after a 5000-hr exposure when tensile testing was done at 1750°F. Oak Ridge[15] has studied the creep properties of Inconel and other nickel-base alloys at elevated temperatures in hydrogen and in argon. The secondary creep rate of these alloys was observed to be greater in hydrogen than in argon. The rupture life was also shorter in hydrogen. This effect was most noticeable in Inconel. There was not, however, an associated decrease in ductility with the reduction in rupture life.

Two stainless steels, AISI types 304 and 347, were also included in a similar investigation and showed similar behavior and secondary creep rates in both hydrogen and argon. Oak Ridge[75] has also pressurized as-received type 304 stainless-steel tubing at 1300°F in air. The results are given in Table IV-10. A number of

Table IV-10 RUPTURE LIFE OF PRESSURIZED AISI TYPE 304 STAINLESS-STEEL TUBING[75] IN AIR AT 1300°F

Tangential stress, psi	Time to rupture, hr
7,951	1077
8,069	2007
9,710	469
9,821	549
11,403	144
11,593	144

other materials have been subjected to an atmosphere of 5 vol.% hydrogen–95 vol.% nitrogen (70 per cent water saturated) at General Electric.[107] The materials studied in creep include types 302, 316, A-286, and 17-7 PH stainless steels, as well as René 41 and Inconel 702, two nickel-base alloys. Test temperatures as high as 1950°F and stresses to 45,000 psi were investigated. The rupture strength of each alloy was less in the gas-mixture atmosphere than in air at high temperatures. The lower temperature creep properties were not influenced by the atmosphere. General Atomic[106] compared the creep properties in air and helium at 1000°F of two materials, a 1.25 wt.% chromium–0.5 wt.% molybdenum steel and type 316L stainless steel. They were found to be the same under these conditions. Creep and creep-rupture data are given for the 1.25 wt.% chromium steel at 1000 and 1200°F and for the type 316L stainless steel at 1300 and 1500°F.

Mechanical Properties of Miscellaneous Metals

The tensile and creep properties of unalloyed tantalum have been studied at Battelle[99b] at elevated temperatures. The tensile strength ranged from 25,000 psi at room temperature to 31,000 psi at 500°C. The rupture and creep properties were determined at 750 and 1200°C.

The mechanical properties of molybdenum and molybdenum-base alloys were studied at Climax.[99c] Alloys containing 0.5 wt.% titanium, 0.05 wt.% zirconium, and 0.5 wt.% titanium plus 0.07 wt.% zirconium were tested at room temperature, 1800, and 2400°F. The effect of carbon contents varying from 0.019 to 0.053 wt.% was investigated. The best elevated-temperature strength was shown by the molybdenum–0.5 wt.% titanium–0.07 wt.% zirconium alloy. There did not appear to be any change in properties associated with the carbon content.

The tensile, compressive, stress-rupture, and creep shear properties of QMV beryllium have been investigated by Brush[99d,99e] in the room temperature to 1500°F range. The effects of purity, grain size, and other processing variables were evaluated on the basis of mechanical properties. The temperature dependency of these properties is illustrated. The creep properties were studied for beryllium having high oxide content. The data indicate that the oxide improved the creep strength of beryllium. The degree of anisotropy was shown to influence the creep resistance at low temperatures but did not significantly affect the properties at the elevated temperatures. Workers at Oak Ridge[75] have examined the stress-rupture strength of beryllium tubing machined from hot-pressed blocks. The method of metal preparation and fabrication definitely influences the creep properties. The results are shown in Fig. IV-16.

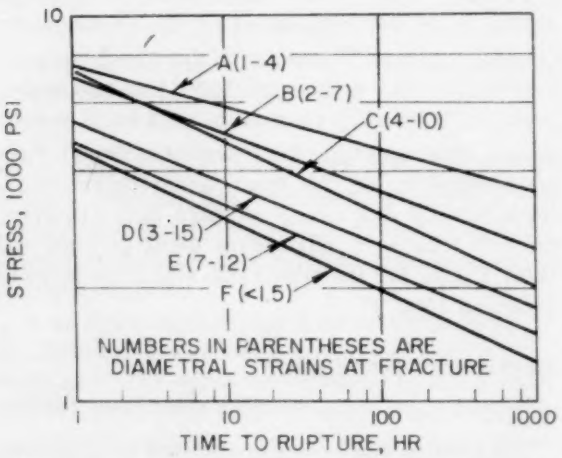

Fig. IV-16 Stress rupture of beryllium tubes[75] at 600°C. *A*, machined from hot-pressed block, Brush Beryllium Co. *B*, machined from warm-extruded rod, Brush Beryllium Co. *C*, warm extruded, Brush Beryllium Co. *D*, Pechiney. *E*, Imperial Chemical Industries. *F*, Chesterfield.

Investigations pertaining to the development of niobium and niobium-base alloys are being conducted at Westinghouse. The effect of oxygen and nitrogen additions on the hardness and fabrication properties of niobium were studied at Westinghouse.[99f] The tensile yield strength of several ingots of niobium prepared by different techniques was evaluated over the –200 to 250°C temperature range. The purest material gave the lowest strength values.

A good summary of the mechanical and physical properties of magnesium and magnesium alloys has been prepared by the British.[14] This data manual includes 34 references, among which are a few pertaining to properties measured after irradiation. (F. R. Shober)

References

1. J. V. Cathcart and F. W. Young, Jr., Influence of Reactor Radiation on the Oxidation of Niobium, *Corrosion*, 17(2): 77–79 (February 1961).
2. D. M. Lakhiani and L. L. Shrier, Crystallization of Amorphous Niobium Oxide During Anodic Oxidation, *Nature*, 188: 49–50 (Oct. 1, 1960).
3. T. Hurlen et al., Oxidation of Niobium, Technical (Scientific) Note No. 1, Norwegian Report NP-7850, April 1959.
4. J. C. Bokros and H. E. Shoemaker, Maritime Gas-Cooled Reactor Program. Reactor Materials Compatibility with Impurities in Helium, USAEC Report GA-1508, General Atomic Div., General Dynamics Corp., Jan. 12, 1961.
5. Oak Ridge National Laboratory, Feb. 9, 1961. (Unpublished)
6. Oak Ridge National Laboratory, Mar. 9, 1961. (Unpublished)
7. R. Bakish, Metallographic Manifestations of the Air Oxidation of Tantalum at 750°C, *J. Electrochem. Soc.*, 105(2): 71–74 (February 1958).
8. Sylvania-Corning Nuclear Corp., High-Temperature Oxidation-Resistant Coatings for Tantalum-Base Alloys, Report SCNC-323, March 1961.
9. W. D. Klopp et al., Development of Protective Coatings for Tantalum-Base Alloys, Feb. 15, 1961.
10. Aerojet-General Nucleonics, Army Gas-Cooled Reactor Systems Program, Semiannual Progress Report, July 1 to December 31, 1960, USAEC Report IDO-28567, Feb. 22, 1961.
11. A. Moskowitz and L. Redmerski, Corrosion of Superalloys by Selected Fused Salts, Report WADD-TR-60-115, Crucible Steel Co. of America, March 1960.
12. R. Bakish and F. Kern, Selective Corrosion of Inconel, *Corrosion*, 16: 533t–534t (November 1960).
13. Nuclear Fuels and Materials Development,

USAEC Report TID-11295(Suppl.), February 1961.
14. B. J. Seddon and E. L. Francis (Comps.), Magnesium Data Manual, British Report DEG-R-90, Jan. 5, 1960.
15. Oak Ridge National Laboratory, Apr. 6, 1961. (Unpublished)
16. J. J. Gill, Physical Condition of SRE Zirconium, USAEC Report NAA-SR-Memo-5842, Atomics International, Nov. 1, 1960; see also USAEC Report NAA-SR-5970, Dec. 15, 1960.
17. M. Makansi et al., Thermodynamic Properties of Sodium, *J. Chem. Eng. Data*, 5(4): 441–452 (October 1960).
18. W. Rostoker et al., *Embrittlement of Liquid Metals*, Reinhold Publishing Corp., New York, 1960.
19. Argonne National Laboratory, Chemical Engineering Division Summary Report for July, August, and September 1960, USAEC Report ANL-6231.
20. Argonne National Laboratory, Reactor Development Program Progress Report for October 1960, USAEC Report ANL-6253, Nov. 15, 1960.
21. W. F. Zelezny, Metal-Water Reactions: Rates of Reaction of Aluminum and Aluminum-Uranium Alloys with Water Vapor at Elevated Temperatures, USAEC Report IDO-16629, Phillips Petroleum Co., Nov. 25, 1960.
22. Phillips Petroleum Co., Materials Testing Reactor–Engineering Test Reactor Technical Branches Quarterly Report for January 1–March 31, 1960, USAEC Report IDO-16633, Oct. 3, 1960.
23. R. S. Nelson and M. W. Thompson, Atomic Collision Sequences in Crystals of Copper, Silver, and Gold Revealed by Sputtering in Energetic Ion Beams, *Proc. Roy. Soc. (London)*, A259(1299): 458–479 (Jan. 24, 1961).
24. A. V. Granato and T. G. Nilan, Stored Energy Release Below 80°K in Deuteron-Irradiated Copper, *Phys. Rev. Letters*, 6(4): 171 (1961); also see USAEC Reports TID-11311 and TID-12368.
25. T. H. Blewitt et al., Energy Release in Reactor-Irradiated Copper: II, 600° to 700°K Release, *Phys. Rev.*, 122(1): 53–57 (1961).
26. T. H. Blewitt et al., Radiation Hardening of Copper Single Crystals, *J. Nuclear Materials*, 2(4): 277–298 (1960).
27. M. J. Makin and F. J. Minter, Irradiation Hardening in Copper and Nickel, *Acta Met.*, 8(10): 691–699 (October 1960).
28. I. G. Greenfield and H. G. F. Wilsdorf, Observations Concerning the Radiation Hardening in Copper and Nickel, *Naturwissenschaften*, 47: 395–396 (1960).
29. A. N. Goland, Radiation-Enhanced Helium Precipitation in Copper, *Phil. Mag.*, [8] 6(62): 189 (February 1961).
30. T. W. Blewitt et al., Annealing Kinetics of Neutron-Irradiated Aluminum and Copper, *Australian J. Phys.*, 13(2a): 347–353 (July 1960).
31. D. R. Muss and J. R. Townsend, Energy Dependence of Radiation Damage in Tungsten, *J. Appl. Phys.*, 32(2): 189 (1961).
32. A. A. Johnson, Deformation, Fracture, and Radiation Damage in B.C.C. Transition Metals, *J. Less-Common Metals*, 2: 241 (1960).
33. F. W. Albaugh, Reactor and Fuels Research and Development Operation Monthly Report, December 1960, USAEC Report HW-67954-A, Hanford Atomic Products Operation, Jan. 15, 1961. (Classified)
34. C. Cassayre et al., Resistivity of Pure Neutron-Irradiated Iron, French Report CEA-1718. Reprinted from *Compt. rend.*, pp. 370–372 (1960).
35. J. B. Niday, Radiochemical Study of the Ranges in Metallic Uranium of the Fragments from Thermal Neutron Fission, *Phys. Rev.*, 121(5): 1471–1483 (Mar. 1, 1961).
36. V. A. J. van Lint et al., Range of 2- to 60-Kev Recoil Atoms in Cu, Ag, and Au, *Phys. Rev.*, 121(5): 1457 (1961).
37. D. I. Porat and K. Ramavataram, Rate of Energy Loss and Ranges of Carbon and Oxygen Ions in Solids, *Proc. Phys. Soc. (London)*, 77(493): 97–102 (January 1961).
38. C. W. Tucker and F. J. Norton, On the Location and Motion of Rare Gas Atoms in Metals, *J. Nuclear Materials*, 2(4): 329–334 (December 1960).
39. G. J. Ogilvie and A. A. Thompson, Influence of Temperature and Bombardment Rate on Disorientation of Silver Single Crystals by Ion Bombardment, *J. Phys. and Chem. Solids*, 17(3/4): 203–209 (January 1961).
40. H. Kronmuller et al., Ferromagnetic Hysteresis by Interstitial Atoms in Neutron-Irradiated Nickel, *Z. Naturforsch.*, 15a: 740–741 (August 1960).
41. G. J. Ogilvie, Bombardment of Metals by Inert Gas Ions, *Australian J. Phys.*, 13(2a): 402 (July 1960).
42. R. H. Kernohan and M. S. Wechsler, Neutron Irradiation of Cu-Al at Elevated Temperatures, *J. Phys. and Chem. Solids*, 18(2/3): 175–180 (February 1961).
43. R. C. Hall et al., Irradiation Effects on Single Crystals of Soft Magnetic Materials, Report ARL-TN-60-110, Westinghouse Electric Corp., June 1960.
44. G. K. Williamson and C. Baker, A Comparison of Vacancy and Interstitial Loops in Graphite, *Phil. Mag.*, [8] 6(62): 313 (February 1961).
45. W. T. Eeles, Small Angle X-Ray Scattering by Pile-Irradiated Graphite, *Nature*, 188: 287–289 (Oct. 22, 1960).
46. G. E. Bacon, Radiation Damage in Graphite, *J. chim. phys.*, 57: 828–836 (October 1960).
47. E. C. H. Silk and R. S. Barnes, Examination of

Fission Fragment Tracks with an Electron Microscope, *Phil. Mag.*, [8] 4(44): 970–972 (1959).

48. R. W. Dayton and C. R. Tipton, Jr., Progress Relating to Civilian Applications During March 1961, USAEC Report BMI-1509, Battelle Memorial Institute, April 1961. (Classified)
49. R. D. Maurer, Light Scattering by Neutron Irradiated Silica, *J. Phys. Chem. and Solids*, 17 (1/2): 44–51 (1960).
50. M. Lambert et al., Precipitation de Lithium dans les Monocristaux de Fluorure de Lithium Irradies aux Neutrons Thermiques, *J. Phys. Chem. and Solids*, 18(2/3): 129–138 (February 1961).
51. J. M. Luthra and V. M. Padmanabhan, X-Ray Study of Neutron Irradiated Barite ($BaSO_4$), *J. Sci. Ind. Research (India)*, 19B: 406–407 (October 1960).
52. M. Yoshida, Distribution of Interstitials and Vacancies Produced by an Incident Fast Neutron, *J. Phys. Soc. Japan*, 16(1): 44–50 (January 1961).
53. C. Lehmann, Zur Bildung von Defekt-Kaskaden in Kristallen Beim Beschuss mit Energiereichen Korpuskularstrahlen, German Report NP-9141, 1959.
54. M. Balarin and O. Hauser, Energy Considerations for Production of Radiation Defects, *Kernenergie*, 3: 973–978 (October–November 1960).
55. T. Iwata et al., On the Energy of the Interstitial Atom in Graphite, *J. Phys. Soc. Japan*, 16(2): 197–205 (February 1961).
56. R. R. Hasiguti, Impurity Trapped Interstitials and the Low Temperature Annealing Stages of Irradiated Copper, *J. Phys. Soc. Japan*, 15(10): 1807–1814 (October 1960).
57. G. Schottky, Theoretische Untersuchungen über Leerstellenkomplex in Edelmetallen, *Z. Physik*, 159(5): 584–601 (1960).
58. G. Schottky, Zur Deutung der Abschreckexperimente an Gold, *Z. Physik*, 160(1): 16–32 (1960).
59. J. S. Wicklund, Effects of Spectrum on Neutron Radiation Damage in Solids, Report DOFL-TR-803, Diamond Ordnance Fuze Laboratories, Dec. 15, 1959.
60. M. W. Thompson, Radiation Damage in Body-Centered Metals, British Report AERE-R-3560, October 1960.
61. M. W. Thompson, The Damage and Recovery of Neutron Irradiated Tungsten, *Reactor Core Materials*, 3(4): 38 (November 1960); *Phil. Mag.*, 5(51): 278–296 (March 1960).
62. G. H. Kinchin and M. W. Thompson, Irradiation Damage and Recovery in Mo and W, *Reactor Core Materials*, 3(4): 38 (November 1960); *J. Nuclear Energy*, 6(4): 275–284 (May 1958).
63. M. W. Thompson, The Observed Nature of Primary Radiation Damage, British Report AERE-R-3561, December 1960.
64. J. S. Koehler, The Nature of Irradiation Damage in the Noble Metals, University of Illinois Technical Report No. 17.
65. R. S. Barnes, Radiation Effects in Cladding Material, *Nuclear Power*, 5(53): 122–123 (September 1960).
66. D. Peckner, Radiation Damage in Metals, *Materials in Design Eng.*, 51(1): 89–93 (January 1960).
67. F. Seitz, Effect of Radiations on Metals, *J. chim. phys.*, 57: 677 (September 1960).
68. D. S. Billington et al., Advances in Radiation Effects, *Nucleonics*, 18(9): 63–86 (September 1960).
69. R. Smith, Irradiation-Induced Phase Transformations in Metals and Alloys, *J. Australian Inst. Metals*, 5(2): 163–172 (August 1960).
70. B. S. Hickman, Nucleation and Growth of Gas Bubbles in Irradiated Metals, *J. Australian Inst. Metals*, 5(2): 173–181 (August 1960).
71. D. S. Billington and J. H. Crawford, *Radiation Damage in Solids*, Princeton University Press, Princeton, N. J., 1961.
72. J. E. Minor, Irradiation Effects in Cladding Materials, USAEC Report HW-64688, Hanford Atomic Products Operation, Apr. 8, 1960.
73. B. Rubin, Examination of PWR Core 1 Blanket Fuel Rods for Microstructure, Hydrogen Pickup, and Burst Strength, USAEC Report WAPD-TM-264, Westinghouse Electric Corp., Bettis Atomic Power Laboratory, February 1961.
74. M. J. Graber and J. H. Ronsick, ETR Radiation Damage Surveillance Programs Progress Report I, USAEC Report IDO-16628, Phillips Petroleum Co., Jan. 27, 1961.
75. Oak Ridge National Laboratory, Gas-Cooled Reactor Project Quarterly Progress Report for Period Ending December 31, 1960, USAEC Report ORNL-3049, Mar. 9, 1961.
76. J. W. Joseph, Jr., Mechanical Properties of Irradiated Welds in Stainless Steel, USAEC Report DP-534, Savannah River Laboratory, December 1960.
77. J. R. Hawthorne and L. E. Steele, Preliminary Observations on the Effectiveness of Heat Treatment for Recovery of Properties of Irradiated Steels, Report NRL-5582, Naval Research Laboratory, Feb. 16, 1961.
78. F. W. Albaugh, Reactors and Fuels Research and Development Operation Monthly Report, February 1961, USAEC Report HW-68712-A, Hanford Atomic Products Operation, Mar. 15, 1961. (Classified)
79. Armour Research Foundation, Illinois Institute of Technology, Dispersed Phase Strengthening of Corrosion-Resistant Aluminum, USAEC Report ARF-2176-6, May 6, 1960.
80. S. G. Roberts, Research Study for Development of Aluminum Base Alloys by Powder Metallurgy Techniques, Report AD-241213, Kaiser Aluminum and Chemical Corp., Aug. 12, 1960.

81. V. N. Svechnikov and V. M. Pan, On the Phases of the Chromium-Nickel-Niobium System, *Dopovidi Akad. Nauk Ukr. R.S.R.*, No. 5: 634–637 (1960).

82. V. N. Svechnikov and V. M. Pan, On Transformations in a Chromium-Nickel System, *Dopovidi Akad. Nauk Ukr. R.S.R.*, No. 7: 917–920 (1960).

83. V. V. Baron, K. I. Ivanova, and E. M. Savitskii, The Phase Diagram of the Niobium-Molybdenum-Vanadium System and Certain Properties of Its Alloys, *Izvest. Akad. Nauk S.S.S.R.*, No. 4: 143–149 (1960).

84. E. K. Storms and N. H. Krikorian, The Niobium-Niobium Carbide System, *J. Phys. Chem.*, 64: 1471–1477 (October 1960).

85. A. Fourdeax and A. Berghezan, Observation by Transmission Electron Microscopy of Stacking Faults in a Body-Centered Cubic Metal: Niobium, *J. Inst. Metals*, 89: 31–32 (September 1960).

86. D. I. Boley, Elastic Constants of Single Crystals of the bcc Transition Elements V, Nb, and Ta, *J. Appl. Phys.*, No. 32: 100–105 (January 1961).

87. D. O. Hobson, A Preliminary Study of the Aging Behavior of Wrought Columbium–1% Zirconium Alloys, USAEC Report ORNL-2995, Oak Ridge National Laboratory, Jan. 27, 1961.

88. A. K. Mukherjee and J. W. Martin, Hardening of a Molybdenum Alloy by Nitride Dispersions, *J. Less-Common Metals*, 2: 392–398 (October 1960).

89. J. Croeni et al., Zirconium-Dysprosium Equilibrium Diagram, USAEC Report BM-RI-5688, Bureau of Mines, Sept. 10, 1959.

90. Westinghouse Electric Corp., Bettis Atomic Power Laboratory, Zirconium Highlights, USAEC Report WAPD-ZH-26, December 1960.

91. Atomic Energy of Canada, Ltd., 1961. (Unpublished)

92. R. F. Domagala, Phase Diagram Studies Final Report, USAEC Report APEX-583, General Electric Co., Aircraft Nuclear Propulsion Dept., March 1961.

93. B. Love, The Metallurgy of Yttrium and the Rare Earth Metals, Report WADD-TR-60-74, Nuclear Corp. of America, Research Chemicals Div., May 1960.

94. J. W. Droege, Thermal Diffusion in a Solid Solution of Hydrogen in Beta Zirconium, USAEC Report BMI-1502, Battelle Memorial Institute, Feb. 24, 1961.

95. R. E. Westerman, Thermal Redistribution of Hydrogen in Zircaloy-2 Process Tubes, USAEC Report HW-66196, Hanford Atomic Products Operation, August 1960.

96. P. Lublin, Analysis of Aluminum-Nickel Diffusion Couples by X-Ray Absorption, in *Advances in X-Ray Analysis*, Vol. 3, pp. 1–10, edited by W. M. Muelle, Plenum Press, New York, 1960.

97. P. L. Gruzin, Diffusion Laws and the Distribution of Elements in Alloys (in Russian), *Metalloved. i Termichesk. Obrabotka Metal., Sbornik Statei*, No. 10: 5–13 (October 1960).

98. Westinghouse Electric Corp., Bettis Atomic Power Laboratory, Zirconium Highlights, USAEC Report WAPD-ZH-25, October 1960.

99. Symposium on Newer Metals, *ASTM Special Tech. Publ. No. 272* (1960).
   a. J. G. Goodwin et al., Effect of Heat Treatments on the Tensile and Corrosion Properties of Zircaloy-2.
   b. F. C. Holden et al., High-Temperature Mechanical Properties of Tantalum.
   c. M. Senchyschen and R. Q. Barr, Mechanical Properties of Molybdenum and Molybdenum-Base Alloy Sheet.
   d. W. W. Beaver et al., Effect of Purity and Manufacturing Variables on Elevated-Temperature Properties of Beryllium.
   e. J. N. Hurd et al., Stress Rupture and Creep Properties of QMV Beryllium Metal.
   f. R. T. Begley and L. L. France, Effect of Oxygen and Nitrogen on Workability and Mechanical Properties of Columbium.

100. Westinghouse Electric Corp., Bettis Atomic Power Laboratory, Zirconium Highlights, USAEC Report WAPD-ZH-27, February 1961.

101. E. I. du Pont de Nemours & Co., Heavy Water Moderated Power Reactors Progress Report for December 1960, USAEC Report DP-575, March 1961.

102. R. L. Mehan and F. W. Wiesinger, Mechanical Properties of Zircaloy-2, USAEC Report KAPL-2110, Knolls Atomic Power Laboratory, February 1961.

103. G. C. E. Olds and J. E. Harris, Improvement in Zirconium Alloys, British Patent 857,835, Jan. 4, 1961.

104. V. K. Grigorovich and Y. S. Safronov, Relation Between the Heat Resistance and Creep of Alloys and Their Constitution Diagrams (in Russian), *Izvest. Akad. Nauk S.S.S.R., Otdel. Tekh. Nauk Met. i Toplivo*, No. 5: 38–46 (1960).

105. F. W. Schmidt et al., Effects of Various Aging Heat Treatments and Solution Annealing and Aging Heat Treatments on Tensile Creep and Stress-Rupture Strengths of Inconel X Sheet to Temperatures of 1400°F, Report NASA-TN-D-374, National Aeronautics and Space Administration, June 1960.

106. General Atomic Div., General Dynamics Corp., Maritime Gas-Cooled Reactor Program Quarterly Progress Report for the Period Ending March 31, 1960, USAEC Report GA-1259, March 1960.

107. R. A. Baughman, Gas Atmosphere Effects on Materials, Report WADC-TR-59-511, General Electric Co., Flight Propulsion Laboratory Dept., May 1960.

Section V

SPECIAL FABRICATION TECHNIQUES

Melting, Casting, Heat-Treatment, and Hot Working

The continued interest in the more advanced methods of melting and consolidating materials is evidenced by the increased number of reports and patents concerned with electron-beam and vacuum consumable-electrode arc melting. One recent reference[1] to an electron-beam melting and casting apparatus utilizing the multichamber principle reviews the utility of the electron beam for melting the more volatile or gassy metals and alloys and stresses the fact that, regardless of the outgassing rate of the charge, the beam energy and contour are unaffected. It is stated that furnace pressure may reach 3×10^{-2} mm Hg, whereas the pressure in the beam chamber remains at less than 1×10^{-4} mm Hg.

The Bureau of Mines has recently designed and constructed an electron-beam melting apparatus with the objective of studying the limitations and potentials of this technique.[2] The application of some of the techniques to the preparation of the niobium–15 wt.% tungsten–5 wt.% molybdenum–1 wt.% zirconium alloy has been investigated at Crucible Steel.[3] It was found that double-electron-beam-melted material varied considerably in both carbon and zirconium concentrations. Carbon contents of 0.004 to 0.04 wt.% and zirconium contents of 0.40 to 0.76 wt.% were noted within a melt. When compared to material prepared by vacuum arc melting, the electron-beam-melted material contained fewer interstitials than the arc-melted material and was more fabricable. The best quality ingots were produced by initially melting by electron-beam techniques and then vacuum arc melting. Facilities to electron-beam melt plutonium have recently been completed at Hanford.[4] Cesium and uranium have been used as stand-ins for the plutonium.

Although electron-beam melting is receiving more attention as increased facilities become available, there are continued efforts to improve the more conventional melting and casting techniques. As in the past, efforts are being expended to refine the as-cast grain size and reduce the pipe in uranium and uranium-alloy castings. Utilization of vibratory energy in the range of 50 to 1000 cps for this purpose is covered in a British patent.[5] It is claimed that the pipe in small (7.4 kg) uranium ingots is decreased in length from an average of 10 in. to 1 to 2 in. by the use of the vibrated molds.

The use of tantalum crucibles for the melting and casting of plutonium and plutonium alloys has been investigated at Los Alamos.[6] Pouring is accomplished by melting a melt-out plug in the bottom of the crucible when the desired temperature is attained. Charges up to 6 kg have been melted using the tantalum crucible. In conjunction with the evaluation of the tantalum crucibles, steel crucibles coated with CaF_2 have also been investigated. No pickup due to the CaF_2 coating in melts heated to 1000°C was reported.

Hanford's efforts to injection cast aluminum-plutonium alloys have been concerned with decreasing the centerline porosity in the injection-cast fuel elements. Some success has been achieved by utilizing an aluminum wire along the axis of the zirconium tube into which the molten metal was injected.

Another melting achievement of note is contained in the announcement by Oak Ridge of the production of the largest known (5 g) melt (inert electrode arc) of technetium.[7] The metal is soft and inherently ductile, although the formation of columnar grains limited the reduction by

rolling to approximately 50 per cent. Larger melts of this material are planned.

The heat-treatment and fabrication of uranium have continued to be of interest.[8] National Lead has reported on its investigation of induction heat-treating of uranium cores and has compared the resultant structures to those obtained by the conventional salt-bath treatments. They have noted that the induction beta-heat-treated cores are comparable in grain size, orientation, and structure to the material treated in the salt baths. Vacuum outgassing of solid uranium core blanks in the alpha temperature range has been investigated at Mallinckrodt.[9] Treatments in the temperature range of 950 to 1150°F were investigated. It was noted that above 950°F the hydrogen was removed more effectively but the structure was coarser. At this time it appears that the process is feasible but limited by economic considerations. It is also stated that grain refinement of the beta-treated structure can be achieved by alpha annealing.

One method of surmounting the problems of the shaping of oxygen-sensitive metals was described in a British patent.[10] The method pertains to drawing and extruding processes in molten-salt media. In other particular fabrication developments, the ability to alpha extrude cast hollow billets of uranium into thin-walled tubes has been reported by Mallinckrodt.[9] A process yield in excess of 65 per cent is reported when material was extruded at 1150°F. The material exhibited a normal fine-grained, high-alpha structure.

An aluminum-plutonium alloy wire containing 15.5 to 16.05 wt.% plutonium was successfully produced by extruding 0.375-in.-diameter cylinders at 450 to 500°C through a shear-face die.[11] Pressures of 150,000 to 220,000 psi were required for an 87:1 reduction in area. Although only three of six extrusions were successful, it is believed that the poor recovery was due to the finish of the die and billet container and not to the technique employed. (E. L. Foster)

Cladding

Cladding by Rolling and Swaging

New innovations not previously reported in detail include cold-roll forming of pressure-tube joints and ultrasonic roll bonding of fuel plates. Some degree of success was reported on the roll cladding of beryllium-clad fuel elements. Swage cladding and densification of UO_2 are still being emphasized, although many of the data covered in the previous issue did not demonstrate any significant advances.

A limited degree of success was reported by Nuclear Metals[12] with the beryllium roll cladding of uranium–10 wt.% molybdenum and uranium–61 vol.% UC fuels. The cladding was formed by hot-press forging beryllium powder around the cores in an evacuated mild-steel envelope. The container was then removed, and the sample was machined square and inspected for faults. After rejacketing, the samples were given a 3:1 total reduction in the 1800 to 1950°F temperature range. Both fuel systems were crack-free after fabrication, but the uranium-molybdenum samples cracked during thermal cycling.

Roll cladding of wrought plutonium-bearing fuels with Zircaloy was attempted at Hanford.[13] A 90 to 95 per cent reduction at 1380 to 1470°F was necessary for sound Zircaloy-to-Zircaloy bonding. This appears excessive in the light of previous work reported by Knolls and Bettis. Successful bonding of the fuel systems was not achieved because failure of the evacuation envelopes halted the fabrication process.

Preliminary fabrication studies for producing dimpled and honeycomb fuel elements were initiated at Nuclear Metals.[14] Extruded rods of Zircaloy-4-clad uranium–10 wt.% molybdenum were rolled to thin ribbons at 1650°F for forming studies.

Ultrasonic roll bonding is a relatively new fuel-element fabrication technique which shows some promise. This process, which was conceived by Combustion Engineering,[15,16] utilizes a continuous ultrasonic welder which promotes solid-state bonding with a minimum of heating and deformation. Although work has consisted mainly of development of equipment, satisfactory joining of type 304 stainless steel was reported. Also, self-bonding of aluminum alloys and bonding of multilayered aluminum-foil side ribs to aluminum–UO_2 dispersions appeared feasible.

In support of the CANDU reactor program, Smith and coworkers at Battelle[17,18] are investigating cold-roll forming as a means of joining Zircaloy-2 to type 410 stainless steel. Various surface preparations have been studied to determine parameters necessary to give cold metallurgical bonding. Mating surfaces were

finished to 300 μin. rms and scrubbed in a solution of $MgO-Na_2CO_3$. Metallurgical bonding was achieved with a single 45 to 50 per cent cold reduction.

Wire type fuel elements were produced by a process that included cold drawing and a combination of swaging and hot drawing. Fuel elements 35 mils in diameter which embody UO_2 cores clad with a nickel–20 wt.% chromium alloy cladding were cold drawn from 0.250 diameter. The final density of the UO_2 core was 90 per cent of theoretical. Type 347 stainless-steel-clad, uranium-zirconium cores were rotary swaged and then hot drawn to 0.065 in. in diameter by Sylcor.[20] Final end closure was made by etching out 1/4 in. of the core and flash welding in a stainless-steel end plug.

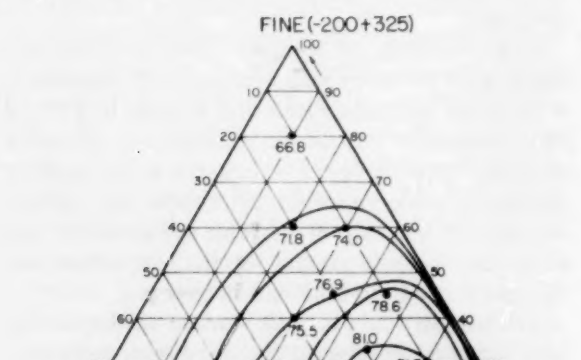

Fig. V-1 UO_2 densities after vibrational compaction of various particle-size compositions.[21]

Figure V-1 illustrates results of work at Hanford[21] on vibratory compaction of UO_2 prior to swaging. Various compositions of particle fractions were blended, vibratory compacted, and then cold swaged 15 per cent. According to the data in Fig. V-1, the highest density was obtained with 60 per cent coarse (–14 +20), 20 per cent medium (–65 +100), and 20 per cent fine (–200 +325) particles. However, they mention previous work where 90 per cent densities were obtained using different particle sizes.

Lamartine[22] at Oak Ridge studied the cold swaging of UN in type 304 stainless steel. A total reduction of 56 per cent produced 82 per cent dense fuel material. Diffraction patterns of the core material indicated the presence of some UO_2 and U_2N_3. The author believed that higher densities could be achieved with a decrease in impurities.

Swage cladding of UC with niobium–0.75 wt.% zirconium was reported by Union Carbide.[23] Full densification of the cold-pressed core was obtained by swaging 40 to 50 per cent at 1600°C. Some core-to-cladding reaction product, presumably NbC, was noted. (H. D. Hanes)

Pressure Bonding

A process that involves the use of gas pressures at elevated temperatures to produce bonds has been termed pressure bonding or isostatic bonding. This process is currently being utilized to bond or clad numerous metals, ceramics, cermets, and dissimilar metals. The process is also being used to compact ceramic and cermet materials under a hydrostatic gas pressure at elevated temperatures.

The gas-pressure-bonding technique is being investigated as a method for fabricating low-cost, stainless-steel-clad, uranium dioxide fuel elements.[24] With pressure-bonding conditions of 3 hr at 2100°F and 10,000 psi, it is possible to achieve both densification of the oxide and high-integrity stainless-steel bonds in a single operation. Fuel-element geometries considered in this study have included rod, flat plate, and tubular configurations. Modifications of the basic designs, such as corrugated rods, compartmented flat plates, and compartmented rods, have been fabricated.

Uranium dioxide structures pressure bonded at temperatures ranging from 2100 to 2300°F have exhibited densities from 82.5 to 99.5 per cent of theoretical, depending on the type of oxide employed. The highest density structures were attained with mixtures of 30 to 60 wt.% ceramic-grade oxide with fused oxide. This particular range of mixtures also permits high initial packed or pressed densities and minimized densification effects in stainless-clad elements.

Final specifications are being established for the preparation of in-pile test specimens of stainless-steel-clad uranium oxide.[25] These pressure-bonded, rod type elements will be prepared with as-green-pressed cores and will measure 0.400 in. in diameter by 36 in. in length. Specifications for the preparation of these elements are being based on the background of in-

formation achieved during the bonding of rod elements approximately 24 in. in length. These elements contained green-pressed oxide pellets consisting of a mixture of 60 wt.% fused–40 wt.% ceramic UO_2 with a Ceremul "C" binder. Other binder materials are also being studied on smaller scale specimens to determine the effects of these binders on green-pellet density, pellet handling characteristics, final density, and final stoichiometry after bonding.

Process variables and specifications are being studied at Bettis[26] to establish final production methods for the fabrication of blanket and seed oxide-bearing fuel plates for PWR core 2.

Considerable experience has been gained at Bettis on the pack bonding of blanket elements which brings the state of knowledge of the two modifications of pressure bonding (direct isostatic bonding of Zircaloy-clad elements and pack bonding of elements in a disposable container) to an equivalent level. Factorial experiments have been made to evaluate the effects of pressure, rib upset, and cleaning cycles on bonds achieved during pack bonding. The pressures in the range studied (6500 to 7500 psi) did not alter the properties of the Zircaloy-to-Zircaloy bonds achieved. Bond quality was not affected in the range of rib upset of 8 to 17 mils; however, bonds were generally better than those previously observed with less than 8 mils of rib upset. The cleaning techniques for production fabrication were established and are reported.

Present plans now call for utilizing the isostatic process for the preparation of the blanket for PWR core 2, while the seed elements will be produced by pack bonding. Such development effort as time permits before the start of production bonding will be devoted to refining these processes to assure meeting all requirements of drawings and specifications. To assure optimum corrosion behavior in both the blanket and seed regions, it is now planned that all fuel elements be subjected to a beta heat-treatment after bonding.

Studies are being conducted at Bettis on the effectiveness of pyrolytic carbon as a barrier to prevent reaction between Zircaloy and UO_2 during bonding or heat-treating of bonded elements at 1850°F. It was observed that increased bonding temperatures up to 1650°F produced only slight increases in diffusion between core and cladding with the pyrolytic carbon barrier layer.

Surface roughness as a function of bonding was further investigated by Bettis.[26] Metallographic evaluation of the effect of surface roughness of abraded components on the bond quality of isostatic-pressure-bonded oxide plate samples confirmed previous indications that surface roughness in the range of 80 to 190 μin. results in the best and most reproducible bond quality. Higher or lower surface roughnesses adversely affect bond quality and reduce reproducibility. Bond quality for each surface-roughness condition was observed to improve as bonding temperature was increased above 1500°F.

The self-bonding of beryllium as a function of surface preparation and bonding parameters is being studied at Battelle.[25,27] In addition, the core-to-cladding reaction between beryllium and UO_2 as a function of bonding parameters is being investigated.

In an attempt to determine whether sound bonds could be achieved between all members of a compartmented fuel plate composed of several parts, a beryllium structural specimen in the form of an I-beam was prepared by pressure bonding at 1600°F and 10,000 psi. The beryllium surfaces were conditioned for bonding by abrading with silicon carbide under water. Metallographic examination of the I-beam structure revealed that a series of small grains formed along the bond interfaces of the mating surfaces. The beryllium surfaces were apparently cold worked enough during abrading to result in recrystallization and grain growth across the original bond interface with no apparent bond-line contamination. (E. S. Hodge)

Diffusion Bonding

A process for coating fissionable fuel with niobium films has been patented by the British,[28] as discussed later under Canning. If this is successful, an attempt will be made to pressure bond the niobium-plated fuel to aluminum cladding by isostatic pressing. As a parallel effort, the roll bonding of niobium-to-uranium fuel is being studied; if successful, these plates are to be bonded to aluminum cladding by isostatic pressing or a second roll-bonding operation. No significant results were yet available.

(D. C. Carmichael)

Coextrusion

Development of the coextrusion process for the fabrication of aluminum-plutonium alloy

fuel elements was conducted by Hanford.[29] Fabrication of 144 coextruded fuel elements with aluminum–7.35 wt.% plutonium alloy cores clad with aluminum (X-8001 alloy) was accomplished. The fuel elements were in the form of rods 0.94 in. in diameter by 60 in. in length, each containing 83.3 ± 4.2 g of plutonium. Essentially, as-cast fuel cores were used as coextrusion billets which reduced the amount of core machining required and fuel-alloy chips generated. The cladding thickness was 0.040 to 0.120 in. All fuel rods were coextruded in an extrusion press which was mounted in a glove box or hood. The extruded rods were easily decontaminated. Plug and socket type end fittings were machined on all the coextruded fuel rods with no radioactive contamination on the machined surfaces being detected. It was demonstrated that the coextrusion process which was developed is capable of producing metallurgically bonded fuel elements of this type.

(C. B. Boyer)

Canning

A process has been described for enclosing the uranium core of a nuclear fuel element by placing the core in an aluminum cup and closing the open end of the cup over the core.[30] As the metal of the cup is brought together in a weld over the center of the end of the core, it is extruded inwardly as an internal projection into a central recess in the core and outwardly as an external projection. Thus oxide inclusions in the weld of the cup are spread out into the internal and external projections and do not interfere with the integrity of the weld.

A suggested approach[21] to the problem of detecting areas of poor heat transfer on canned slugs involves heating the slug internally and, with the jacket wall bathed in coolant, scanning the surface with a suitable probe to indicate the spots of high and low temperature. Several variations of this principle have been tried. The most successful technique involved external heating and percussion welding of two aluminum studs to the canning jacket. The ends of the studs were threaded to fit the tip socket of an electric soldering iron. Thermocouples were attached to the studs at their junction with the slug jacket and at the base of the threaded portion the same distance apart on each stud. Comparison of the equilibrium temperatures of the two stud-cladding junctions indicated that the stud welded to the known unbonded portion of the slug was 5°C hotter than that on the sound bond stud. This result would indicate that the difference in heat-transfer capacity of the two jacket areas could be measured by this technique. However, this test is a destructive one and would not be suitable for production.

A diffusion-canning process is described in which uranium fuel is clad with a zirconium can by passing the element through a die.[31] The operation takes place at a temperature varying between 500 and 1000°C. The heating is accomplished by passing a low-voltage current through the can. This process differs from the coextrusion process in that the uranium is not deformed. A vacuum is maintained between the uranium core and zirconium can during the drawing operation. Subsequent to drawing, the element is heat-treated at 800°C to obtain the final diffusion. The quality of this core-clad bond is dependent on the initial surface conditions of the components used and the degree of vacuum maintained during the drawing operation.

A fabrication process for producing integral finned tubing has been described which avoids the thermal barriers resulting from joining fins to tubes.[32] The fabrication is performed on tubes with integral fins either of the longitudinal or helical variety in this manner: a series of transverse cuts is made in the shorter fins at equal intervals along the tube length, and each fin segment is twisted at the top so that its tip is either inclined or longitudinal to the tube axis. An integral finned tube may be made which has improved heat transfer and reduced tendency to bow under reactor irradiation and thus is particularly suited for canning reactor fuel elements.

A process has been patented for coating fissionable fuel with niobium films preparatory to cladding with an aluminum can to prevent reaction between core and can.[28] Such films are 0.1 to 0.2 μ thick and may be applied by evaporation onto the fuel elements in a chamber in which a niobium piece is attached to a tantalum heater.

An improved process for cladding uranium with aluminum is outlined in a recent British patent.[33] A thin layer of nickel (0.250 in.) is sandwiched between the metals to be joined. Joining is completed by heating the sandwich in the 535 to 625°C temperature range under pressures of 11 to 25 psi for 8 min to produce a solid-state weld. In this manner, alloying be-

tween the uranium and aluminum and subsequent formation of brittle diffusion products are said to be prevented.

Several niobium-, vanadium-, and tantalum-base alloys are being considered for canning materials for use in future fast reactors.[34] These alloys possess the necessary compatibility with most fuels and sodium coolant at temperatures in excess of 900°C.

(E. G. Smith, Jr.)

Nonelectrolytic Chemical-Plating Techniques

Coatings on Extended Surfaces. Studies of the deposition rate of titanium from titanium tetraiodide can be aided by the use of heat- and mass-transfer models.[35] Such models consist of aluminum rods arranged in a $\frac{1}{4}$-scale pattern with a recirculating air supply. The dependence of local and averaged rates of heat transfer and consequent metal transfer upon outlet geometry, number of rods, position upon a rod, and air flow rate is established for flow patterns created by radial and tangential air inlets.

A brief review[36] of advanced coating methods included a discussion of the application of ceramic and refractory-metal coatings by means of chemical vapor deposition.

Included in a report[37] describing the experimental coating of uranium with zirconium by chemical vapor deposition was an excellent historical review of the art as well as a useful discussion of reaction mechanisms.

A reasonably protective coating for niobium can be secured by exposing heated niobium to zinc vapor.[38] A niobium specimen, together with a small (stoichiometric) amount of zinc, is placed in an evacuated and sealed silica capsule. By maintaining the temperature of the niobium specimen a few degrees above that of the zinc source and air cooling the container after the coating cycle, a surface layer of $NbZn_3$ can be produced. The coating is self-healing in air at temperatures approaching 2000°F, since a tight protective layer of ZnO is formed.

A continuing program at High Temperature Materials, Inc.,[39–41] is aimed at the development of methods for forming massive deposits of pyrolytic hafnium carbide, niobium carbide, and tantalum carbide. The methods are equally useful in the preparation of coatings of these carbides.

Choice of a suitable graphite substrate, of expansion compatible with that of hafnium carbide, permitted the formation of reasonably uniform crack-free hafnium carbide coatings 10 to 44 mils thick. The microhardness number of such coatings lies in the 3500 to 4000 DPH range. Niobium carbide was deposited on a hot wire at temperatures in the 1700 to 2100°C range. Other parameters included metal halide-to-methane ratios from 1:4 to 1:1 and reduced pressure (1 to 15 mm Hg). The microhardness numbers of the deposits were in the 2440 to 2732 DPH range, which compares favorably with those of commercial material (2400 to 2470 DPH). Numerous tantalum carbide coating experiments were carried out on various substrates, including flat plates, rocket-nozzle inserts, and full-scale rocket nozzles. The physical properties and oxidation resistance of the deposits were evaluated.

Coatings of pyrolytic carbon also were prepared.[42,43] The internal surfaces of tubes, made of refractory materials, were used as substrates. The coating atmosphere was an inert gas with a low concentration (e.g., 2.5 vol.%) of methane or propane. Coatings, 21 mils thick, were formed in 4 hr at 2000°C and were quite uniform, with a maximum thickness variation of 10 per cent. X-ray methods were used to determine crystallite dimensions.

Titanium nitride coatings on graphite were formed by chemical vapor deposition.[44] The atmosphere was a mixture of commercial hydrogen, containing nitrogen, and $TiCl_4$ vapor prepared by bubbling the hydrogen through liquid $TiCl_4$. This mixture was passed over a hemicylindrical specimen of AGX graphite, induction heated to 1200°C in a quartz tube. At a hydrogen flow rate of 1.6 liters/min, 20 mg of TiN per square centimeter of substrate was deposited in 12 min. Such coatings are protective for at least 60 sec in a Mach 2 air stream with a stagnation temperature of 2200°C; the TiN coating is converted to the oxide. Uncoated graphite specimens, subjected to the same test conditions, were damaged after 20 sec and were destroyed at the end of the 60-sec test cycle.

Uniform, dense coatings of Al_2O_3, 5 to 15 μ thick, can be formed on 44- to 350-μ UO_2 particles by hydrolysis of Al_2Cl_6 vapor in a fluidized bed of the particles[45] at 1830°F. Such coated particles are resistant to HNO_3 leaching, to oxidation in 1830°F air, and to thermal cycling

between 600 and 2500°F. After low neutron-irradiation exposures, coated particles show excellent fission-gas retention at temperatures up to 2400°F in inert gas. The coating process should be feasible on a commercial scale. Typical operating conditions include the following:

Particle-bed weight: 100 g
UO_2 particle size: 105 to 149 μ
Reactor-wall temperature: 1830°F
Aluminum chloride-vaporizer temperature: 300 to 320°F
Water-vaporizer temperature: controlled on basis of a previous calibration
Gas flow through aluminum chloride vaporizer: 0.75 standard liter/min
Gas flow through water vaporizer: 0.75 standard liter/min
Main fluidizing gas flow: 2 standard liters/min
Reactant composition: 96.5 mole % H_2, 1.3 mole % Al_2O_3, 2.2 mole % H_2O
Coating rate: 3 g/hr
Fraction of Al_2O_3 as coating: 50 wt.% Al_2Cl_6 conversion 95 per cent
Coating rate: 0.8 μ/hr

Alumina coatings were deposited on UO_2 particles by hydrolysis of Al_2Cl_6 vapor in a fluidized bed.[27,46] First, a 5-μ coating of dense Al_2O_3 was applied. Subsequently, 5-, 20-, 40-, and 45-μ-thick coatings of dense Al_2O_3 were applied at 1000°C. A 12-μ coating of porous amorphous Al_2O_3 was applied at 700°C. Test data indicated that this amorphous Al_2O_3 may undergo a transition to the crystalline form of Al_2O_3 during subsequent thermal cycling.

Fuel particles were coated with pyrolytic carbon by the decomposition of hydrocarbons in a tumbling-bed reactor at temperatures above 1500°C and in a fluidized bed of the particles at temperatures[27,46] below 1500°C. Owing to particle agglomeration, nonuniformity of coating, and adherence to reactor walls, future work will be confined to temperatures below 1500°C until a high-temperature fluidized-bed reactor can be set up. Evaluation of the carbon coating embodies microscopic examination, measurement of hardness, direct alpha count, and measurement of fission-gas release on postirradiation heating. (E. M. Sherwood)

Electroplating

The preparation of thorium for corrosion-protective nickel plate influences the protective quality of the coating.[47] Electropolishing in a sulfuric acid–phosphoric acid solution was more effective than chemical pickling in a nitric acid–hydrofluosilicic acid bath. Removing 4 mils of thorium from the surface by electropolishing gave better results than the removal of 2 mils. Small blisters developed in thorium specimens plated with 1 to 2 mils of nickel after 50 to 100 hr of exposure to water-saturated air at 200°F. The blistering is associated with hydrogen pickup during activation and plating, which is minimized by electropolishing in place of chemical pickling. In subsequent work at Battelle, metallographic examinations of cross sections showed that the blistering occurred below the thorium surface.[27] With slow heating to 500°F in a vacuum and with 1- to 2-hr holding periods at 200, 300, and 400°F, hydrogen was outgassed with no blister formation.[46]

In Hanford studies along the same lines, tensile shear tests with an epoxy resin adhesive indicated that chemical pickling was more effective than electropolishing for pretreating thorium surfaces.[18]

After electroplating uranium with copper, nickel, or chromium, electrochemists at the Bureau of Standards[48] observed black films between the uranium and the coating which they attributed to the oxidation product of a moisture film adsorbed on the uranium surface during cleaning or during the initial stage of the plating process. The black oxide film was not eliminated when coating thicknesses were increased to 0.008 in. to ensure dense, pore-free coatings. When uranium was rinsed, after cleaning, in an oleic acid–ethyl ether solution or in formamide and ethyl ether and then plated with aluminum in a nonaqueous, aluminum chloride–ethyl ether–lithium hydride bath, good adhesion was obtained and no black films were formed, provided the aluminum was at least 0.004 in. thick. Under thinner coatings, the black oxide usually was apparent.

Other laboratories have been able to plate nickel in aqueous solutions with no evidence of black, oxide-film formation between the uranium and the coating.[49–52] Comparison of the Bureau of Standards procedures with those of others reveals differences in the preparation of the uranium that may account for the difference in results. Anodic treatment in phosphoric acid or chemical treatment in chromic acid solutions probably produced a film of phosphate, chromate, or oxide film which interfered with good adhesion and supplied the oxygen respon-

sible for the formation of the black film observed under the electroplate. If uranium is chemically treated in nitric acid solution after any anodic treatment in a phosphoric acid solution to remove the anodic film, good adhesion can be obtained with no tendency for black, oxide-film formation after nickel plating.[49,50,52]

Methods for electroplating nickel and other metals on uranium, disclosed in two recent British patents,[53,54] include diffusion alloying of the nickel at 700 to 800°C to improve its adherence to uranium. Coatings of lead, copper, chromium, or aluminum-silicon alloy can be applied over the nickel after diffusion bonding, according to these patents.

Nickel and zirconium-nickel alloy were electroplated with good adhesion to urania, at Gladding-McBean.[55] Coating thicknesses were 0.005 to 0.01 in. The alloy contained 15 per cent zirconium and 85 per cent nickel.

Chemical plating with nickel is effective for improving the corrosion resistance of aluminum-clad fuel elements.[56] The organic acid and the concentration used in the electroless nickel bath influence corrosion resistance and the ductility of the nickel deposit.

While exploring the feasibility of cathodically depositing uranium oxide for fuel elements, Hanford investigators[57] discovered that UCl_4 in the deposit could be reduced by utilizing low-melting electrolytes such as the potassium chloride–lead chloride eutectic, melting at 411°C. Adherent, crystalline UO_2 deposits containing 200 ppm lead and potassium were obtained.

A diaphragm cell was devised which includes a porous crucible in which an anode, a cathode, and fused melt are inserted.[58] The anode and cathode are separated by a porous glass, silica, beryllia, or alumina diaphragm to hold impurities in the anode compartment. When electrolysis is completed, the crucible is drained of electrolyte and heated to melt the reduce metal. Uranium was produced in this manner with iron, nickel, manganese, and carbon impurity contents of only 7, 1, 1, and 90 ppm, respectively. This is compared with the 200 ppm iron, 12 ppm nickel, 15 ppm manganese, and 1700 ppm carbon impurities found in the uranium fluoride additions to the fused eutectic mixture.

Purified hafnium was recovered at the Bureau of Mines[59] from zirconium-containing sludge from one electrolyte by subjecting it to electrolysis in a second cell. The first deposit, produced during 11 amp-hr, contained 92.9 wt.% zirconium. Subsequent deposits contained successively less zirconium and more hafnium. The hafnium content of the cathode deposit reached 97 wt.% after 27 hr of electrolysis. Yttrium deposition was facilitated by using a low-melting, lithium–potassium chloride electrolyte in place of fused potassium chloride.

(W. H. Safranek)

Ceramic Coatings

The oxidation resistance of silicon-SiC coated graphite support sleeves is being evaluated at Oak Ridge.[60] When heated in flowing air for 6 to 24 hr at 420 to 650°C, coated graphite type 901S showed no loss in weight. The loss observed with coated graphite type 580 ranged from one-third to nearly equal that of an uncoated specimen. The difference in the results with types 901S and 580 graphite was explained as being due to the anisotropy of the latter.

Aerojet-General[61] has experimented with silicon-SiC coatings on graphite. A two-step process is embodied in a technique in which a silicon layer is first reacted with the graphite to form SiC, and a second silicon layer is then applied and fused. Better oxidation resistance at 1000°C in air was obtained when silicon was initially bonded to the graphite with a solution of VYNS resin in cyclohexanone than when it was applied as a suspension in acetone.

The feasibility of coating Zircaloy with porcelain-enamel type coatings has been demonstrated by Argonne.[34] It was further shown that 5 wt.% Gd_2O_3 could be introduced into these coatings.

Commercial coatings for molybdenum are being evaluated by General Electric.[62] Specimens coated with Climax Molybdenum aluminum-chromium-silicon, Linde LM-5, and Chromalloy W-2 have been evaluated. Some data are presented, but no conclusions have been reached regarding the relative merits of the coatings. Under thermal-shock flexure tests,[63] Chromalloy and Climax coatings lasted 10 hr, and Linde coatings withstood the test for 5 hr. Failure in each coating resulted from cracks perpendicular to the base which exposed the molybdenum to attack by oxygen.

Attempts are being made to adapt a coating consisting of glass-impregnated, flame-sprayed alumina for the protection of molybdenum.[62,63] The maximum life obtained was 100 hr under static oxidation testing at 2300°F.

A British patent[64] describes a technique for coating titanium, zirconium, beryllium, and their alloys with complex fluorides. Metal surfaces are dipped in a solution containing 2 wt.% of a complex acid of fluorine such as fluosilicic, fluoboric, fluophosphoric, or fluosulfuric acid.

(B. W. King)

Welding and Brazing

A new bibliography of interest in the welding field was issued recently,[65] presenting 270 additional references on this subject.

Further studies of the crack susceptibility of the nickel-molybdenum alloy, INOR-8, are being made.[66] The studies are designed to evaluate the effect of composition and deoxidation practice on the cracking susceptibility. A large number of test weldments have been prepared and examined for evidences of cracking. Hot-ductility-test samples also are being made. Cracking can apparently be eliminated by assuring purification and deoxidation of the melt during initial casting. An addition of 20 per cent niobium to the basic composition appears to eliminate the weld-metal cracking problems.

Oak Ridge investigators also are continuing their studies of beryllium joining.[60] Recent work has included refinement of fusion-welding techniques, development of high-temperature brazing alloys, and fabrication of a large number of tube-burst specimens. Measurements of the weld-metal grain size in beryllium fusion welds have established that the grains are between 45 and 90 μ in diameter. Welding and brazing of 155 beryllium tube-burst specimens were accomplished. These specimens were fabricated from 0.3-in.-ID by 0.040-in.-wall beryllium tubing. End caps were inserted with a light taper and were fusion welded at each end of the tube. A type 318 stainless-steel tube was inserted in one of the end caps and was sealed in place by brazing with a 49 wt.% titanium–49 wt.% copper–2 wt.% beryllium brazing alloy. About 10 per cent of the total number of specimens were rejected because of leaks in the weld or brazed joints. The highest rejection rate was observed in the specimens fabricated from Pechiney tubing. The welds in this material also contained much more evidence of porosity than welds in the remaining materials. In all, 31 per cent of the welds contained porosity. However, specimens containing porosity are included in the burst program. No failures have occurred in either the welded or brazed joints.

Canadian experience in the solid-phase bonding of Zircaloy-2 by resistance heating is described.[68] The work was conducted on a conventional welding machine; however, welding conditions were set so that fusion of the base metal did not occur. It was concluded that spot type joints with shear strengths comparable to those required in the U. S. military aircraft specifications for titanium could be made. Adequate joints were obtained between surfaces prepared by pickling, abrading, or machining. The shear strength was sensitive to thickness variation. The tolerances of the process for variation in settings of current, electrode force, and welding time were established.

(R. E. Monroe)

Explosive Forming

A state-of-the-art report on explosive metalworking has been published by the Defense Metals Information Center (DMIC) at Battelle.[69] The report describes the principles of explosive forming and its effect on material properties; covers applications such as forming, powder compaction, welding, flanging, hardening, cutting, forging, and punching; and discusses the advantages and disadvantages of explosive metalworking.

The manner in which the load is released, as well as applied, is quite important in explosive forming. When a material is subjected to an explosive load, such as the type encountered with contact charges, it can momentarily accept a large amount of elastic energy. The majority of this elastic compression is released after the pressure pulse has reached its peak and the load begins to decrease. The material tends to revert to its original energy state during this decrease in loading, and if the load is released too rapidly, it will overextend itself, thereby inducing tensile stresses which will cause a distortion or fracture of the material. It is usually possible to avoid this effect by increasing the time-pressure profile to permit a more gradual release of the load.

Critical impact velocities and relative particle velocities are also of considerable importance in explosive metalworking. The critical impact velocity is defined as that velocity at which the material will fracture in a brittle

manner at the point of impact. The critical-impact-velocity concept can be extended to include relative particle velocity, a value which represents the difference in velocity existing between two adjacent body elements under dynamic conditions. The relative particle velocity also possesses an upper limit that a material can sustain without fracture. This value, called the critical relative particle velocity, is usually assumed to be equal to the critical impact velocity of the material. The application of the critical-relative-particle-velocity concept is most useful when considering explosive-metal systems in which abrupt changes in particle velocity due to the propagation and interaction of stress waves exist. In most sheet-metal forming operations, however, there exists a continuous gradient of relative particle velocity along the workpiece. In such cases the critical relative particle velocity or critical impact velocity becomes less meaningful in terms of quantitative values.

In many forming operations, fracturing of the workpiece may be due to factors other than exceeding the relative particle velocity of the material. These other factors include thinning of the workpiece, work hardening, and conditions of dynamic stress concentration. Thus other factors must be included in the determination of the particle velocity which should be used to perform a specific forming operation with a given material.

The effect of explosive forming on the properties of a material and the behavior of the material during an explosive forming operation are subjects of considerable debate. Although several theories have been postulated to explain what occurs within a metal body during explosive forming, there is a general consensus that, when a metal is subjected to an impulsive load, it passes through a phase during which it behaves as a viscous fluid and, while in this fluid condition, forms to the contour of the die. From a practical standpoint, during explosive forming the metal undergoes severe plastic deformation, and the metal behavior during a forming operation may frequently be studied by means of a mathematical analogy based on a fluid model. Under explosive pressures, metals behave plastically and do not become fluid; they move through the elastic to the plastic range and take permanent set in a few millionths of a second.

A technical paper describing some of the basic methods presently being used in explosive compaction of metal powders and a monograph discussing typical results obtained by explosive compaction have been prepared by Battelle.[69,70] The extreme pressures generated by the detonation of a high-explosive charge, from 2,000,000 to 4,000,000 psi for a contact charge, are quite desirable for metal-powder-compaction operations. Such pressures, although short lived, have been effective in producing deformation at ambient temperature in many common and high-strength metals during explosive-forming operations and consequently would also be expected to produce similar deformation in powder metal particles.

Possible methods for compacting metal powders with explosives range from those utilizing familiar powder-compacting die designs to those techniques in which pack assemblies rather than dies are required. The choice of system, of

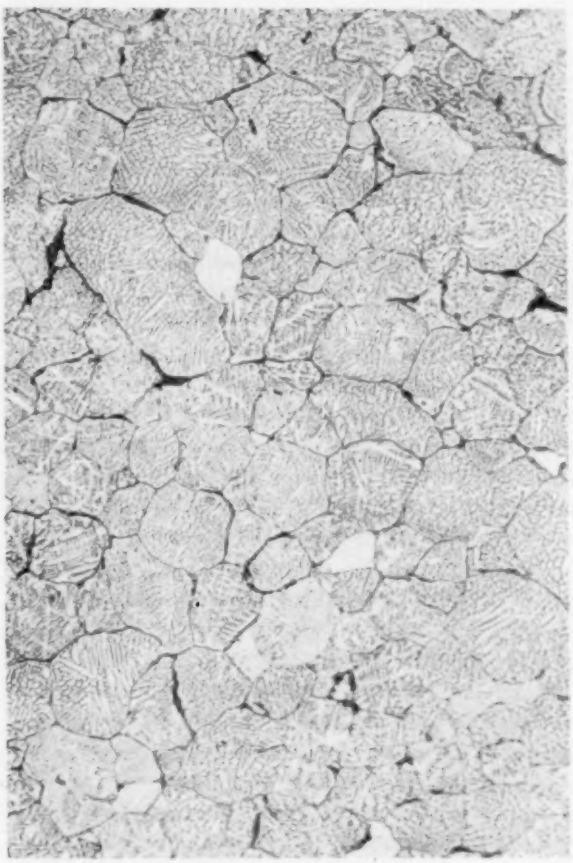

Fig. V-2 Haynes Stellite alloy 25 powders compacted at ambient temperature with explosives. Density measured at 94.6 per cent of theoretical.[69] Magnification 250×.

Fig. V-3 Typical microstructure in unsintered BeO body fabricated by explosive compaction.[69]

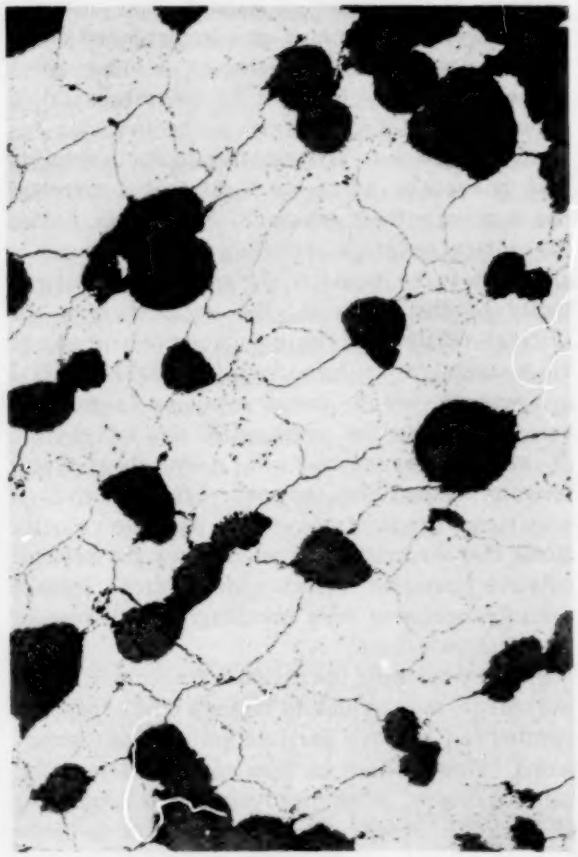

Fig. V-4 Explosively compacted 30 wt.% UO_2–tungsten cermet in the unsintered condition.[70] Magnification 100×.

course, depends on the final size and geometry desired and the properties of the metal powder in question. With each system the compacting characteristics are dependent on parameters such as weight of charge, media, buffers, axiality, and detonation patterns.

In general, high final densities on the order of those normally achieved through pressing and sintering have been attained in the explosive compaction of metal powders. For a given set of experimental conditions, the density obtained and the resultant green strength are dependent on the ductility and particle sizing of the individual powders. In many instances, interparticle bonding has been indicated, although no tests have been directed at establishing the degree of such bonding.

In Battelle experiments, ceramic, cermet, and metallic materials have been compacted into such shapes as rods, tubes, fluted tubes, and flat plates. Figures V-2 to V-4 show typical structures obtained by this method.

Nonoxide ceramics, such as borides, carbides, silicides, and graphite, have also responded favorably to explosive compaction. The following is a list of several materials compacted at Battelle along with their as-compacted densities.

Materials	Percentage of theoretical density
25 wt.% UO_2–75 wt.% nickel	95
Tungsten	94.8
Haynes Stellite alloy 25	95
Titanium	88.4
20 wt.% $MoSi_2$–80 wt.% ZrB_2	95.6
25 vol.% UN–75 vol.% TiC	96.2
$MoSi_2$	98.1
Graphite	93.5
Beryllium	96
Zircaloy-2	97
Thoriated tantalum	97
30 wt.% UO_2–70 wt.% tungsten	96.8

Basic and applied research investigations regarding the dynamics of metal-explosive systems, the effects of explosive loading on material properties, the physics of stress waves and their effects, fracture dynamics, and other related subjects have been conducted at the U. S. Naval Ordnance Test Station at China Lake.[71] In a report on this work, the energy sources available for conducting explosive-metalworking operations are discussed. Some of the characteristics of deflagrating and detonating explosives are given in Table V-1; Table V-2 gives the detonation velocities for a number of common explosives.

Table V-1 CHARACTERISTICS OF HIGH AND LOW EXPLOSIVES[71]

Property	High explosives	Low explosives
Method of initiation	Primary high explosives: ignition, spark, flame, or impact Secondary high explosives: detonator, or detonator-booster combination	Ignition
Conversion time	Microseconds	Milliseconds
Conversion rate	6000 to 28,000 ft/sec	A few inches to a few feet per second
Pressures	Up to about 4,000,000 psi	Up to about 40,000 psi

Table V-2 TYPICAL DETONATION RATES[71]

Explosive	Rate of detonation, ft/sec
Amatol, 50-50	21,000
Ammonium nitrate	8,800
Composition A-3	26,500
Composition B	25,600
Composition C-3	25,000
Composition C-4	26,300
Dynamites, ammonia	8,800–15,000
Dynamites, ammonia gelatin	14,400–18,700
Dynamites, gelatin	13,100–20,300
Dynamites, straight	14,400–19,300
Lead azide	16,700
Lead styphnate	17,100
Mercury fulminate	17,700
Nitroglycerin	25,200
PETN	27,200
Tetryl	25,700
TNT	22,600

A study concerning the explosive forming of refractory metals is presently being conducted by the Chromalloy Corporation.[72] The objectives of this program are (1) to develop techniques for the explosive forming of refractory metals, (2) to investigate the effects of detonation waves on these materials, (3) to determine the feasibility of using explosive techniques as a means of joining refractory metals, and (4) to obtain some measure of the deformation rate and its effect on the explosive forming of refractory metals. The major emphasis during this program is being placed on molybdenum, with tungsten, niobium, and tantalum also being considered.

Several tests have been run with pure molybdenum and a ½ per cent titanium-molybdenum alloy. The charge used during this phase of the study was 15 per cent dynamite, and the transfer medium was 325-mesh powdered alumina. The charge weights used were 35 g for 0.010-in.-thick material, 50 g for 0.020-in.-thick material, and 70 g for 0.040-in.-thick material. These charges, although greater than those used in earlier work, have been found to be optimum. Other parameters investigated during this period included strain rate and metal deformation velocity.

A program to develop a fabrication process for the cold joining of Zircaloy-2 to type 410 stainless-steel pressure tubes is presently being conducted at Battelle.[17] One of the fabrication processes being considered is explosive joining. Initial studies to determine the surface preparation and charge weight required to produce a good bond have been conducted with flat-plate assemblies. Surface finishes of 300 μin. rms, with subsequent cleaning and scrubbing with a MgO-Na_2CO_3 slurry, have been found to produce the best bonds. The optimum charge weight was found to consist of 16 g of EL-506A-2 sheet explosive.

Hanford[72a] has been experimenting with the compacting of UO_2 powder by high-energy impact with a Dynapak machine. Instantaneous pressures of approximately 500,000 psi have been developed by using Bridgman anvil punches, with expendable steel reinforcing rings placed around the stainless-steel capsule containing the UO_2.

It was found that by having a slight excess of oxygen in the UO_2 the plasticity and achievable density were increased. It was necessary to use a vented capsule for this operation since, when the UO_2 was heated, some of the excess oxygen was released. With a sealed capsule, an

internal pressure was built up by this released gas, which caused porosity in the compacted UO_2.

Micronized UO_2, −200-mesh fused UO_2, and −200-mesh sintered and crushed UO_2 have been compacted at 1200°C by high-energy impact, using the Bridgman anvil technique. The densities to which the materials were compacted and their final oxygen-to-uranium ratios were 99.5 per cent of theoretical density with a ratio of 2.0397, 99.5 per cent of theoretical density with a ratio of 2.0018, and 99.0 per cent of theoretical density with a ratio of 2.0046, respectively.

(C. C. Simons)

Nondestructive Testing

Nondestructive Testing by Means of Ultrasonic Energy

A recently published book[73] should be very useful to those faced with nondestructive-testing problems. An impressive list of subjects is included which cover the principles of a large number of nondestructive-testing methods in language that is easily understood by the layman.

Mode conversion, a result of the ability of a solid to transmit many ultrasonic wave types at different velocities, often causes confusion in interpreting ultrasonic nondestructive-testing data. Although there are claims that rough wall surfaces on a cylinder eliminate all but the fastest modes, work at Argonne[74] shows that rough surfaces do not reliably prevent mode conversion.

Actually, mode conversion is an indication of the versatility of ultrasonic testing; for example, inspection for nonbond regions in clad structures by means of Lamb waves is being done at Oak Ridge.[2,75] A wave incident on an unbonded area is converted to Lamb waves in the thin delaminated section. Only the Lamb wave is detected, and its presence is an indication of a delamination or nonbond. This method is sensitive to nonbond areas $\frac{1}{16}$ by $\frac{3}{16}$ in.

Oak Ridge has been evaluating another nonbond test in which a beam directed normal to the surface of a 0.065-in.-thick type 304 stainless-steel can surrounding the copper cylinders of a liquid-metal boiler is able to detect areas of nonbond. This method is sensitive to nonbonds as small as $\frac{3}{32}$ in. in diameter in small experimental specimens. The full-size test pieces are more difficult to inspect by this method because the method is sensitive to thickness variations.

An interesting method of determining bond quality in PWR fuel elements is being investigated at Armour Research.[26,76,77] This method, called charge scanning, is based on a principle that has been used in other systems for visualizing acoustic fields; i.e., producing an acoustic image on a piezoelectric crystal. The charge on the face of a piezoelectric crystal is a function of the pressure across the crystal. If the faces of the crystal are connected to electrodes, the voltage measured across the crystal is an integrated value. By contrast, in the Armour charge-scanning procedure, the electrical charges on the reverse side of the receiving crystal are detected incrementally by scanning the crystal either with a fine wire or with the electron beam of an iconoscope type vacuum tube. Since the charge at any point is a function of the sound pressure at that point, it should be possible to obtain contrast between defective and nondefective areas by a drop in signal.

Both eddy currents and an immersed ultrasonic-resonance technique are being studied[26] as means of detecting and measuring the thinning of cladding in seed elements. Reasonably standard equipment of either type can detect thinning in areas as small as $\frac{1}{8}$ in. in diameter. The ultrasonic method was considered a little more promising at the time the reference report was written because it was not affected by configuration and because it was a faster method.

An eddy-current system and an ultrasonic system have been combined at Hanford[78] to produce a multiple nondestructive-testing station for NPR fuel elements. Eddy currents at 20 kc are used to measure the cladding thickness within approximately ±0.002 in. Eddy currents at 120 kc reveal discontinuities in the cladding. Simultaneously, ultrasonic energy at 15 Mc is used to inspect the bond between the zirconium and uranium. The energy that passes through a good bond reveals defects in the core. In the absence of defects, the attenuation of the pulse is used as a measure of the average grain size of the uranium. Hanford uses a low-Q lithium sulfate crystal with a short focal length. The low Q enables the transducer to be used over a wide range of frequencies, the same transducer being used for core-integrity measurements[79] at 5 Mc.

There are interesting basic studies being conducted at Argonne,[80] the results of which

will be of benefit to the field of nondestructive testing. For instance, Argonne is investigating the velocity and attenuation in three steel cylinders $^{3}/_{16}$ in. in diameter by $1^{7}/_{8}$ in. long. The initial pulse must be considerably shorter than 1.3 μsec. Argonne is trying to obtain an initial pulse of $^{1}/_{2}$ μsec which would be 5 cycles at 10 Mc or 10 cycles at 20 Mc. It will be interesting to see how this is accomplished with sufficient intensity to obtain the measurements desired.

Argonne has also measured shear-wave velocities on a single crystal of alpha zirconium using frequencies[80] in the range 40 to 45 Mc. These measurements were made continuously over the 20 to 870°C temperature range, thus making possible the precise determination of the elastic modulus. Although the alpha-beta transformation point of zirconium reportedly is 862°C, this single crystal did not change structure, the velocities at given temperatures below 822°C being identical both before and after heating the crystal to 870°C. (D. Ensminger)

Eddy-Current and Other Nondestructive-Testing Techniques

An eddy-current transducer has been developed[2] to measure the spacing between fuel plates. The eddy-current coil is mounted between a leaf spring and the end of a tape measure. By scanning the fuel-plate spacing, the leaf spring translates the spacing measurement to eddy-current readings from the coil. The range of this unit was for spacings of 0.110 to 0.160 in. This would seem to have wide application since, if the eddy-current parameters were chosen properly, the coil would be sensitive only to the movements of the spring. The calibration could then be constant for any material one might choose to measure. In fact, a similar system[81] is being adapted for the measurement of the inside diameter of tubes. The spring idea has been varied by using an encircling coil around the metal spring-loaded feeler.

The dual-frequency, probe type, eddy-current inspection technique previously developed by Argonne[82] has been employed successfully in the inspection of Zircaloy-2 tubing used as the jacket for the ZrO_2-CaO-UO_2 spike fuel for the EBWR.[23] This method employs a small-diameter probe and is capable of detecting small internal cracks in the tubing on a production basis. The inspection rate was not disclosed; however, in the earlier communication[82] the rate calculates to approximately 11.7 in./min, with the suggestion that it could be increased by 100 per cent.

An unusual electro-potential test was developed for detecting voids in the coatings on graphite.[7] A galvanic cell is established with the coating as one electrode, a suitable electrolyte, and a second electrode. In one experiment for a silicon-SiC coating, the electrolyte was made up of a dilute solution of chromic and sulfuric acids. The second electrode was made of zinc. The electromotive force generated by the silicon-SiC/Zn cell was 0.75. For the graphite/zinc cell (901S graphite), the potential was 2.1. Measurements showed that exposed zones of $^{1}/_{16}$, $^{5}/_{32}$, $^{11}/_{32}$, and $^{15}/_{32}$ in. in diameter in the coatings produced voltages of 1.2, 1.6, 1.9, and 2.1 volts, respectively. These readings seem to indicate that the technique should be very sensitive to very small exposed areas and that beyond a $^{15}/_{32}$-in.-diameter zone little change would be recorded. This should be a very useful tool if the immersion into the electrolyte is not detrimental to the product being inspected.

An investigation[83] was made to compare the relative usefulness of various nondestructive methods for the inspection of small-diameter tubing. The methods explored were visual (magnifying glass), eddy current, dye penetrants (visual and fluorescent), magnetic particle, ultrasonics, radiographic, and hydrostatic. The conclusion drawn from this work was that the eddy-current technique was the most versatile and useful for the inspection of small-diameter tubing. The authors recognized one major problem, however, which is that the eddy-current technique is extremely difficult to calibrate.

Bettis[26] reports significant progress in the development of a fiber-optic device for fuel-element inspection. Surface patterns simulating corrosion-product stains were well defined using a 24-in.-long, 2-in.-wide fiber probe and photography. Probes having two 50-in. lengths are to be used for the inspection of the PWR core 2 and early PWR subassemblies.

(C. L. Seale)

References

1. M. von Ardenne, A 45-kw Electron Beam Multichamber Furnace for Melting and Casting Various Metals, *Kernenergie*, 3: 507–517 (June 1960).

2. Nuclear Fuels and Materials Development, USAEC Report TID-11295, February 1961.
3. P. F. Darby and R. O. Carson, The Development of Optimum Manufacturing Methods for Columbium Alloy Forgings. Phase IIA: Evaluation of Four Techniques for Consolidation of a Columbium Base Alloy (F48) Containing 15% W, 5% Mo, and 1% Zr, Report AMC-TR-7-782(II), Crucible Steel Co. of America, Midland Research Laboratory, September 1960.
4. O. J. Wick, Plutonium Metallurgy Operation Quarterly Progress Report, October, November, and December 1959, USAEC Report HW-64136, Hanford Atomic Products Operation, Feb. 25, 1960. (Classified)
5. H. Lloyd and M. L. Noahes, Improvements in or Relating to Metal Casting, British Patent 856,785, Dec. 21, 1960.
6. F. Miley and J. W. Anderson, Bottom-Pour Re-Usable Melting Crucibles for Plutonium Casting, USAEC Report LA-2480, Los Alamos Scientific Laboratory, Feb. 17, 1961.
7. Oak Ridge National Laboratory, March 1961. (Unpublished)
8. F. L. Cuthbert, Summary Technical Report for Period October 1, 1960, to December 31, 1960, USAEC Report NLCO-825, National Lead Co. of Ohio, Jan. 31, 1961. (Classified)
9. Mallinckrodt Chemical Works, Process Development Quarterly Progress Report, October–December, 1960, USAEC Report MCW-1463, Feb. 1, 1961.
10. Deutsche Gold und Silber-Scheideanstalt Vornols Roesster, Process and Apparatus for the Hot-Shaping of Metals and Metal Alloys, British Patent 843,362, Aug. 4, 1960.
11. L. C. Lemon and W. T. Ross, Fabrication of Aluminum Clad Plutonium-Aluminum Alloy Pin Elements, USAEC Report HW-66757, Hanford Atomic Products Operation, Sept. 1, 1960.
12. J. Greenspan, Fabrication Development of Beryllium-Clad Uranium–3.9% Silicon, Uranium–10% Molybdenum, and Uranium–Uranium Monocarbide Cermets, USAEC Report NMI-1236, Nuclear Metals, Inc., Aug. 30, 1960.
13. F. W. Albaugh, Reactor and Fuels Research and Development Operation Monthly Report, January 1961, USAEC Report HW-68350-A, Hanford Atomic Products Operation, Feb. 15, 1961. (Classified)
14. Nuclear Metals, Inc., Fundamental and Applied Research and Development in Metallurgy, Progress Report for August 1960, USAEC Report NMI-2088, Sept. 30, 1960.
15. Combustion Engineering, Inc., and Aeroprojects, Inc., A Program To Study the Feasibility of and Develop an Apparatus for the Ultrasonic Roll Bonding of Fuel Plates, USAEC Report CEND-93, December 1960.
16. Aeroprojects, Inc., February 1961. (Unpublished)
17. S. W. Porembka, Zircaloy–Stainless Steel Bonding Program, First Quarterly Report, December 1960 to March 1961, USAEC Report BMI-X-166, Battelle Memorial Institute, Mar. 7, 1961.
18. R. W. Dayton and C. R. Tipton, Jr., Progress Relating to Civilian Applications During March 1961, USAEC Report BMI-1509, Battelle Memorial Institute, Apr. 1, 1961. (Classified)
19. Reference canceled.
20. W. P. Chernock, Investigations in Wire-Type Fuel Elements, USAEC Report SCNC-300, Sylvania-Corning Nuclear Corp., March 1960. (Classified)
21. Hanford Atomic Products Operation, Quarterly Progress Report on Fuels Development Operation for July, August, and September 1959, USAEC Report HW-62656, Oct. 15, 1959. (Classified)
22. J. L. Lamartine, Oak Ridge National Laboratory, private communication.
23. Nuclear Fuels and Materials Development, USAEC Report TID-11295(Suppl.), February 1961.
24. S. J. Paprocki (Ed.), Progress on the Use of Gas-Pressure Bonding for Fabricating Low-Cost Ceramic, Cermet, and Dispersion Fuels, USAEC Report BMI-1475, Battelle Memorial Institute, Nov. 7, 1960.
25. R. W. Dayton and C. R. Tipton, Jr., Progress Relating to Civilian Applications During December 1960, USAEC Report BMI-1489(Rev.), Battelle Memorial Institute, Jan. 1, 1961.
26. Westinghouse Electric Corp., Bettis Atomic Power Laboratory, Pressurized Water Reactor (PWR) Project Technical Progress Report for October 24, 1960, to December 23, 1960, USAEC Report WAPD-MRP-89.
27. R. W. Dayton and C. R. Tipton, Jr., Progress Relating to Civilian Applications During January 1961, USAEC Report BMI-1496, Battelle Memorial Institute, Feb. 1, 1961.
28. B. N. Watts and D. Shaw, Improvements Relating to the Canning of Fuel Elements for Use in Nuclear Reactors, British Patent 859,206 (to British Thomson-Houston Co., Ltd.), Jan. 18, 1961.
29. W. J. Bailey et al., Fabrication of Aluminum-Plutonium Alloy Fuel Elements by Coextrusion, USAEC Report HW-63151, Hanford Atomic Products Operation, Dec. 1, 1959.
30. G. A. Last, Process for Jacketing a Core, U. S. Patent 2,945,293 (to USAEC), July 19, 1960.
31. M. Gauthron, Canning by the Diffusion Caused by a Heated Die, USAEC Translation AEC-tr-4384, 1959 (translated by M. S. Feldman from French Report CEA-1296).
32. E. W. V. Acton and M. C. Hartnell-Beavis, Improvements in or Relating to Methods of Manufacturing Protective Cans for Nuclear Reactor Fuel Elements, British Patent 858,294 (to General Electric Co., Ltd.), Jan. 11, 1961.

33. S. Storchheim, Cladding Uranium with Aluminum, British Patent 859,503 (to Sylvania-Corning Nuclear Corp.), Jan. 25, 1961.
34. Argonne National Laboratory, Reactor Development Program Progress Report, February 1961, USAEC Report ANL-6328, Mar. 15, 1961.
35. G. H. Kesler et al., The Use of Heat and Mass Transfer Model Studies in the Evaluation of the Rates of Deposition of Metals in Complex Systems, *Trans. Met. Soc. AIME*, 221: 9–13 (February 1961).
36. L. McD. Schetky, Try the Advanced Coating Methods, *Metalworking*, 17: 14–19 (March 1961).
37. O. Flint, Vapour-Phase Deposition of Metals on Uranium, Part I, British Report AERE-R-3535, November 1960.
38. B. F. Brown et al., Protection of Refractory Metals for High-Temperature Service: Progress Report 1, July 1, 1960, The Zinc-Base Coating for Niobium, Report NRL-5550, Naval Research Laboratory, Nov. 28, 1960.
39. High-Temperature Materials, Inc., Pyrolytic Carbide Development Program, 9th Monthly Progress Report (for) December 1960–Jan. 11, 1961.
40. High-Temperature Materials, Inc., Pyrolytic Carbide Development Program, 10th Monthly Progress Report (for) January 1961, Jan. 31, 1961.
41. High-Temperature Materials, Inc., Pyrolytic Carbide Development Program, 11th Monthly Progress Report (for) February 1961, Feb. 28, 1961.
42. J. D. Batchelor, Improvement of the Usefulness of Pyrolytic Graphite in Rocket Motor Applications, 8th Monthly Progress Report (for) Dec. 20, 1960, to Jan. 20, 1961, Feb. 3, 1961.
43. J. D. Batchelor, Improvement of the Usefulness of Pyrolytic Graphite in Rocket Motor Applications, 9th Monthly Progress Report (for) Jan. 20 to Feb. 20, 1961, Feb. 28, 1961.
44. N. T. Wakelyn, Titanium Nitride: An Oxidizable Coating for the High Temperature Protection of Graphite, Report NASA-TN-D-722, National Aeronautics and Space Administration, February 1961.
45. M. F. Browning et al., Alumina Coating of UO_2 Shot by Hydrolysis of Aluminum Chloride Vapor, USAEC Report BMI-1471, Battelle Memorial Institute, Oct. 25, 1960.
46. R. W. Dayton and C. R. Tipton, Jr., Progress Relating to Civilian Applications During February 1961, USAEC Report BMI-1504(Del.), Battelle Memorial Institute, Mar. 1, 1961.
47. R. W. Dayton and C. R. Tipton, Jr., Progress Relating to Civilian Applications During November 1960, USAEC Report BMI-1480, Battelle Memorial Institute, Dec. 1, 1960.
48. D. E. Couch and A. M. Brown, Coatings for Uranium, National Bureau of Standards–Project 0506-20-05465 (3262), to Sandia Corporation (Order AL 59-1022), March 1 to July 1, 1960.
49. J. G. Beach et al., Electroplating Metals on Uranium, USAEC Report BMI-912(Del.), Battelle Memorial Institute, May 7, 1954.
50. J. G. Beach and C. L. Faust, Electroclad Aluminum on Uranium, *J. Electrochem. Soc.*, 106: 654 (1959).
51. C. Chanvin et al., Protection of Uranium by Electrodeposition and Diffusion of Nickel, *Electrochim. Acta*, 1: 177–189 (July 1958).
52. M. H. Binstock, Fuel Element Development for Piqua OMR, USAEC Report NAA-SR-5119, Atomics International, June 30, 1960.
53. Electroplating Metals with Protective Metals, British Patent 853,521, Nov. 9, 1960.
54. Nickel Coatings and Methods of Applying, British Patent 853,522, Nov. 9, 1960.
55. Gladding, McBean & Co., March 1961. (Unpublished)
56. F. W. Albaugh, Reactor and Fuels Research and Development Operation Monthly Report, December 1960, USAEC Report HW-67954-A, Hanford Atomic Products Operation, Jan. 15, 1961. (Classified)
57. L. K. Mudge et al., Hanford Atomic Products Operation, November 1960. (Unpublished)
58. John Edward Antill, British Patent 847,912, Sept. 14, 1960.
59. Bureau of Mines, Boulder City Metallurgy Research Laboratory, Electrochemical Studies of Hafnium, Zirconium, and Yttrium, USAEC Report TID-6481, 1960.
60. Oak Ridge National Laboratory, Gas-Cooled Reactor Project Quarterly Progress Report for Period Ending December 31, 1960, USAEC Report ORNL-3049, Mar. 9, 1961.
61. R. Carpenter and A. Del Grosso, Summary Report on Materials for the GCRE-II, USAEC Report IDO-28564, Aerojet-General Nucleonics, Dec. 30, 1960.
62. W. B. Hall, Protective Coatings for Molybdenum Alloys, Interim Report No. 2, Report AD-234943, General Electric Co., Flight Propulsion Laboratory Dept., Oct. 15, 1959.
63. General Electric Co., Flight Propulsion Laboratory Dept., Protective Coatings for Molybdenum Alloys, Quarterly Report No. 3, Report AD-234944, Jan. 15, 1960.
64. Pyrene Company, Ltd., Improvements in and Relating to the Coating of Metallic Surfaces, British Patent 843,054, Aug. 4, 1960.
65. Office of Technical Services, Welding (Supplement to CTR's 324-331), OTS Selective Bibliography, Report SB-402, March 1960.
66. Oak Ridge National Laboratory, Mar. 9, 1961. (Unpublished)
67. T. Duff, Solid Phase Bonding of Zircaloy-2 by Resistance Heating, Canadian Report AMFC-59-2, Feb. 9, 1960.
68. C. C. Simons, Explosive Metalworking, Report DMIC-Memo-71, Defense Metals Information Center, Battelle Memorial Institute, Nov. 3, 1960.

69. S. W. Porembka and C. C. Simons, Compacting Metal Powders with Explosives, ASTME Creative Manufacturing Seminars 1960-1961, Paper No. SP60-102.

70. C. C. Simons, Battelle Memorial Institute. (Unpublished)

71. J. Pearson, The Explosive Working of Metals, Report NOTS-TP-2421 (NAVORD-7033), U. S. Naval Ordnance Test Station, Feb. 4, 1960.

72. R. L. Wachtell, Explosive Forming of Refractory Metals, Report NP-9137, Chromalloy Corp., May 1, 1960.

72*a*. D. W. Brite and R. J. Anicetti, Hanford Atomic Products Operation, November 1960. (Unpublished)

73. W. J. McGonnagle, *Nondestructive Testing*, McGraw-Hill Book Company, Inc., New York, 1961.

74. W. J. McGonnagle et al., Argonne National Laboratory, December 1960. (Unpublished)

75. R. W. McClung et al., Oak Ridge National Laboratory, Mar. 13, 1961. (Unpublished)

76. W. E. Lawrie, Ultrasonics and Ceramic Coatings, Quarterly Progress Report No. 2 for July 1 to September 30, 1960, Report ARF-6043-11, Illinois Institute of Technology, Armour Research Foundation, 1960.

77. W. E. Lawrie, Ultrasonics and Ceramic Coatings, Quarterly Progress Report No. 3 for October 1 to December 30, 1960, Report ARF-6043-14, Illinois Institute of Technology, Armour Research Foundation, Jan. 9, 1961.

78. T. G. Lambert, A Multiple Nondestructive Test Station for NPR Fuel Elements, USAEC Report HW-65910, Hanford Atomic Products Operation, June 28, 1960.

79. P. L. Farnsworth and K. M. Haws, Fabrication and Evaluation of Zircaloy-2 and Zircaloy-4 Tubing for Use in Cladding Uranium Dioxide and Aluminum-Plutonium Fuel, USAEC Report HW-66810, Hanford Atomic Products Operation, Oct. 1, 1960.

80. Argonne National Laboratory, April 1961. (Unpublished)

81. C. V. Dodd, Oak Ridge National Laboratory, February 1961. (Unpublished)

82. C. J. Renken, Argonne National Laboratory, 1961. (Unpublished)

83. J. R. Grieve and A. M. Bounds, Nondestructive Testing of Small Tubing, *Metal Progr.*, 78(6): 110–114 (December 1960).

NUCLEAR SCIENCE ABSTRACTS

The U. S. Atomic Energy Commission, Division of Technical Information, publishes *Nuclear Science Abstracts (NSA)*, a semimonthly journal containing abstracts of the literature of nuclear science and engineering.

NSA covers (1) research reports of the U. S. Atomic Energy Commission and its contractors; (2) research reports of government agencies, universities, and industrial research organizations on a world-wide basis; and (3) translations, patents, books, and articles appearing in technical and scientific journals.

Complete indexes covering subject, author, source, and report number are included in each issue. These are cumulated quarterly, semiannually, and annually providing a detailed and convenient key to the literature.

Availability of *NSA*

SALE *NSA* is available on subscription from the Superintendent of Documents, U. S. Government Printing Office, Washington 25, D. C., at $18.00 per year for the semimonthly abstract issues and $15.00 per year for the four cumulated-index issues. Subscriptions are postpaid within the United States, Canada, Mexico, and all Central and South American countries, except Argentina, Brazil, British and French Guiana, Surinam, and British Honduras. Subscribers in these Central and South American countries, and in all other countries throughout the world, should remit $22.50 per year for subscriptions to semimonthly abstract issues and $17.50 per year for the four cumulated-index issues.

EXCHANGE *NSA* is also available on an exchange basis to universities, research institutions, industrial firms, and publishers of scientific information. Inquiries should be directed to the Division of Technical Information Extension, U. S. Atomic Energy Commission, P. O. Box 62, Oak Ridge, Tennessee.